Etude de transformations de phases dans des alliages d'aluminium par la technique des couples de diffusion

Rocio Valdés

N° d'ordre : 2363

THESE

présentée

pour obtenir

LE TITRE DE DOCTEUR
DE L'INSTITUT NATIONAL POLYTECHNIQUE DE TOULOUSE

École doctorale : Matériaux Structure Mécanique

Spécialité : Science et Génie des Matériaux

par

Bertha Rocío VALDES LOPEZ

Etude de transformations de phases dans des alliages d'aluminium par la technique des couples de diffusion

Soutenue le **13 juillet 2006** devant le jury composé de :

M.	**Eric ANDRIEU**	Professeur, I.N.P. à Toulouse	Président
M.	**Alain HAZOTTE**	Professeur, LETAM	Rapporteur
M.	**Miguel A. CISNEROS**	Professeur, I.T. de Saltillo	Rapporteur
M.	**Jacques LACAZE**	Directeur de recherche C.N.R.S	Directeur de thèse

Etude de transformations de phases dans des alliages d'aluminium par la technique des couples de diffusion.

RESUME

Cette étude décrit les équilibres de phases dans différents alliages d'aluminium en vue de mieux connaître le rôle du magnésium, du manganèse et du fer dans les alliages Al-Si. Les travaux expérimentaux ont essentiellement porté sur l'analyse de couples de diffusion solide/solide et solide/liquide. Le système Al-Mg-Si a été étudié en premier en associant un alliage Al-Si à différents alliages Al-Mg-Si. Ces résultats, complétés par des essais d'ATD, ont permis d'améliorer la description thermodynamique de ce système selon la méthode CALPHAD. Le système Al-Mg-Mn-Si a ensuite été étudié expérimentalement en associant des alliages Al-Mn-Si et Al-Mg-Si. Le principal résultat obtenu dans cette partie est la non-substitution du Mg dans les composés définis du système Al-Mn-Si. La dernière partie présente une étude par MET des composés définis contenant Al, Si, Mn et Fe dans des alliages d'aluminium assemblés par brasage, procédé que l'on peut rapprocher des couples solide/liquide.

ABSTRACT

The purpose of the present work is to describe phase equilibria in different aluminium alloys for a better understanding of the role of magnesium, manganese and iron in Al-Si commercial alloys. The experimental support was the analysis of solid/solid and solid/liquid diffusion couples. Firstly, the Al-Mg-Si system was studied by associating an Al-Si alloy to different Al-Mg-Si alloys. These results, supplemented by DTA tests, made it possible to improve the thermodynamic description of this system according to CALPHAD method. The Al-Mg-Mn-Si system was then studied by diffusion couples with Al-Mn-Si and Al-Mg-Si alloys as end members. The main result obtained in this part of the work is that Mg does not substitute in the ternary Al-Mn-Si compounds. Finally, a TEM study of the compounds containing Al, Si, Mn and Fe in some aluminium alloys assembled by brazing is presented. This latter process can be compared to the solid/liquid couple technique.

Keywords:

- Diffusion couple
- Magnesium
- Calphad
- Aluminum
- Manganese
- Intermetallics
- Silicon
- Microanalysis
- Phase diagrams

A la mémoire de ma mère.
En témoignage de ma grande affection.

Remerciements

Ce travail de thèse a été réalisé au sein de l'équipe MEMO – Mécanique –Microstructure – Oxydation du Centre Interuniversitaire de Recherche et d'Ingénierie des Matériaux de Toulouse (CIRIMAT) dirigé par Monsieur Francis Maury.

Ce thèse s'est effectuée sous la direction de Monsieur Jacques Lacaze, directeur de recherche au Centre National de la Recherche Scientifique. Je souhaite lui exprimer ma profonde reconnaissance pour m'avoir tellement apporté scientifiquement et humainement.

Je tiens à remercier Monsieur Eric Andrieu, Professeur à l'Institut National Polytechnique de Toulouse, pour avoir accepté de présider le jury, malgré ses nombreuses obligations. Je remercie également Monsieur Miguel A. Cisneros, Professeur à l'Institut Technologique de Saltillo, et Monsieur Alain Hazzote du LETAM, professeur à l'Université de Metz, d'avoir accepté d'être les rapporteurs de mes travaux de thèse.

Je ne saurais oublier Monsieur Bernard Viguier et Moukrane Dehmas, qui m'ont fait profite de leur riche expérience en cristallographie.

Je tiens également à exprimer ma plus haute estime et ma profonde gratitude à Madame Marie-Christine Lafont et à Monsieur Djar Quab. Je les remercie très vivement pour leur aide constante en matière de microscopie électronique en transmission et à balayage.

Mes remerciements s'adressent également à Jany et Aline pour leur amitié et leur soutien administratif.

Merci également à tous les permanents du laboratoire, Dominique, Daniel, Jb-Deschamps, Yannick, Alexandre, Nadine, Christine, Gérard et Philippe Maugis. Merci pour vos précieux conseils et leur soutien.

Je remercie très sincèrement tous mes camarades de laboratoire pour leur amitié et leur soutien dans les moments difficiles, Nadia, Mayerling, Cat, Jonathan, Raluca, Sandrine, Julien, Loïc, JB-J, Fabienne, Cristel, Emilie, Simon. Je remercie plus particulièrement mes camarades de bureau, Séverin, Greg et Nakari, qui trouvent ici toute mon affection. Je vous souhaite de tout mon cœur une très grande réussite.

Je tiens aussi à remercier toute ma famille pour son soutien de l'autre côté de l'océan.

Enfin, je pense très fort à celui qui a partagé mon quotidien, qui m'a toujours soutenu : Merci cher Oliver, pour m'avoir accompagné dans cette grande aventure.

Encore une dernière fois, merci à tous.

SOMMAIRE 2

Cette thèse comprend sept compléments *:*

I. MICAST- The effect of magnetically controlled fluid flow on microstructure evolution in cast technical Al-alloy.

II. X-ray characterization of Al-Mg-Si alloys.

III. Phase equilibria and solidification of Mg-rich Al-Mg-Si alloys.

IV. Diffusion couples Al-Si/Al-Mg-Si, preparation and exploitation.

V. Calphad-type assessment of the Al-Mg-Si system.

VI. Phase equilibria and solidification in Al-Mg-Si-Mn system.

VII. Identification of intermetallic precipitates formed during re-solidification of brazed aluminium alloys.

Introduction

I.1 Le programme MICAST

Les travaux de cette thèse s'inscrivent dans le cadre du programme MICAST "Microstructure Formation in Casting of Technical Alloys under Diffusive and Magnetically Controlled Convective Conditions – MICAST" financé par l'ESA (Agence spatiale européenne). Ce programme a associé des partenaires universitaires (ACCESS, CGL, CIRIMAT-INPT, DLR-IRS, EPM-MADYLAM, SGMU) et industriels (DUNAFERR, HYDRO, MAL, TITAL) et portait sur l'analyse de la formation de la microstructure de solidification d'alliages d'aluminium du type A356 contenant du fer et manganèse sous différentes conditions convectives (microgravité, gravité terrestre et confinement magnétique). Des revues des résultats expérimentaux et théoriques ont été publiées dans des journaux et des actes de conférences internationales [1-3]. L'une de ces publications [1] est incluse dans ce manuscrit comme le premier complément.

Huit groupes de travail (work-packages) avaient été constitués :

- WP1 : Préparation, exécution et analyse d'essais sur Terre devant servir de références ;
- WP2 : Développement du réseau dendritique en trois dimensions ;
- WP3 : Thermodynamique ;
- WP4 : Conditions industrielles ;
- WP5 : Analyse des champs magnétiques de déplacement ;
- WP6 : Développement et application des modélisations en champs de phase ;
- WP7 : Développement et application des modélisations globales ;
- WP8 : Préparation, exécution et analyse des essais en vol.

Nos travaux se situaient dans le cadre du groupe de travail 3 et avaient pour objectif une meilleure connaissance du système Al-Mg-Si-(Mn-Fe). Bien que ce système ait déjà été largement étudié, sa complexité est source de nombreuses ambiguïtés qui justifient une nouvelle approche.

I.2 Présentation et composition des matériaux

Dans une première partie de notre étude, nous avons travaillé sur le système Al-Mg-Si. A partir de la section isotherme du diagramme de phase Al-Mg-Si calculée à 300 °C avec la base de données COST 507 [4] et présentée en Figure I-1, nous avons choisi les compositions de quatre alliages localisées dans différents domaines de phase. Dans cette figure les lignes en trait épais sont les limites entre différents domaines de phases, les phases présentes étant indiquées sur le côté droit du diagramme. Les symboles (Al) et (Mg) représentent les solutions solides riches en Al et Mg respectivement, et les symboles Al_3Mg_2-β, $Al_{30}Mg_{23}$-ε, $Al_{12}Mg_{17}$-γ et Mg_2Si désignent les composés binaires des systèmes Al-Mg et Mg-Si dont les diagrammes sont représentés en Figure I-2. Dans le diagramme Al-Mg, on note que la phase gamma présente un large domaine d'homogénéité. Des travaux récents de Donnadieu [5, 6] ont montré que les structures des phases β et γ sont complexes. L'analyse du diagramme de phases binaire Mg-Si montre la présence du composé intermétallique stœchiométrique Mg_2Si à point de fusion élevé.

Les compositions de trois alliages (croix) ont été choisies suivant la ligne en trait interrompu de sorte qu'elles soient situées dans trois domaines triphasés différents. Un quatrième alliage, contenant 30 % en poids de magnésium et 0.5 % en poids de silicium, a été préparé pour cette étude et est représenté par un carré dans la Figure I-1.

Les trois premiers alliages étudiés ont été préparés au CRC (Casting research center, Australie) et le quatrième par le DLR (Allemagne). Des analyses chimiques ont été effectuées au centre d'analyses du CNRS, avec un soin spécial pour détecter la présence de fer et de manganèse. La composition de ces différents alliages est indiquée dans le Tableau I-1.

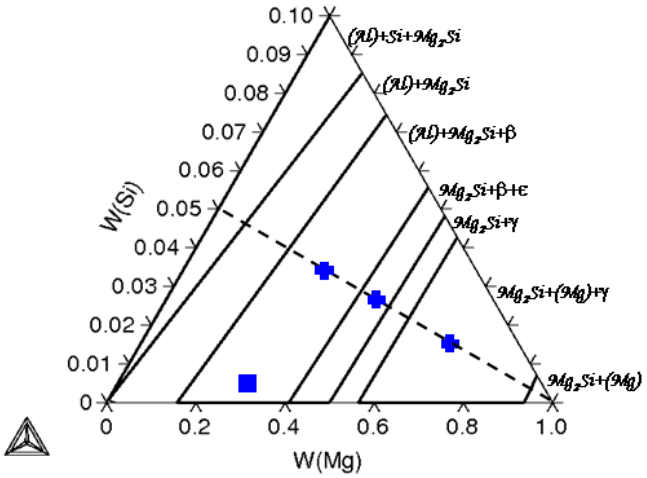

Figure I-1 : Section isotherme à 300 °C du système Al-Mg-Si.

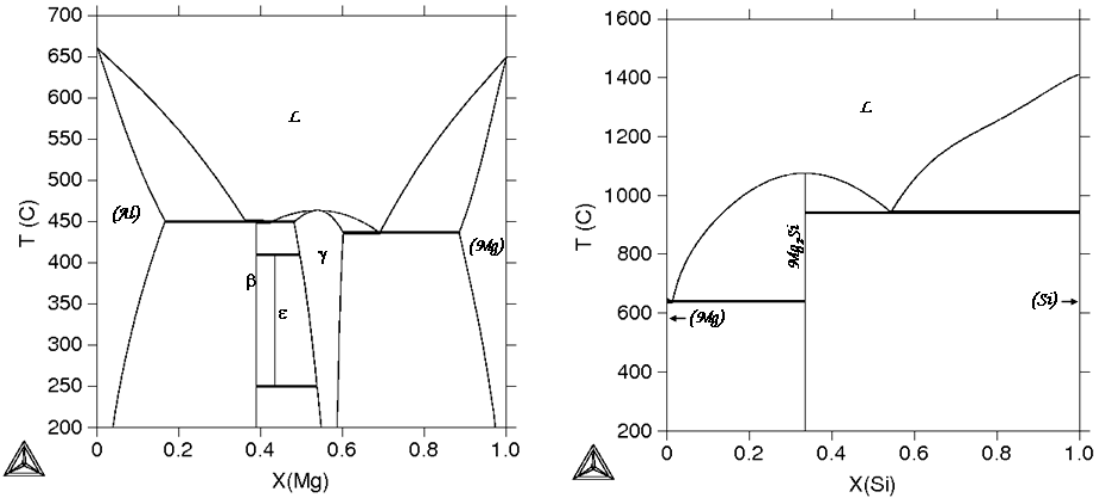

a) *b)*

Figure I-2 : Diagrammes de phases des systèmes binaires Al-Mg a) et Mg-Si b) calculés à l'aide de la banque COST-507 [4] et du logiciel thermocalc.

Dénomination	*Al*	*Mg*	*Si*	*Fe*	*Mn*
A30	66.70	28.68	3.55	0.05	0.01
A45	46.38	50.11	2.91	0.02	0.01
A70	27.96	68.05	1.23	0.18	0.02
D30	70.01	29.40	0.89	0.07	< 50 ppm

Tableau I-1 : Composition des alliages étudiés (% en poids).

Pour l'étude des phases à équilibre dans le système Al-Mg-Si, nous avons essentiellement utilisé la technique de couples de diffusion à l'état solide en associant l'un des alliages présentés ci-dessus à un alliage binaire Al – 5 % en poids de silicium préparé au DLR, Allemagne.

Dans une deuxième étape, des "incursions" dans le système Al-Mg-Mn-Si ont été effectuées en associant l'alliage Al-Mg-Si A70 et différents alliages du système Al-Mn-Si fournis par le Professeur J.C. Schuster (Université de Vienne). La composition chimique de ces alliages est présentée dans le Tableau I-2. Leur préparation a été décrite par Du et coll. [7].

Référence de l'alliage	***Al***	***Mn***	***Si***
N59	45	45	10
N55	36	45	19
E	20	45	35
N72	30	40	30
F	10	40	50
A	5	75	20
B	20	70	10
C	65	20	15

Tableau I-2 : Composition nominale des alliages ternaires Al-Mn-Si (en pourcentages atomiques).

Enfin, une étude MET a porté sur des alliages d'aluminium plaqués et assemblés par brasage utilisés dans les échangeurs thermiques pour automobiles. Ces alliages sont constitués d'un matériau de cœur en alliage AA3003 plaqué sur ses deux faces avec un alliage AA4343. Après pliage et pré-assemblage, un traitement thermique à 600 °C permet de braser les pièces entre elles par fusion des placages. Ce traitement induit la formation de précipités contenant les éléments Al, Mn, Fe, Si lors de la re-solidification. Nous avons étudié ces précipités par MET dans le cadre d'une collaboration informelle avec S. Tierce du groupe "Corrosion" du laboratoire.

I.3 Techniques de caractérisation

Les différentes techniques de caractérisation des microstructures qui ont été employées sont : la microscopie optique, la microscopie électronique à balayage (MEB) et l'analyse EDX, la microscopie électronique à transmission (MET) et la diffraction de rayons X.

I.3.1 Microscopie optique

La préparation métallographique des échantillons consiste à les polir mécaniquement avec des papiers abrasifs en carbure de silicium, du grade 600 jusqu'au grade 4000, puis à la pâte diamantée de 1 μm. Pour mettre en évidence les phases présentes, il faut ensuite réaliser une attaque chimique avec différents réactifs. Pour les alliages A30, A45 et D30 nous avons utilisé le réactif Keller constitué de 2.5 ml d'acide nitrique, 1.5 ml d'acide chlorhydrique, 1 ml d'acide fluorhydrique et 95 ml d'eau. 30 secondes d'attaque suivies d'un rinçage à l'eau permettent de révéler la phase Al_3Mg_2-β. Pour l'alliage A70, nous avons utilisé une solution de 0,5 % d'acide nitrique dilué dans l'éthanol. Les microstructures des alliages cités ci-dessus à l'état brut de coulée sont présentées sur la Figure I-3.

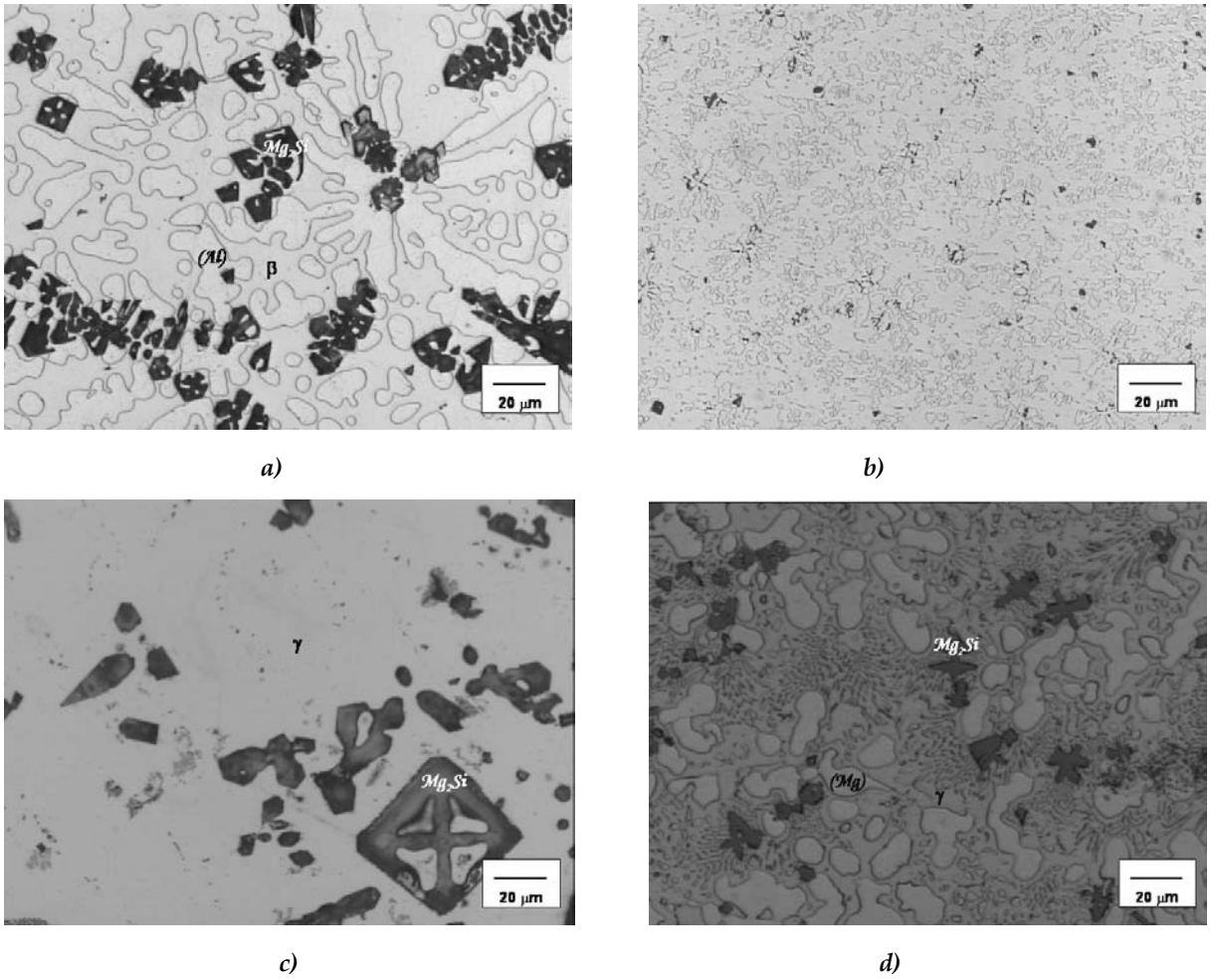

Figure I-3 : Microstructures des alliages après attaque chimique. Pour les quatre alliages les précipités gris foncé correspondent au composé stœchiométrique Mg_2Si. Pour l'alliage A30 a) les dendrites d'aluminium sont entourées de la phase Al_3Mg_2-β, pour D30 b) la microstructure est la même que A30 mais plus fine du fait d'une plus grande vitesse de refroidissement, pour A45 c) la matrice est composée de la phase $Al_{12}Mg_{17}$-γ et pour A70 d) les dendrites de magnésium sont entourées de $Al_{12}Mg_{17}$-γ plus un eutectique biphasé $Al_{12}Mg_{17}$-γ + (Mg)

I.3.2 Diffraction des rayons X

La diffraction des rayons X permet l'identification des phases présentes. Les deux diffractomètres utilisés sont :

- Un appareil SEIFERT 2000 équipé d'une cathode de cuivre ($K\alpha_1$ = 1,54056 Å, $K\alpha_2$ = 1,54439 Å).
- Un appareil INEL équipé d'une cathode de cobalt (Kα = 1.7889 Å).

Les enregistrements ont été effectués soit sur des échantillons de 10x18x2 mm^3 prélevés sur matériau brut de coulée et polis, soit sur des poudres obtenues par broyage. L'emploi de l'une ou l'autre des méthodes sera précisé lors de la présentation des résultats. Les diffractogrammes ont été enregistrés dans la configuration θ-2θ pour 2θ variant entre 20 et 80°, avec une vitesse de balayage de 0.04 °.min^{-1}. L'indexation des diffractogrammes a été faite à l'aide du programme Carine v3.1 [8] à partir des données de Pearson [9]. CaRine v3.1 [8] est un logiciel de cristallographie qui permet le calcul des diffractogrammes en ayant généré la structure cristalline des phases d'intérêt à partir de leur groupe d'espace et de leurs paramètres de maille. Le Tableau I-3 regroupe les données utilisées pour indexer les pics des diffractogrammes des alliages Al-Mg-Si. Du fait de la complexité des structures des phases Al_3Mg_2-β et $Al_{12}Mg_{17}$-γ, les résultats correspondants sont présentés dans le complément numéro deux.

Phase	***Prototype***	***Symbole de Pearson***	***Group d'espace***	***Paramètre de maille (Å)***
Al-α	Cu	cF4	$Fm\bar{3}m$	a = 4.0494
Mg-hcp	Mg	hP2	$P6_3/mmc$	a = 3.2094 c = 5.2112
Diamant	Si	cF8	$Fd\bar{3}m$	a = 5.4311
Mg_2Si	CaF_2	cF12	$Fm\bar{3}m$	a = 6.35
Al_3Mg_2-β	Al_3Mg_2	cF1832	$Fd\bar{3}m$	a = 28.239
$Al_{30}Mg_{23}$-ε	$Co_5Cr_2Mo_3$	hR53	$R\bar{3}$	a = 12.8254 c = 21.7478
$Al_{12}Mg_{17}$-γ	α –Mn	cI58	$I\bar{4}3m$	a = 1.05438

Tableau I-3 : Description des phases utilisée pour l'indexation des diagrammes DRX des alliages Al-Mg-Si.

I.3.3 Microscopie électronique à balayage (MEB)

L'acquisition des images a été réalisée à l'aide d'un microscope électronique à balayage de type LEO 435 VP équipé d'un spectromètre à dispersion d'énergie (EDS) de type IMIX-PC de PGT avec un détecteur en germanium. Le système d'analyse IMIX permet l'acquisition d'analyses ponctuelles et de cartographies élémentaires X. Les

observations des échantillons ont été faites très souvent en mode rétrodiffusé, ce qui permet de mieux visualiser les différentes phases. Une distance de travail de 19 mm et un angle d'incidence de 35° sont imposés par la géométrie de l'appareil afin d'optimiser les conditions de détection des rayon X.

I.3.4 Microanalyse X

L'analyse EDS permet une caractérisation chimique des différentes phases. Le principe consiste à bombarder l'échantillon par un faisceau d'électrons d'énergie de l'ordre de 10 à 40 kV. L'impact provoque l'émission de rayons X (raies K, L, M) caractéristiques des éléments constituant l'échantillon. La zone d'interaction dans laquelle sont émis les électrons et les photons forme un volume, appelé "poire d'interaction" [10], dont la taille dépend de la tension d'accélération des électrons et du matériau étudié. La tension d'accélération du faisceau d'électrons incident est l'un des paramètres importants de la microanalyse.

- Les électrons incidents ne peuvent pas éjecter des électrons d'une énergie supérieure à la leur. Le spectre s'arrête sur l'axe des énergies à la valeur qui correspond à la tension d'accélération.
- Le volume analysé dépend aussi de la tension d'accélération. Le logiciel Casino [11] a permis de faire un calcul approximatif de la trajectoire des électrons par une simulation Monte-Carlo en prenant en compte la composition chimique des phases. Les images de la Figure I- 4 représentent une analyse ponctuelle avec un faisceau d'électrons accélérés avec une tension de 15 ou 8 kV pour un précipité de MnSi dans un alliage Al-Mn-Si. Pour une tension d'accélération de 15 kV, la distance de pénétration des électrons est plus grande que pour une tension de 8 kV. Nous pouvons voir que les électrons perdent progressivement leur énergie en pénétrant dans le matériau. Pour les analyses de phases à l'interface des couples de diffusion

à l'état solide/liquide du système Al-Mg-Mn-Si, la tension d'accélération a été fixée à 8 kV de manière à ce que la taille du volume d'analyse soit la plus proche possible de celle des précipités.

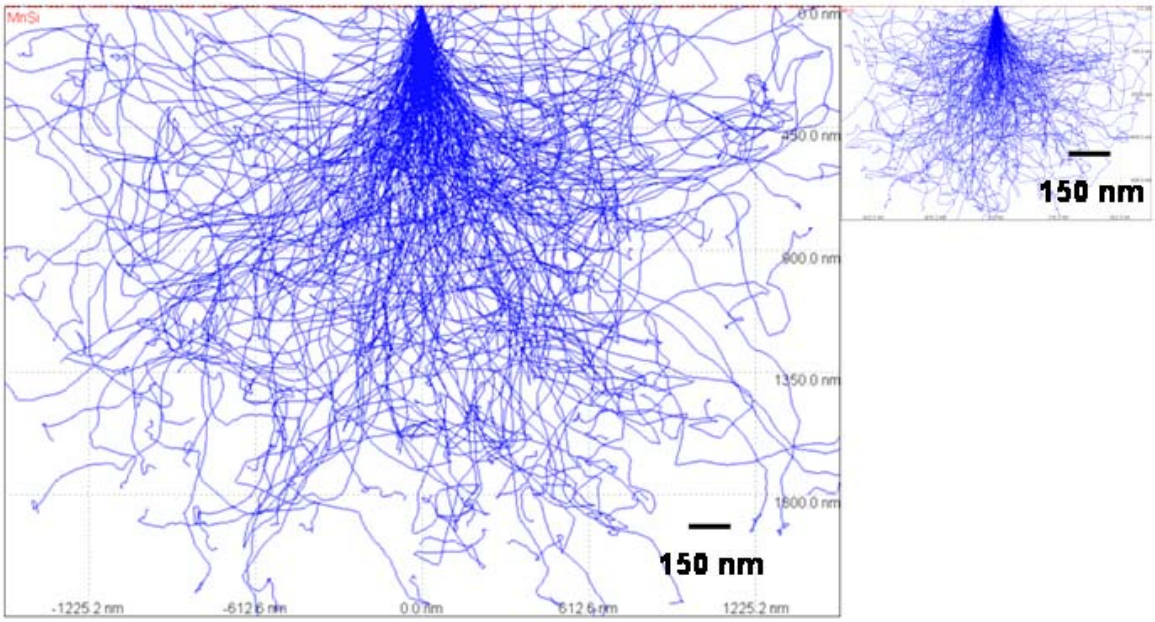

a) 15 kV ***b) 8 kV***

Figure I- 4 : Comparaison des poires d'interaction des électrons à 15kV a) et 8 kV b) calculées à l'aide du logiciel casino [11].

- La quantité de photons produite dans une gamme d'énergie est aussi fonction de la tension d'accélération. Les analyses EDS sont fiables lorsque l'énergie des électrons du faisceau incident dépasse 1,5 fois l'énergie de la raie dans la série sélectionnée (K, L ou M) pour l'élément à analyser. Il est donc important de choisir une tension d'accélération compatible avec les éléments (donc les raies) que l'on analyse. Des tensions faibles pour les éléments légers devront être utilisées alors que l'on privilégiera des tensions plus fortes pour les éléments lourds. Les valeurs des raies pour les éléments présents dans les échantillons sont indiquées dans le Tableau I- ***4***.

Elément	*Numéro atomique*	K_α	K_β	L_α	$L_{\beta 1}$	$L_{\gamma 1}$
Mg	12	1.25	1.29			
Al	13	1.48	1.55			
Si	14	1.73	1.82			
Mn	25	5.89	6.48	0.637	0.649	0.652

Tableau I- 4 : Valeur d'énergie d'émission des rayons X (eV) [10].

On constate qu'une tension d'accélération de 8 kV, pour les analyses dans les phases Al-Mn-Si, n'est pas bien appropriée pour la raie K_α du manganèse, et qu'il faudrait donc travailler avec la raie L_α. Toutefois nous avons remarqué par des analyses ponctuelles, faites sur des précipités MnSi, une différence de concentration de l'ordre de 10 pour cents pour le Mn par rapport à celles effectuées avec une tension de 15 kV (raie $K_{\alpha Mn}$) ainsi qu'indiqué dans le Tableau I-5. Nous supposons que cette différence est liée à des phénomènes d'absorption par la matrice et au fait de l'existence de plusieurs raies L qui peuvent se confondre et être plus ou moins absorbées dans le volume d'analyse. C'est pourquoi nous avons malgré tout décidé de travailler avec la raie $K_{\alpha Mn.}$ On note dans le Tableau I-5 que les valeurs obtenus à 8 kV sur la raie $K_{\alpha Mn}$ sont effectivement proches de celles obtenus à 15 kV. En résumé, pour les couples de diffusion dans le système Al-Mn-Mg-Si, une tension d'accélération de 8 kV a été choisie de manière à réduire la poire d'interaction. Pour les alliages et les couples Al-Mg-Si, une tension de 15 kV a été employée.

Elément	**8 kV (raie $L_{\alpha Mn}$)**	**8 kV (raie $K_{\alpha Mn}$)**	**15 kV (raie $K_{\alpha Mn}$)**
Mg	0.18	0.21	0.25
Al	5.18	6.10	6.04
Si	37.25	44.31	44.92
Mn	57.40	49.40	48.80

Tableau I-5 : Comparaison des mesures à 8 et 15 kV avec différentes raies du Mn.

Suivant les cas, une tension d'accélération de 15 ou de 8 kV a été utilisée avec des temps d'acquisition de 100 et 200 secondes respectivement. Dans tous les cas, le courant de sonde est de 1.5 nA, il est contrôlé à l'aide d'un pico-ampèremètre.

Dans le cas des analyses à 8 kV le temps d'acquisition a été augmenté à 200 secondes pour améliorer la précision de l'analyse en termes de statistique de comptage, c'est-à-dire pour diminuer la longueur de l'intervalle de confiance. La précision est calculée par le programme par l'équation :

$$\Delta C > \frac{2.33 \times C \times 2(N_p)^{1/2}}{N_{p-b}}$$

Où C est la concentration en fraction (% en poids), N_P est le nombre de coups au pic, y compris le bruit de fond, et $N_{P\text{-}b}$ est le nombre de coups nets au pic.

La quantification des analyses a nécessité l'élaboration d'une bibliothèque de standards (témoins réels). Les spectres des différents éléments à l'état pur (Al, Mg, Mn, Si) ont été acquis dans les mêmes conditions que celles de l'analyse des échantillons (tension d'accélération, courant de sonde, temps d'acquisition….). Avant l'acquisition des spectres des témoins, le courant de sonde a été mesuré et stabilisé pendant une heure, puis régulièrement contrôlé pendant les acquisitions des spectres pour éviter d'éventuelles fluctuations.

Le traitement des spectres d'émission X (IMIX) utilise le modèle de correction ZAF qui prend en compte le numéro atomique (Z), l'absorption (A) et la fluorescence (F). Il n'est applicable en toute rigueur que si la zone analysée est monophasée. Dans ce travail, la principale source d'erreur est la présence éventuelle d'une seconde phase dans le volume analysé. Les analyses ont été multipliées pour minimiser les incertitudes de ce type.

I.3.5 Microscopie électronique à transmission (MET)

Pour réaliser une partie de cette étude il a fallu la préparation d'échantillons amincis mécaniquement, puis ioniquement (PIPS). Le microscope utilisé est un JEOL 2010, équipé d'un détecteur EDS de marque Voyager.

I.4 Équilibre des phases et solidification d'alliages riches en magnésium dans le système Al-Mg-Si

Pour l'étude des phases en équilibre dans le système Al-Mg-Si, nous avons utilisé la technique de couples de diffusion entre un alliage binaire Al- 5 %Si et l'un des alliages Al-Mg-Si présentés ci-dessus. La zone de diffusion est constituée de bandes (couches) mono-phasées ou biphasées successives ainsi que l'illustre la Figure I-5. Les détails et l'exploitation des résultats sont présentés dans le complément numéro quatre. La composition des phases formées dans la zone d'interdiffusion a été évaluée à partir des analyses en pointés. Les composés binaires formés ne contiennent pas de silicium (moins de 0.1 % en poids), et on peut donc comparer leur composition à celle établie dans le diagramme de phases Al-Mg calculé avec la base COST 507 [4].

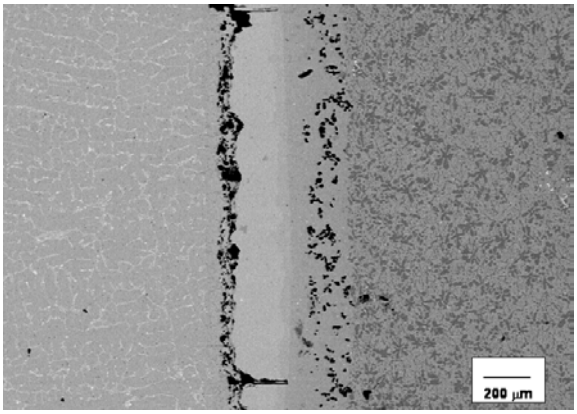

Figure I-5 : Zone de diffusion dans le couple Al5Si/A70.

Des analyses thermiques différentielles ont été effectuées sur les alliages Al-Mg-Si (Tableau I-1) pour déterminer les températures des transformations des phases. Deux

réactions eutectiques ont été déterminées : Liquide ↔ (Al) + β+ Mg_2Si à 448°C et Liquide ↔ (Mg) + γ + Mg_2Si à 436°C et sont en accord avec celles présentées dans la littérature. L'une des difficultés a été la mise en évidence de la réaction eutectique Liquide ↔ (Al)+ β+ Mg_2Si, d'où le choix de l'alliage D30. Avec ce dernier alliage on a fait d'essais de refroidissement à différentes vitesses, les enregistrements d'ATD sont inclus dans le complément trois.

I.4.1 Couples de diffusion Al-Si/Al-Mg-Si et profils de diffusion

La base de ce travail consistait à étudier la zone d'interdiffusion Al-5Si/Alliages riches en magnésium dont la nature dépend du diagramme de phase. Les résultats et leur exploitation ont été le point de départ du quatrième complément. De premiers couples ont été élaborés avec les alliages A30, A45 et A70 à 300 °C maintenus pendant 24 jours mais le contact entre les deux parties des couples était insuffisant.

Le traitement a été réalisé de nouveau pour une durée de 7 mois et a donné des couples exploitables. Des échantillons prélevés dans la zone d'interdiffusion des trois couples ont été préparés pour être observés au microscope électronique à balayage et pour mesurer la composition des phases par EDX. Les cartographies élémentaires X acquises par le système d'analyse IMIX ont été traitées par le logiciel Spirit. Des problèmes sont apparus dans le traitement de ces cartographies pour l'obtention des profils de concentration. En effet, alors que le traitement direct des spectres moyens obtenus sur l'ensemble des cartographies donne des résultats convenables en termes de composition, les profils qui en sont déduits présentent des biais qui, dans le cas présent, se sont manifestés par des taux de silicium très faibles. L'origine de ces biais réside certainement dans la méthode employée par le logiciel Spirit qui traite les cartographies comme des images après les avoir codées sur 255 niveaux de gris. Par suite les informations obtenues par cette méthode doivent être considérées comme qualitatives.

Les chemins des diffusions observés peuvent être retracés sur le diagramme Al-Mg-Si, ainsi qu'illustré en Figure I-6 dans le cas du couple Al-Si/A70. Le chemin de diffusion forme des zigzags parce qu'il traverse des zones plus ou moins riches en précipités de Mg_2Si. Il a été noté que les chemins de diffusion sont en accord avec la microstructure observée et avec les changements de domaines de phases dans le système Al-Mg-Si, tout en restant proches du binaire Al-Mg.

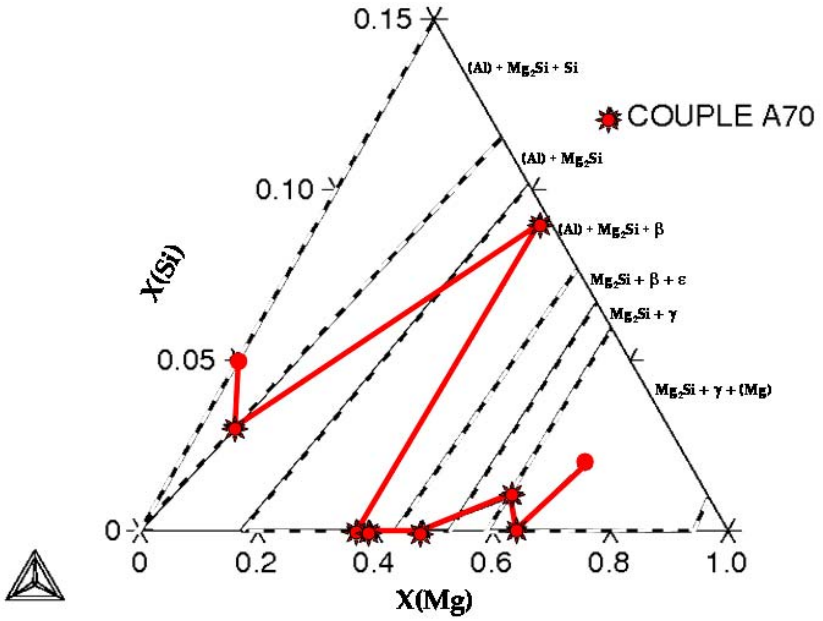

Figure I-6 : Profil de composition moyenne du couple Al-Si/ A70 dans le système Al-Mg-Si, ou chemin de diffusion. Les cercles pleins correspondent aux compositions initiales des éléments du couple, les étoiles à la composition aux frontières des différents domaines microstructuraux. Les lignes séparent les différents domaines d'équilibre entre phases calcules à 300 °C.

I.5 Evaluation de type Calphad du système Al-Mg-Si (Complément V)

La description des équilibres entre phases dans les systèmes ternaires et d'ordre supérieur requiert des outils de calculs et simulations. La méthode CALPHAD (CALculation of PHAse Diagrams) définit pour chaque phase un modèle permettant de décrire son énergie libre de Gibbs par une fonction de la température et de la composition [12]. Différents modèles ont été développés pour décrire le comportement

thermodynamique des phases existantes, comme les liquides et les solutions solides, les composés stœchiométriques, etc.

Ce travail a permis une amélioration des paramètres ternaires décrivant la phase liquide du système Al-Mg-Si, sans modification des phases solides et donc des équilibres solide-solide. La Figure I-7a montre un agrandissement de la projection du liquidus le long du binaire Al-Mg dans le système ternaire Al-Mg-Si. Les températures calculées E_2 = 448 °C et E_4 = 436 °C dans le complément III sont en accord avec la projection tracée sur la Figure I-7a. La microstructure de l'eutectique ternaire L↔ (Mg) + γ + Mg_2Si est présentée sur la Figure I-7b. L'eutectique est composé de deux phases (Mg) + γ, la troisième étant constituée par de gros cristaux de Mg_2Si (gris clair) indépendants, provenant du dépôt primaire. La composition eutectique a été mesurée par EDS sur des secteurs de 30x40 μm^2 et elle est reportée sur la projection du liquidus de la Figure I-7a et elle est approximativement de 69.9 % en poids de magnésium et 0.8% en poids de silicium.

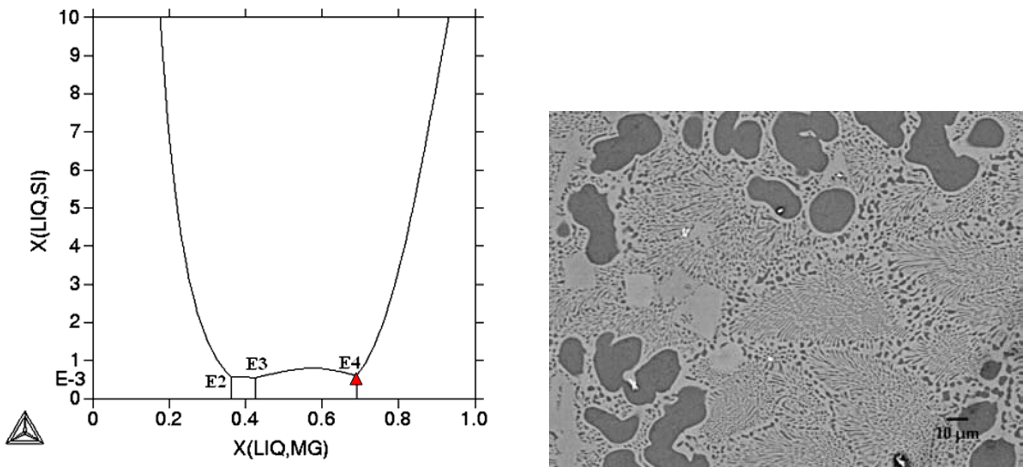

a) *b)*

Figure I-7 : Agrandissement de la projection du liquidus, côte Al-Mg a) Microstructure du l'eutectique dans l'alliage A70 b).

I.6 Équilibre des phases dans le système Al-Mg-Si-Mn

Différentes tentatives ont été effectuées pour étudier les équilibres dans le système Al-Mg-Si-Mn. Le manganèse a été choisi plutôt que le fer pour réaliser des études

expérimentales parce qu'il y a moins de travaux disponibles dans ce système que dans le Al-Mg-Si-Fe. Cette étude nécessite la connaissance de tous les diagrammes de phases binaires et ternaires limitrophes, et cela nous a conduit à nous intéresser plus particulièrement au système Al-Mn. Les deux autres sous sections sont consacrées aux essais réalisés.

I.6.1 Evaluation du diagramme Al-Mn

Le diagramme Al-Mn a été étudié par différents auteurs, dont Jansson [13,14] dont les données sont celles de la base COST 507 [4]. Le diagramme correspondant apparaît sur la Figure I-8a. En accord avec Gödecke et Köster [15], il y a trois phases intermétalliques nommées γ, γ_1 et γ_2 entre 35 et 55 % at. de manganèse. Dans le diagramme proposé par Jansson, la phase Al_8Mn_5 englobe ces trois phases dans une seule structure ($D8_{10}$) du type Al_8Cr_5. D'autre part, Ellner [16] dans son étude avec des rayons X à haute température, a montré que la phase γ a une structure bcc désordonnée (A2). La Figure I-8b montre une évaluation plus récente du diagramme réalisée par Liu [17]. Les phases γ et γ_2 sont prise en compté dans cette alors que la phase γ_1 est intégrée dans la phase γ_2-Al_8Mn_5. Notons que la structure de la phase γ_1 est inconnue. De plus, Liu [17]a montré que la phase γ subit une transformation d'ordre, de A2 à B2. Cette évaluation prend aussi en compte l'extension de domaine de stabilité de la phase ε étudie par [18]. Liu a décrit les phases γ et δ(Mn) avec une même structure désordonnée bcc. J'ai essayé d'utiliser les données présentées par Liu [17] pour calculer le diagramme mais sans succès. D'où l'intérêt d'améliorer le diagramme Al-Mn a partir des données de Jansson en décrivant les phases δ-Mn et γ-AlMn avec une même structure bcc. Dans cette évaluation, la transformation d'ordre de la phase γ-A2 n'a pas été prise en considération. La Figure I-8c montre le diagramme Al-Mn ainsi optimisé.

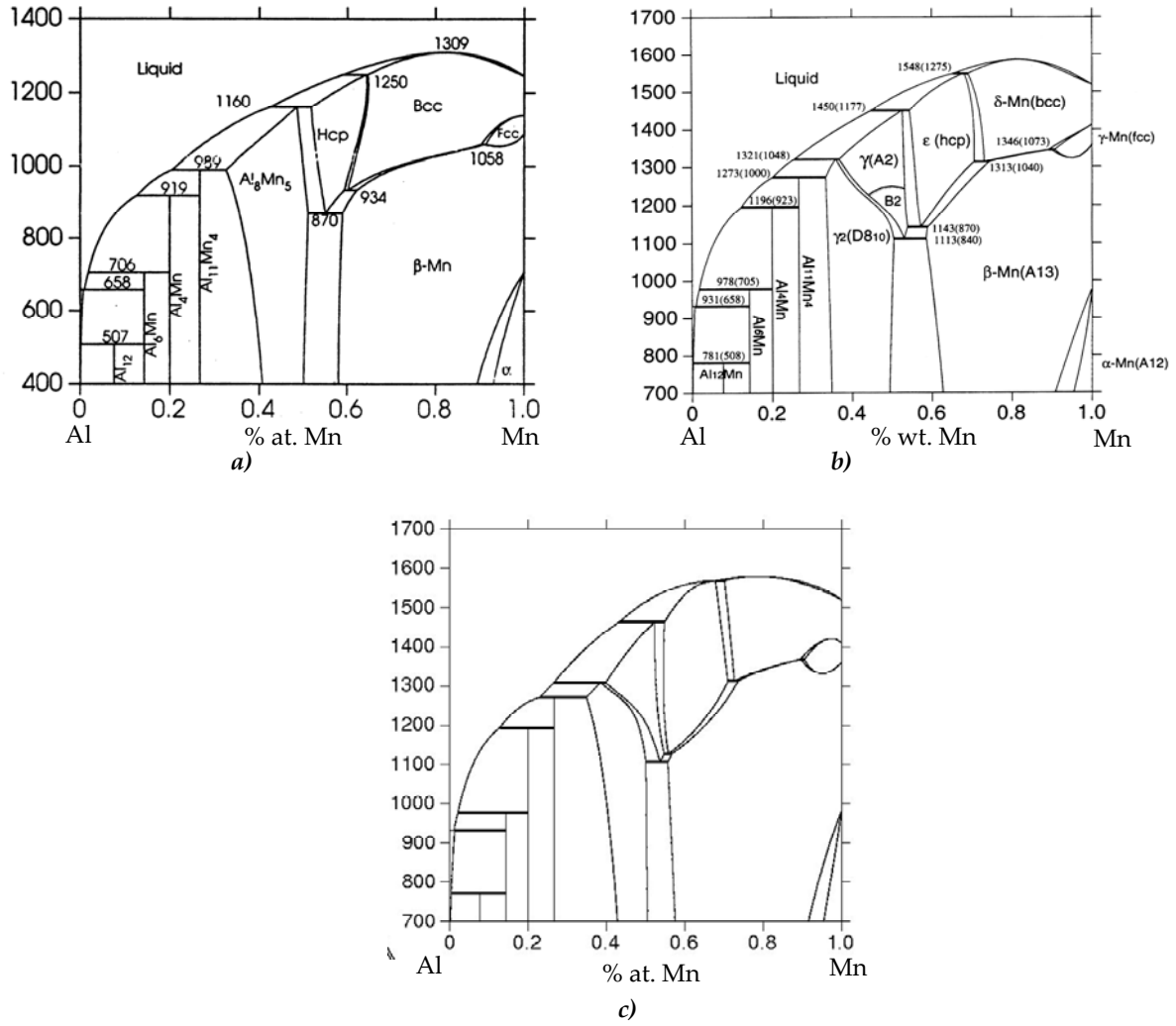

Figure I-8: Diagramme Al-Mn calculé par Jansson [14] a), par Liu [17] b) et diagramme calculé dans cette étude c).

I.6.2 Couples de diffusion à l'état solide entre Al-Mn-Si etAl-Si- Mg

Pour étudier les équilibres possibles dans le système quaternaire, nous avons réalisé des couples de diffusion et des frittages de poudres à l'état solide. Les échantillons préparés n'ont pas permis d'obtenir de résultats. En effet, la présence d'oxydes de magnésium a limité l'homogénéisation des poudres et les phénomènes de diffusion.

L'oxyde de magnésium est observé en blanc sur la micrographie du mélange de poudres Al-Mg-Mn-Si présentée sur la Figure I-9. Ces essais préliminaires, et la revue bibliographique qui avait été faite en parallèle, ont orienté nos travaux postérieurs en vue

de répondre à la question : le magnésium peut-il entrer en substitution dans l'un des nombreux composés intermétalliques du système Al-Mn-Si ?

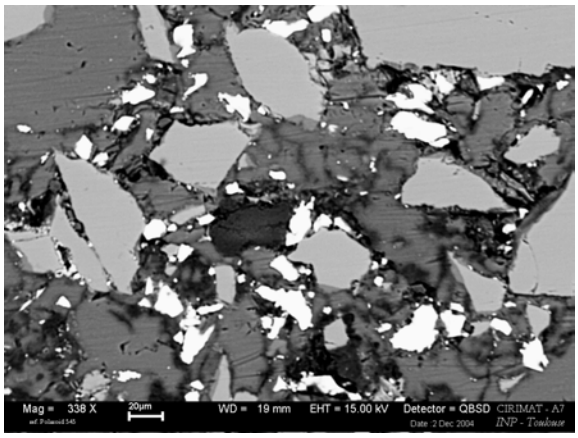

Figure I-9 : Micrographie des poudres de Al-Mg-Mn-Si après frittage.

I.6.3 Couples de diffusion avec une phase liquide

Pour essayer de répondre à la question ci-dessus, nous avons alors cherché à réaliser les équilibres entre une phase liquide riche en magnésium et un des alliages Al-Mn-Si. Pour cela nous avons utilisé des creusets en magnésium contenant une plaquette d'alliages Al-Mn-Si entre deux plaquettes d'alliages A70. Le traitement thermique appliqué pouvant consister en un maintien à une température unique T_1 pendant un temps t_1, ou en deux maintiens successifs (T_1, t_1) puis (T_2, t_2). Les caractéristiques de l'ensemble des essais sont indiquées dans le Tableau I-6. Les observations ont montré que l'on avait soit dissolution des alliages Al-Mn-Si soit croissance d'une couche de $Al_{11}Mn_4$ entre ces premiers alliages et l'alliage A70. Pour répondre à la question initiale, les analyses EDS effectuées sur les intermétalliques du système Al-Mn-Si n'ont pas permis de révéler la présence de magnésium.

Reference	T_1 (°C)	t_1 (min)	T_2 (°C)	t_2 (min)	*Interphase*
N59	600	180			Dissolution
	550	240			$Al_{11}Mn_4$
N55	600	120			Dissolution
	550	180			$Al_{11}Mn_4$
E	600	120			Dissolution
N72	600	15	550	180	$Al_{11}Mn_4$
F	600	5	550	240	Dissolution
A	550	15	450	480	$Al_{11}Mn_4$
B	550	15	450	480	$Al_{11}Mn_4$
C	550	15	450	450	Dissolution

Tableau I-6 : Détails des traitements thermiques réalise et les résultats.

I.7 Etude MET des précipités de Al-Mn-Fe-Si dans un alliage d'aluminium re-solidifié

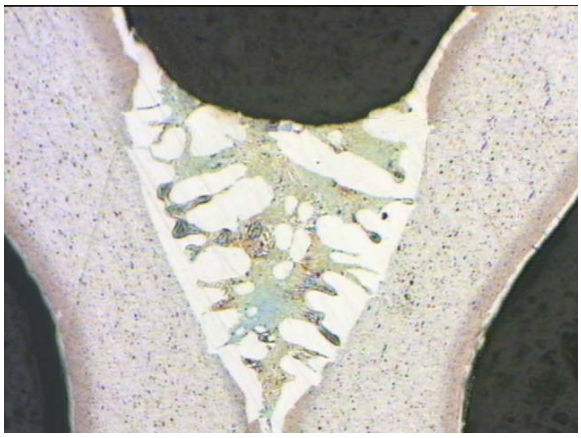

Figure I-10 : Section transverse de matériau après brasage des alliages AA4343 et AA3003.

La littérature fait apparaître de nombreux désaccords pour ce qui concerne les structures et compositions des précipités dans les alliages d'aluminium du système Al-Mn-Fe-Si (complément sept). Nous avons eu l'occasion d'étudier les précipités qui contiennent du silicium, du fer et du manganèse dans un alliage re-solidifié après brasage. Les phases α-Al(Fe,Mn)Si et δ-AlFeSi sont permis les précipités qui contiennent une faible teneur en Fe et en Mn observés dans les brasures telle que celle de la Figure I-10. Les observations faites au MET ont confirmé que la phase α-Al(Fe,Mn)Si a une structure

cubique avec un groupe d'espace Im3 et la phase δ-AlFeSi peut avoir deux structures, soit tétragonale soit orthorhombique. Cette dernière phase n'étant pas attendue à l'issue de la solidification d'alliages ternaires Al-Fe-Si, ces résultats suggèrent qu'elle est stabilisé au détriment de la phase β-Al_4FeSi.

[1] L. Ratke, S. Steinbach, G. Müller, M. Hainke, A. Roosz, Y. Fautrelle, M.D. Dupouy, G. Zimmermann, A. Weiss, J. Lacaze, R. Valdes, G-U. Grün, H-P. Nicolai, G. Gerke-Cantow. MICAST–Microstructure formation in casting of technical alloys under diffusive and magnetically controlled convective condition. Materials Science Forum Vol. 508 (February 2006). pp 131-144. Trans. Tech. Publications 2006, Switzerland.

[2] L. Ratke, S. Steinbach, G. Müller, M. Hainke, J. Friedrich, A. Roosz, Y. Fautrelle, M.D. Dupouy, G. Zimmermann, A. Weiss, J. Lacaze, R. Valdes, G-U. Grün, H-P. Nicolai, H. Gerke-Cantow. MICAST–The effect of magnetically controlled fluid flow on microstructure evolution in cast technical Al-alloys. Microgravity Sci. Tech. 2005; XVI: 99.

[3] L. Ratke, S. Steinbach, G. Müller, M. Hainke, A. Roosz, Y. Fautrelle, M.D. Dupouy, A. Ciobanas, G. Zimmermann, A. Weiss, J. Lacaze, R. Valdes, G-U. Grün, H-P. Nicolai, R. Gerke-Cantow. MICAST–Microstructure formation in Casting of technical alloys under diffusive and magnetically controlled convective conditions. Trans. Indian. Inst. Met. 2005; 58: 631.

[4] I. Ansara, A.T. Dinsdale, Rand MH. Thermochemical database for light metal alloys. 1998 July. European Commission and COST 507.

[5] Donnadieu P., Su H., Proult A., Harmelin M., Effenberg G., Aldinger F. From Modulated Phases to a quasiperiodic structure with a cubic point group and inflation symmetry. Journal de Physique I France 1996; 6: 1153.

[6] Donnadieu P, Harmelin M., Su H., Seifert H., Effenberg G., Aldinger F. A quasicrystal with Inflation Symmetry and no forbidden symmetry Axes in a rapidly solidified Mg-Al Alloy. Z. Metallkd 1997; 88: 33.

[7] Du Y., Schuster J.C., Weitzer F., Krendelsberger N., Huang B., Jin Zhanpeng., Gong Weiping., Yuan Zhaohui., Xu Honghui. A thermodynamic description of the Al-Mn-Si system over the entire composition and temperature ranges. Metallurgical and Materials Transaction A 2004; 35A: 1613.

[8] http://pro.wanadoo.fr/carine.crystallography/. CaRine v3.1.

[9] Villars P. Pearson's Handbook Desk Edition. ASM International 1997.

[10] Friel J. X-ray and image analysis in electron microscopy. Princeton Gamma-Tech 1995.

[11] http://www.gel.usherbrooke.ca/casino/. Casino "Monte Carlo Simulation of Electron Trajectory in Solids".

[12] N. Saunders., A.P. Miodownik. CALPHAD - Calculation of Phase Diagrams. A comprensive guide. Pergamon Materials Series. Series Editor: R.W. Cahn. 1998; Vol.1.

[13] Jansson A. A thermodynamic evaluation of the Al-Mn system. Metallurgical and Materials Transaction A 1992; 23A: 2953.

[14] Jansson A., Chart Tim. A thermochemical assessment of data for the al_rich corner of the al-fe-mn system, and a revision of data for the Al-Mn system. COST 507 1998; 1: 257.

[15] Godecke T., Koster W. (en allemand) Al-Mn. Z. Metallkd 1971; 62:727.

[16] Ellner M. The structure of the high-temperature phase MnAl(h) and the displacive transformation from MnAl(h) into Mn_5Al_8. Metallurgical Transactions A 1990; 21A: 1669.

[17] Liu X., Kainuma R., Ischida K. Thermodynamic assessment of the Al-Mn binary phase diagram. Journal of phase equilibria 1999; 20: 45.

[18] Liu X., Kainuma R., Ohtani H., Ischida K. Phase equilibria in the Mn-rich portion of the binary system Mn-Al. Journal of alloys and compounds 1996; 235: 256.

MICAST – Microstructure Formation in Casting of technical alloys under diffusive and magnetically controlled convective conditions

L. Ratke, S. Steinbach, G. Müller, M. Hainke, A. Roosz, Y. Fautrelle, M.D. Dupouy, A. Ciobanas, G. Zimmermann, A. Weiss, J. Lacaze, R. Valdés, G-U. Grün, H-P. Nicolai, R. Gerke-Cantow. MICAST–The effect of magnetically controlled fluid flow on microstructure evolution in cast technical Al-alloys. Microgravity Sci. Tech. 2005; XVI: 99.

MICAST – Microstructure Formation in Casting of technical alloys under diffusive and magnetically controlled convective conditions

L. Ratke, S. Steinbach[1], G. Müller[2], M. Hainke[2], A. Roosz[3], Y. Fautrelle, M.D. Dupouy[4], G. Zimmermann, A. Weiss[5], H.-J. Diepers[5], J. Lacaze[6], R. Valdes[6], G-U. Grün[7], H-P. Nicolai[8], H. Gerke-Cantow[8]

[1] Insititute of Space Simulation, DLR, Cologne, Germany, Lorenz.ratke@dlr.de

[2] Crystal Growth Laboratory, University of Erlangen, Erlangen, Germany,

[3] Department of Materials Science, University of Miskolc, Hungary

[4] EPM, Madylam, CNRS Grenoble

[5] ACCESS e.V., Aachen, Germany,

[6] Cirimat, Toulouse, France

[7] Hydro Aluminium Deutschland GmbH, Bonn, Germany

[8] Tital Feinguss GmbH, Bestwig, Germany

Keywords: solidification, microstructure, macro-segregation, magnetic fields, modeling, microgravity, AlSi-alloys

Abstract. The MICAST research program focuses on a systematic analysis of the effect of convection on the microstructure evolution in cast Al-alloys. The experiments of the MICAST team are carried out under well defined thermally and magnetically controlled, convective boundary conditions and analyzed using advanced diagnostics and theoretical modeling, involving phase field simulation, micro-modeling and global simulation of heat and mass transport. The MICAST team uses binary, ternary and technical alloys of the Al-Si family. This paper gives an overview on recent experimental results and theoretical modelling of the MICAST team.

Introduction

The MICAST research program, initiated in 1998 to utilize the International Space Station with industrial relevant topics in the field of material science, identified that a detailed knowledge and a quantitative theoretical description about the influence of the convective heat and mass transport on the microstructure formation and segregation in technical alloys is of high scientific and industrial importance. Although numerous paper have been published investigating the effect of fluid flow on e.g. dendrite formation, coarsening of secondary arms, precipitation of intermetallics, micro- and macro-segregation [1-5] and especially a large number of paper investigates experimentally the effect of magnetic fields (static, alternating, rotating) on the cast microstructure [6-8], it has to be said, that the understanding of fluid flow on the liquid to solid transformation is rather in its infancies. Research under microgravity conditions in the last decades has shed light on the importance of fluid flow and it became clear that even in best experimental set-ups used on earth residual flows can change the microstructure appreciably and thus does not allow a detailed quantitative comparison with theoretical predictions [9].

The MICAST research program therefore focuses on a systematic analysis of flow effects on microstructure. Questions are for example, how the intensity of convection and the direction of the flow acts on the evolution of the mushy zone, on macro- and micro-segregation, on the

morphology of dendrites, on the growth mode and spatial arrangement of intermetallic precipitates. The microstructure is characterized by the dendrite tip radius, the dendrite envelope, the primary dendrite stem spacing (PDAS), the secondary arm spacing (SDAS), the distribution and morphology of intermetallic phases, 3D topology of the mushy zone, the lamellae spacing of the interdendritic eutectic and the eutectic fraction. In order to simplify the complex interactions between heat and mass transport and the microstructure evolution, the experiments performed by the MICAST team are carried out under well defined thermal and magnetically controlled convective boundary conditions using directional solidification and advanced in-situ diagnostics and metallographic techniques. The experiments shall provide benchmark data to validate theoretical models. The theoretical modelling involves phase field simulation and micro-modelling as well as global simulation of the heat and mass transport and the magnetically induced fluid flow in the experimental set-ups used by the team. The MICAST project uses binary Al-x wt.%Si alloys (x=5 - 9), two pure ternary AlSi7Mg alloys (Mg=0.3,0.6 wt.%), this ternary enriched with Fe and Mn and the technical A357 alloy. The A357 alloy is a standard casting alloy used for example in automotive applications (cylinder heads, motor blocks).

Thermodynamic of AlSiMg base alloys

The focus of the project on this family of technically important foundry alloys led to the conclusion that precise knowledge and description of the Al-Mg-Si(-Mn-Fe) system is highly necessary. Although the ternary Al-Si-Mg system has been extensively investigated, ambiguities still remain at high magnesium contents. As a basis for further study, an attempt was thus achieved to clarify these uncertainties.

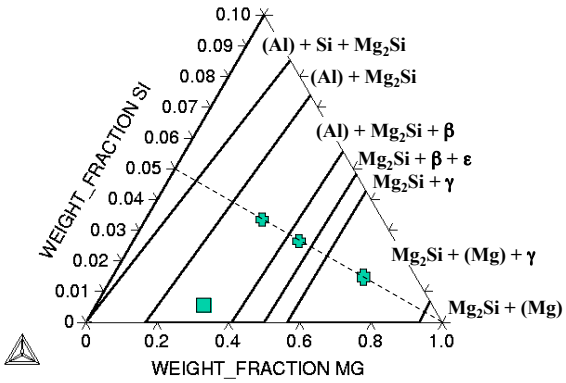

Figure 1 - Isothermal section of the Al-Mg-Si system at 300 °C.

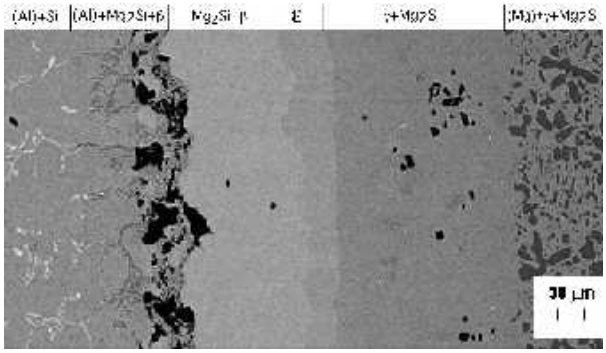

Figure 2 – SEM micrographs showing the junction part of the diffusion couple [10].

Fig. 1 shows an isothermal section of the Al-Mg-Si phase diagram calculated at 300 °C using the COST 507 data bank. The bold lines are limits between various domains, with the phases present indicated on the right side of the diagram. (Al) and (Mg) stand for the fcc and hcp solid solutions respectively rich in Al and Mg, while $Al_{30}Mg_{23}$-ε, Al_3Mg_2-β and $Al_{12}Mg_{17}$-γ designate compounds from the binary Al-Mg system. In this figure, the three alloy compositions shown with crosses were chosen along the interrupted line so that they are located in different three phase fields. A fourth alloy, much closer to the Al-Mg side, was also prepared for this study and is represented with a square in Fig. 1. Differential thermal analysis was performed on these four alloys and the composition of the phases of the as cast and DTA samples were then evaluated by EDX [10]. Also, a diffusion couple was prepared and maintained 7 months at 300 °C to give the composition of the phases in equilibrium in the Mg corner [10]. Using Thermocalc®, a new set

of ternary interaction parameters in the liquid phase of the Al-Mg-Si system was determined [11] which improves the liquidus description with respect to the COST 507 data bank. As no other parameter was modified, the description of the ternary system thus obtained maintains its highly efficiency for the solid-solid equilibria which was due in particular to an appropriate representation of the properties of the Mg_2Si phase [12].

Solidification Experiments

As outlined above, fluid flow is an essential parameter in the experimental investigations of the project. Therefore experiments were already performed under microgravity conditions (see below) to obtain a data base on microstructures as they are obtained under purely diffusive conditions. On the ground the experimental groups at Miskolc, Aachen and DLR developed facilities to directionally solidify alloys under the influence of rotating magnetic fields. Schematics of the two facilities used by DLR and ACCESS are shown in Figs. 3 and 4.

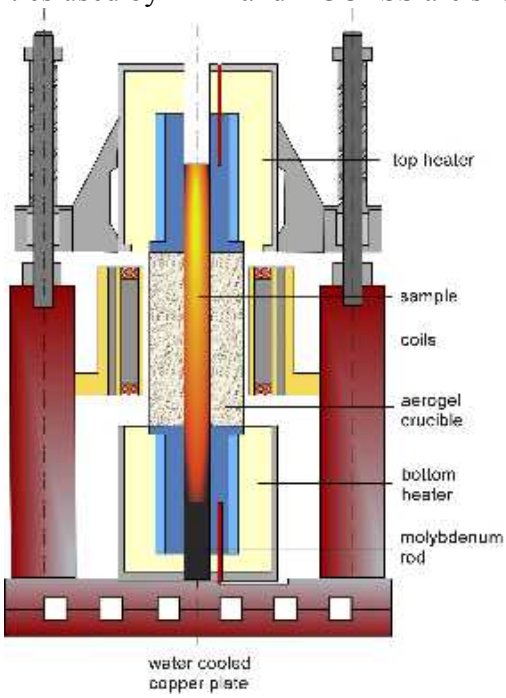

Figure 3 - DLR facility ARTEMIS 3 utilizes aerogels as a crucible and adiabatic zone material. Due to the extremely low thermal conductivity of aerogels the isotherms are planar. Due to the transparency of aerogels especially in the near infrared, the solidification can be observed optically. The facility is equipped with 3 pairs of Helmholtz coils, yielding magnetic fields up to 6 mT at a fixed frequency of 50 Hz [13-16].

At Miskolc university a conventional Bridgman furnace is equipped with the housing of an asynchronous motor allowing to vary the magnetic field strength up to values of 0.76 mT at two different frequencies, 100 and 250 Hz.

The fluid flow field induced by rotating or traveling magnetic fields as a function of the field strength and the frequency was analyzed theoretically by the groups in Erlangen (CGL) and Grenoble (Madylam).

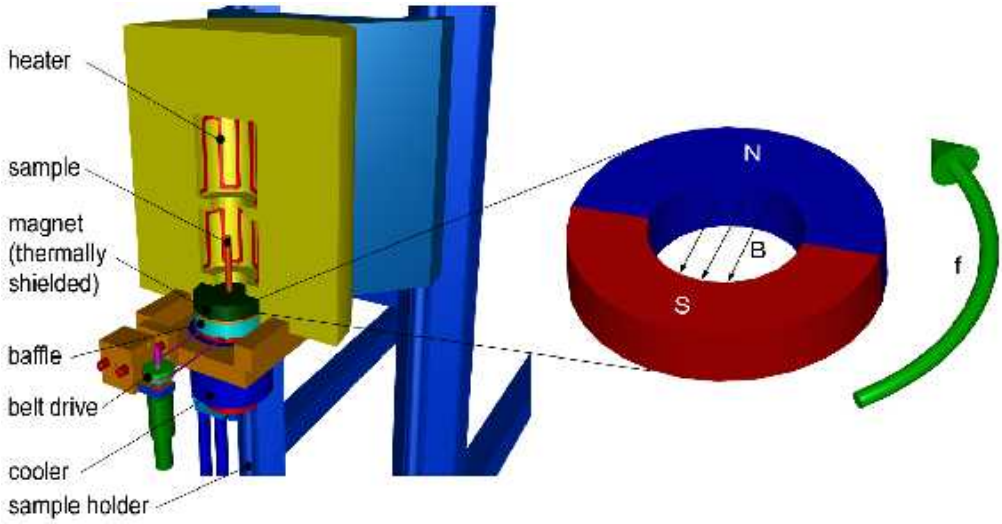

Figure 4 - The Bridgman-Stockbarger type facility at ACCESS uses a permanent magnet of constant magnetic induction of 25 mT. The ring magnet is integrated in the baffle region of the furnace and can be rotated from 0 to 3000 rpm. Thus, the RMF induces forced flow in the melt close to the growing solid-liquid interface..

The essential parameter describing the influence of an alternating magnetic field is the Taylor number defined as

$$Ta_m = \frac{B_0^2 R^4 \sigma \omega}{2\rho\nu^2 p} \qquad (1)$$

with B_0 the magnetic induction, R the sample radius, σ the electrical conductivity of the melt, ω the circular frequency, ρ the fluid density, ν the kinematic viscosity and p the number of poles (here 3).

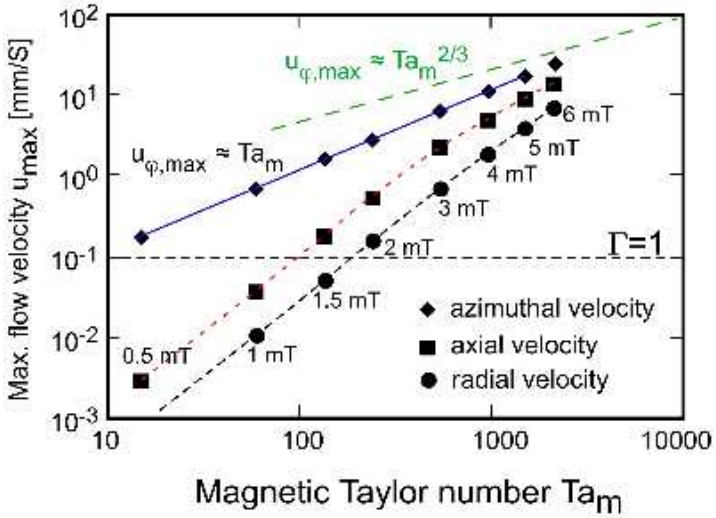

Figure 5 - Result of a numerical modeling of the maximum flow velocities induced by a rotating magnetic field in a cylindrical sample. For laminar flow the azimuthal velocity should be linear in the Taylor number. At very large Taylor numbers this velocity scale as $Ta^{2/3}$. The extrapolation of this analytical result to lower Taylor number is shown as the dashed curve.

The rotating magnetic field induces not only azimuthal flow, as is expected, but also a radial and axial flow (secondary flows) [5,17]. These cannot be neglected, since they become comparable to the azimuthal flow at larger Taylor numbers. A result of a numerical calculation of the flow

velocities in an AlSi melt is shown in Fig.5. At 6mT the flow velocities are around a 1cm/s, whereas at 3 mT they are a factor of ten smaller.

The large magnetic induction of 25 mT used in the ACCESS facility (see Fig. 4) could lead to a flow being probably time dependent or at the onset to a transition to turbulence. This will be analyzed in detail in the future, when thermal and magnetic models of all experimental facilities are developed by CGL and Madylam.

From the larger number of experimental results obtained so far we present only a few ones exemplarily. The influence of rotating magnetic fields (RMF) was measured on the primary dendrite stem spacing (PDAS) in directionally solidified A357 alloys and lead to the result shown in Fig. 6. There the PDAS is shown as a function of solidification velocity for a situation without a RMF and for two different magnetic field strengths. With increasing magnetic field (at fixed frequency of 50Hz) the PDAS decreases. This result was confirmed by experiments performed with the ACCESS facility. The result is shown in Fig.7 confirming the larger the frequency the smaller the primary dendrite spacing.

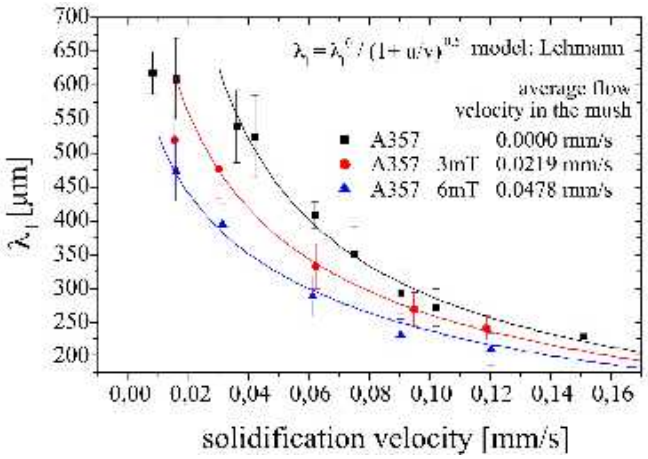

Figure 6 - PDAS in A357 as dependent on solidification velocity. Shown are three curves for different magnetic field strengths of the RMF leading to different flow velocities (see Fig.5). The drawn in curves are a fit with the Hunt and Lu theory [19] modified by the Lehmann []18 criterion (see eq.(2)).

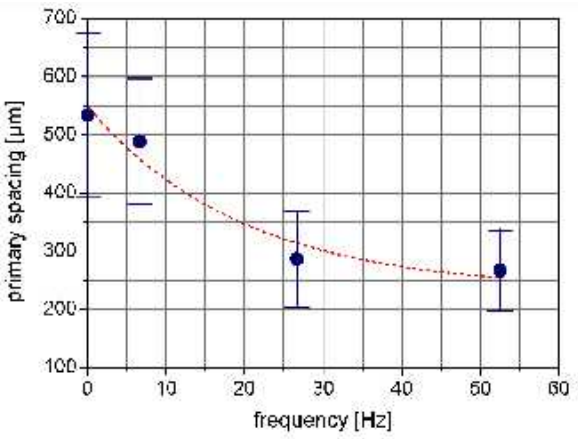

Figure 7 - Primary spacing determined from decanted AlSi samples directional solidified with $G = 10^4$K/m and $v = 4.2\ 10^{-6}$ m/s as a function of different rotational frequencies of the permanent ring magnet.

Both observations are in agreement with an order of magnitude analysis of Lehmann [18]. He showed that the primary spacing with a fluid flow of velocity U at a given solidification velocity v should lead to a reduction in spacing given by a simple relation

$$\lambda_1^{RMF} = \frac{\lambda_1^0}{\sqrt{1+\frac{U}{v}}} = \frac{\lambda_1^0}{\sqrt{1+\Gamma}} \qquad (2)$$

With increasing U the spacing is reduced. Fitting the primary spacing λ_1 without RMF to the theory of Hunt and Lu [19], which works out perfectly, and then applying the expression of eq.(2) to the experimental data of Fig. 6 leads to a perfect agreement and allows to determine the effective flow velocity inside the mush. Such an analysis shows that the real flow velocities in the mushy zone are much smaller than those calculated in the volume (Fig.5). Fluid flow changes also the secondary arm spacing significantly. This will be shown later in the context of micro-modeling and at the end in comparison with microgravity results.

A detailed analysis of possible flow effects on dendrite tips and mushy zone lengths was performed at ACCESS. They developed a special decanting device that allowed to throw off

rapidly the melt from a partially solidified sample by centrifugal forces. If the melt is removed sufficiently fast from the mush, the geometry of the mush and the dendrite tips can be analysed in 3D. Two examples of dendrite tips without and with a rotating magnetic field are shown in Figs. 8a,b. From a careful analysis of the dendrite tip shape (rotating several dendrite tips in the SEM and looking from various sides to them) it could be concluded that within the measurement error the tip radius is not changed by fluid flow.

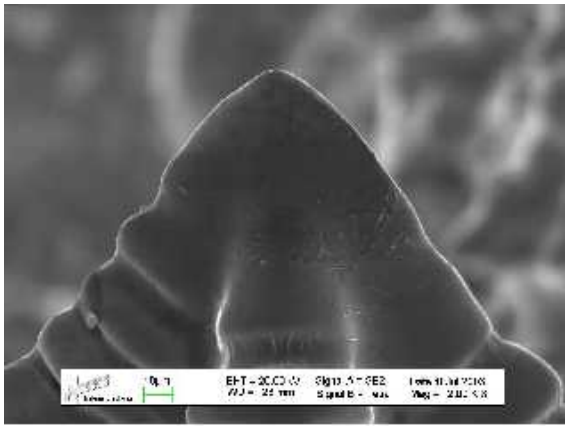

Figure 8a - Tip of a dendrite taken with SEM from a decanted AlSi7 sample, directional solidified without RMF.

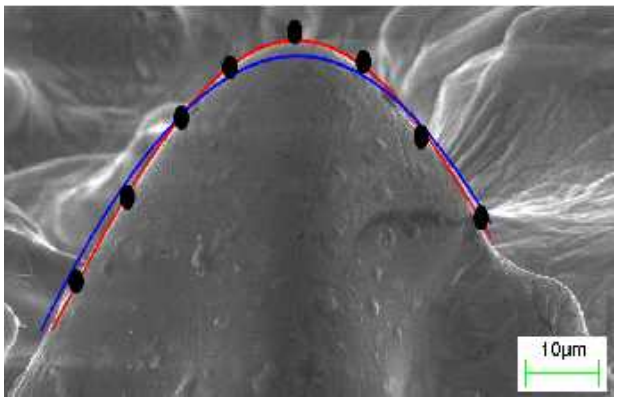

Figure 8b - Tip of a dendrite taken from a decanted sample, which is directionally solidified with a RMF of 50 Hz. The tip contour has been fitted by using different polynomial functions..

The mushy zone length is, however, affected. It decreases with increasing fluid flow, since the fluid flow induces a macro-segregation (see below) and any change in the local concentration changes the solidification interval and thus at a given temperature gradient the length of the mushy zone.

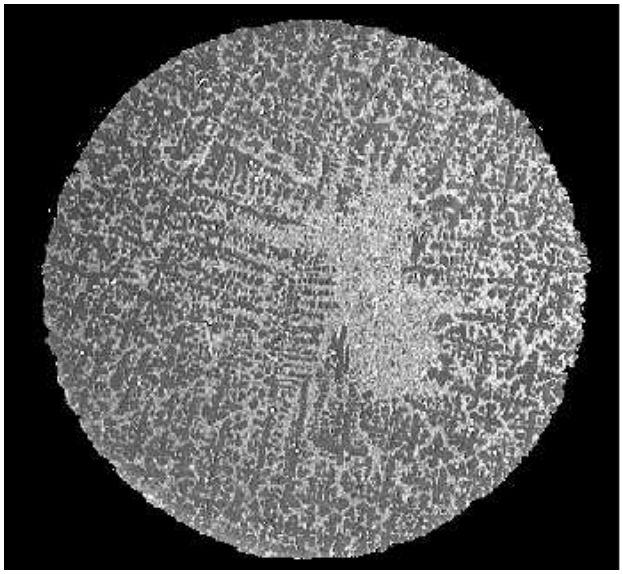

Figure 9 - Cross section through an A357 sample solidified with RMF at 6 mT. Slightly of center is an area free of dendrite. This zone exhibits a eutectic microstructure only.

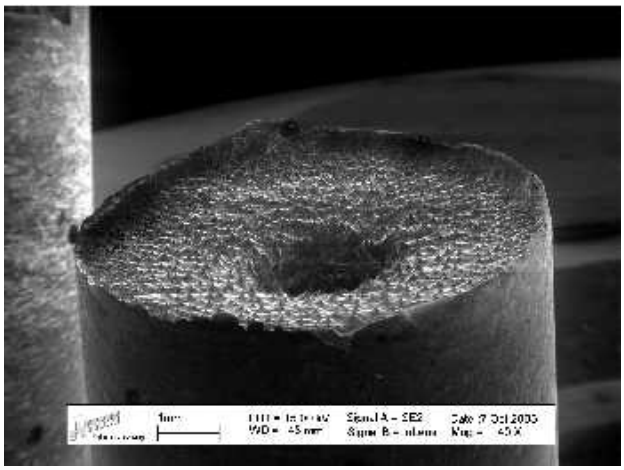

Figure 10 - Solid-liquid interface of a decanted AlSi7Mg0.6 sample solidified with a RMF of 50 Hz showing a deep depression in the center part

An unexpected effect of RMFs on AlSiMg alloys, is the macro-segregation observed. Usually these alloys are not prone to segregation, since the density differences between the components are rather small. Both groups at ACCESS and DLR, however, observed strong segregation (Figs. 9,10), which was predicted by the macro-models at CGL. The cross section through an A357 alloy (Fig. 9) shows close to the center a region with no primary dendrites, but a pure AlSi eutectic. The decanted sample in Fig. 10 shows that there is a channel in the center, where obviously the liquidus temperature was lower than closer to the sample surface (for a more detailed discussion see below).

Numerical Modeling

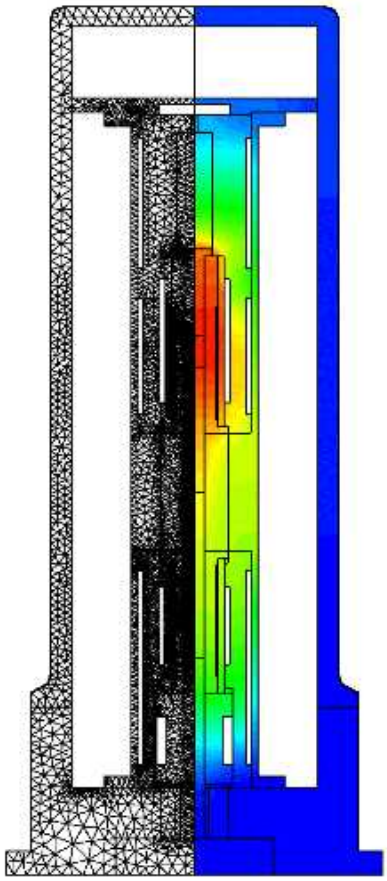

Figure 11 - Thermal model of the ARTEX facility as implemented in CrysVUn.

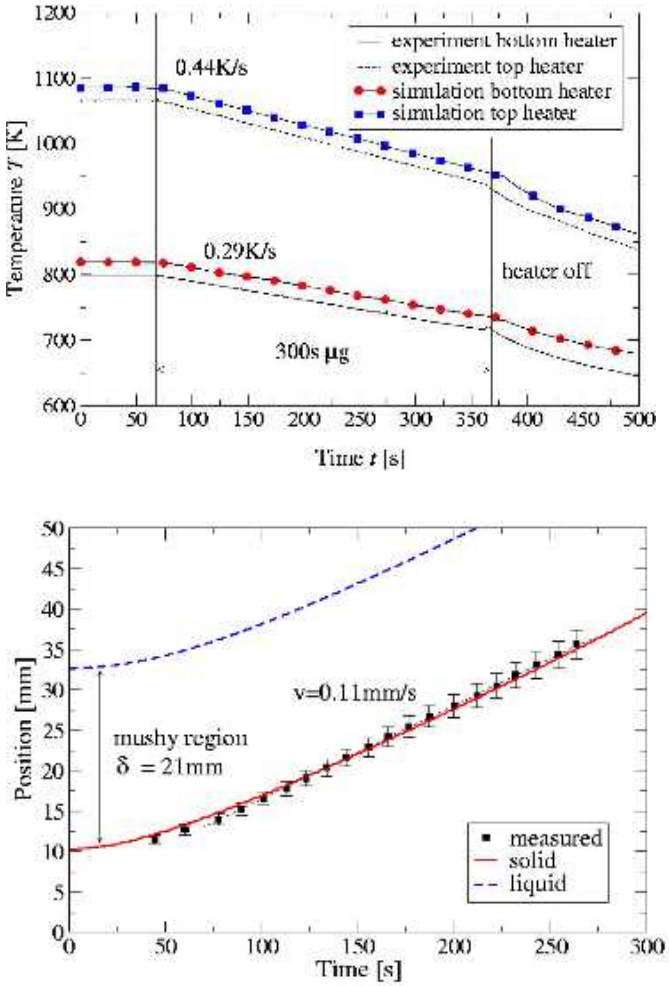

Figure 12 - Temperature profiles for the both heating elements (top) and the resulting solidification process (bottom).

Global Modeling. The global modeling performed by CGL with the software package CrysVUn [17] has the objective to support the design and optimization of the experimental facilities used in the laboratory and under microgravity conditions. The goal is to define process parameters, select proper construction materials and to provide inputs, i.e., boundary conditions, for micro-modeling and phase field simulations. Therefore, global thermal models are developed for all facilities as used in the project and systematically verified by experiments. As an example Fig.11 shows the set-up of the model of the ARTEX facility used on sounding rockets to study the solidification of AlSi alloys under microgravity. The model is based on the CAD drawing of the

furnace, the materials parameters and the thermophysical properties of AlSi6 [20]. The ARTEX facility is based on the aerogel furnace concept of ARTEMIS adapted to the sounding rocket program TEXUS [21]. It consists of two heaters, controlled independently by PID controllers and separated by a cylindrical piece of aerogel. The sample is fixed in a cylindrical hole in the center of the aerogel. Controlling the heaters allows to directionally solidify the sample from the bottom to the top with a planar solidification front, due to the small radial heat fluxes. The alloy used in TEXUS 39 (2002) was a binary AlSi6 alloy. It was solidified with a velocity of 0.13 mm/s within the 6 min. of microgravity TEXUS offers. The temperature gradient was 3 K/mm. The experimentally used temperature profiles for the top and the bottom heater severed as the input parameters for the thermal model of ARTEX. The computed position of the eutectic isotherm and the tip of the mushy zone are compared to experimental measurements in Fig. 12 (bottom). It clearly demonstrates that the model predictions agree nicely with the experimental observation of the position of the eutectic solidification front. The only fit parameter was a shift of the heater temperatures of 20K in order to match the initial position of the solidification front. This may be attributed to thermal contact resistances, e.g., between the Molybdenum cooling rod and the sample, which are not included in the model [17, 20].

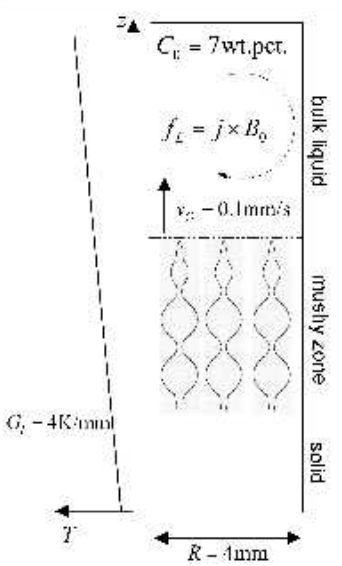

Figure 13 - Schematic overview of the modeling set-up used to analyze the segregation in AlSi-based alloys by CGL.

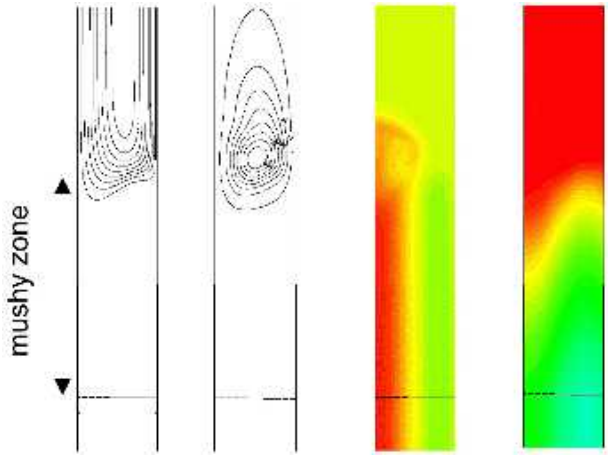

Figure 14 - Interaction of a RMF driven flow with the mushy zone. Shown are (from left to right): isolines of the azimuthal velocity, streamlines in the meridional plane, the mixture concentration and the liquid volume fraction (the axis of symmetry is in each case on the left side).

Macro-segregation modeling. Numerical modeling is performed at CGL and Madylam to investigate the effect of rotating magnetic fields (RMFs) on the Si distribution, i.e., on the resulting macro-segregation. A sketch of the considered problem is shown in Fig. 13. The RMFs are mainly interacting with the bulk liquid, creating a forced flow primarily in the azimuthal direction. Numerical simulations showed that the bulk flow velocities reach up to several cm/s even in such small scale samples [5,17]. Ahead of the solidification front a pressure drop is created, leading to secondary flows, which may create macro-segregation. For the considered alloy and configuration natural convection is negligible in a first approximation. Therefore, the strength of the interdendritic convection (expressed by the coefficient Γ (see eq.(2)) can be mainly attributed to the strength of the magnetic field and the permeability of the mushy zone.

For RMF the magnetic field strength is usually characterized by the magnetic Taylor number Ta_m (eq. (1)). The resistance of the mushy zone on the flow may be expressed in terms of the Darcy number Da, defined as $Da=K/L^2$. Here, K denotes a representative value of the permeability and L a characteristic length scale of the problem. The permeability is a complex function of the mushy zone morphology and several models are available in the literature. The presented results were obtained with the application of the well known Karman-Kozeny equation. The calculations have been performed for an alloy with the nominal composition of Al-7wt.Si, a solidification velocity of 0.1 mm/s a sample radius of 4mm, a height of 100 mm, a temperature gradient of 4 K/mm and RMF with 50 Hz and the magnetic induction varying from 1 – 6 mT. A typical result obtained in the calculations is shown in Fig. 14. As can be seen, the swirl flow in the bulk liquid induces a fluid motion inside the mushy zone. The upward directed interdendritic flow transports solutally enriched liquid out of the two phase region at the axis of the sample. The value of the mixture concentration is increased at the axis of the sample and in consequence a liquid channel is developing inside the mushy zone [5, 17]. The result is in qualitative agreement with the observation made by DLR and ACCESS, shown in Figs. 9 and 10. Future work is devoted to obtain a quantitative agreement. In any case, it is interesting to note, that the bulk flow only enters the mushy zone at the tip of the dendrites.

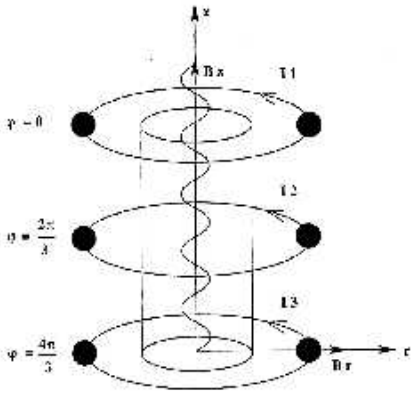

Figure 15 - Scheme of the coil and current arrangement to induce traveling magnetic fields

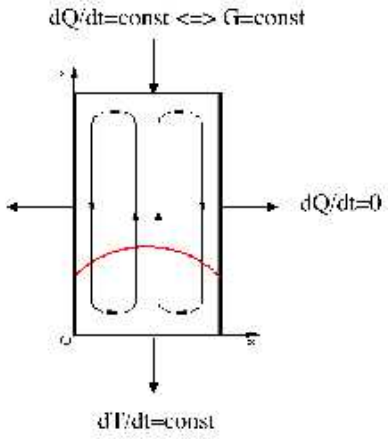

Figure 16 - Cylindrical cavity with boundary conditions used by Madylam to calculate macro-segregation.

Another investigated magnetic field configuration are so-called traveling magnetic fields (TMFs). One way to realize experimentally a TMF is illustrated in Fig.15. Three circular coils are fed from an alternating current (AC) voltage source, with a phase shift of $2\pi/3$ between the coils. The resulting field is a superposition of the magnetic field created by each coil, traveling either in upward or downward direction. The resulting average axial Lorentz force density may be written as

$$\left\langle f_z \right\rangle = \frac{\sigma\omega}{2}\frac{B_0^2}{a} I_1^2(ar) \quad (3)$$

whereby I_1 is the Bessel function of the first order and a being the wave vector. Assuming a cylindrical cavity as shown in Fig.16 with the boundary conditions given there, the group at Madylam calculated the macro-segregation in AlSi samples. Figure 17 shows a result of such a calculation for an AlSi7 alloy with a gradient of 10 K/mm at the top and a cooling rate of 0.2 K/s at the bottom. As in the case of the RMF, an enrichment of Si is found in the center of the sample. Nevertheless, for this field configuration, the traveling direction of the magnetic field is

an additional process parameter. By changing the traveling direction from downward to upward, a Si enrichment at the outer wall of the sample is resulting [22-25].

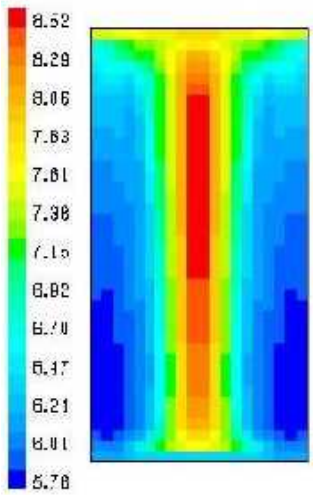

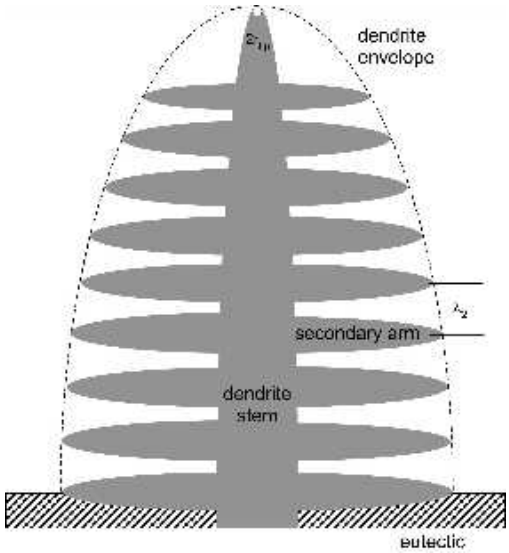

Figure 17 - Macro-segregation of Si in AlSi7 using traveling magnetic fields with a downward direction

Figure 18 - Scheme of a model dendrite explaining used for the micro-modeling.

Micro-Modeling. The prediction of microstructure evolution does not only need a macro-simulation which uses average quantities, but also requires a model that is able to calculate the experimentally observable features, like PDAS; SDAS, eutectic fraction. The model developed by the group in Miskolc uses the binary and ternary phase diagrams, especially the temperature and concentration dependent partition coefficient. It starts by calculating the dendrite tip radius and the tip undercooling using the Kurz, Giovanola, Trivedi model. With this information and for the given temperature gradient the primary dendrite stem is calculated and its envelope, assuming that it can be approximated as a paraboloid of revolution. The SDAS is calculated using the well known equation of diffusive coarsening of secondary arms, that can be described by

$$(4)\quad \lambda_2^3 = \lambda_{2,0}^3 - \int_0^t BM(c_0, T(t))dt$$

with λ_2 the SDAS and M a complex function defined by

$$(5)\quad M(c_0, T) = \frac{D_L(c_0, T)T\sigma(c_L)}{m_L(T)\left[1-k(T)\right]\Delta H(c_0, T(t))\rho(c_L)c_L(T)}$$

and B a geometric factor of the order unity (for details see [26-28]). A few results concerning the SDAS of the calculations are shown in Fig. 20. The SDAS along a directionally solidified sample as measured and calculated is shown in the two pictures in the upper row of Fig. 19 compared to the calculated SDAS. Taking the average SDAS in the samples for different alloy compositions and plotting the measured against the calculated one shows that there is a deviation between both (left picture in the bottom row of Fig. 19). Correcting the calculation by changing the constant B in eq.(4) allows to bring measurement into an agreement with the calculations (right picture in the bottom row of Fig. 19).

Phase field modeling. At ACCESS a phase field model is developed to simulate the microstructure inside the mush of AlSi-based alloys using the real thermodynamics of the alloy. 2D multi-dendrite arrangements are studied as well as 3D dendrite morphologies (see Fig. 20) and compared quantitatively with the results of the decanting experiments and the measurements

of the microstructure carried out by other groups. The conventional phase field model for solutal dendrites was improved to avoid solute trapping inside the growing dendrite [29-31]. With this improvement realistic 2D dendritic arrays have been modelled and the primary spacing was calculated that established after a suitably long growth time. The classical relationship between velocity and spacing was recovered as well as hysteretic effects or history effects have been studied. Thus the phase field model is now able to model the growth of AlSi dendritic arrays (see Fig. 21). Fluid flow was taken into account with a boundary layer model. Up to a diffusion distance D/v away from the dendrite tips the diffusion field is calculated exactly, outside the concentration is set constant everywhere. Performing then the phase field calculations with AlSi7 alloys for different boundary layer extensions showed that the tip radius is constant and not changed by the flow. This is in agreement with the experimental observations taken from the decanting experiments described above.

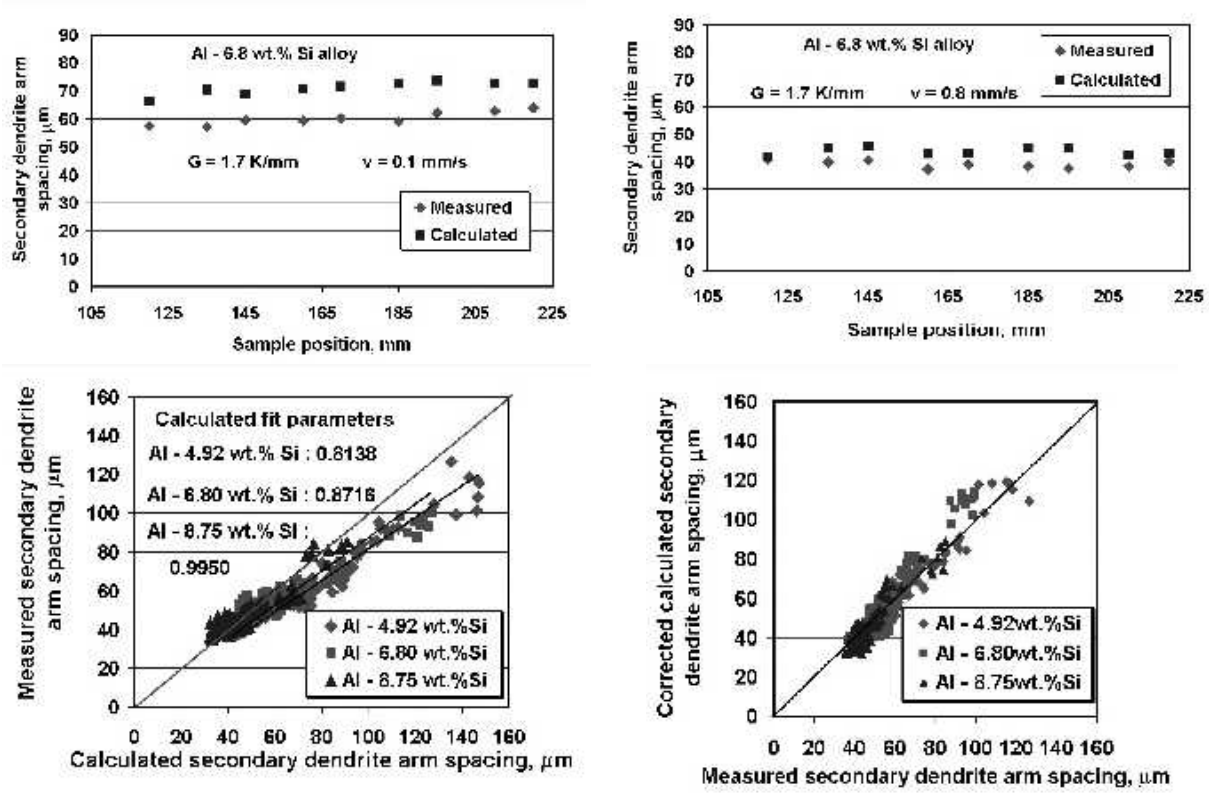

Figure 19 - The SDAS along a directionally solidified sample as measured and calculated is shown in the two figure in the upper row compared to calculated SDAS. Taking the average SDAS in the samples for different alloy compositions and plotting the measured against the calculated one shows that there is a deviation between both. Correcting the calculation by changing the constant B in eq.(4) allows to bring measurement with calculation into an agreement.

Microgravity experiments

The MICAST project performed in 2002 a microgravity experiment in the TEXUS sounding rocket program (TEXUS 39). In the experiment we used an Al-6wt.% Si alloy. The solidification speed was 0.13 mm/s and the gradient 3 K/mm. The experiment performed as planned using the ARTEX facility described above. The microscopic analysis of the sample showed a larger primary stem spacing than the ground based sample, a reduced SADS and a smaller eutectic spacing [32]. Comparing the microgravity result, the laboratory results with and without RMF shows a remarkable difference in SDAS such that one might guess, what the result of the

TEXUS 41 experiment, to be performed in November 2004 (microgravity + RMF) will be. The experimental findings obtained so far are shown in Fig. 22.

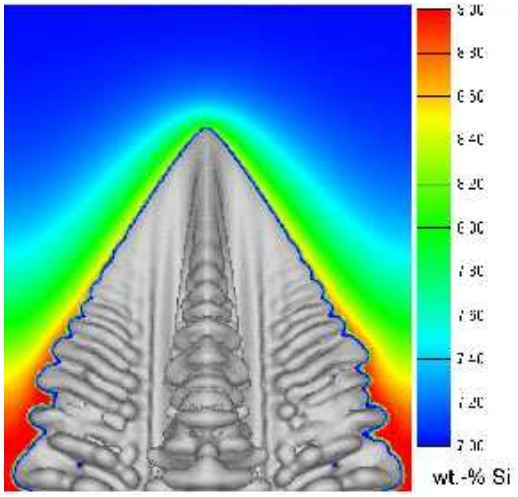

Figure 20 – 3D AlSi7 dendrite simulated by the improved PFM model at ACCESS. The colored contours around the dendrite tip visualize the Si solute content.

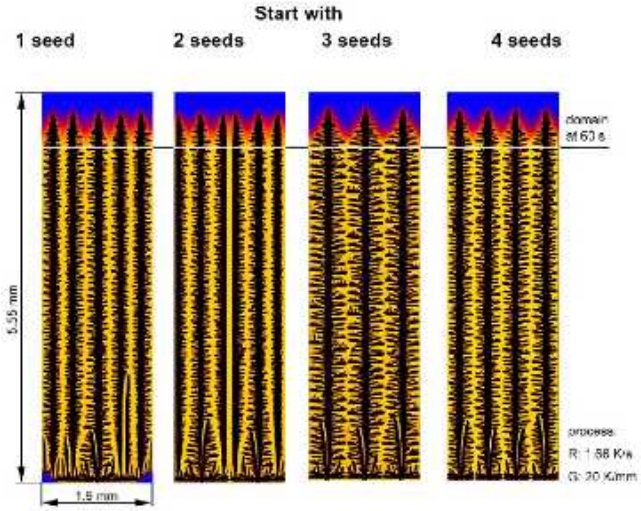

Figure 21 - Phase field modeling of the directional solidification of an AlSi7 alloy showing the selection mechanism in an array of dendrites in 2D. The numerical results are compared with the experiments using the decanting technique at ACCESS and the microstructure features determined in the project..

It is interesting to note that the SDAS depends on local solidification time with a power being greater than 1/3, in contrary to the expectation from eq.(4). Evaluating eq.(4) with the time dependent temperature profile and concentration dependent partitition coefficients the real exponent will be smaller than 1/3. Observing one which is larger points to the effect of fluid flow. Ratke and Thieringer [33] and Diepers and Beckermann [34] showed that fluid flow changes the exponent to 1/2 asymptotically. In reality the exponent will be smaller in agreement with the observation. Interesting in this respect is, however, that a larger exponent than 1/3 is observed although there was no RMF applied (with RMF the group at DLR observed values for the exponent around 0.48). Numerical simulation of the ARTEX facility, described briefly above, shows that there are only minor residual convections originating mainly from radial temperature gradients at those regions where the sample leaves the aerogel and enters the furnaces. The flow velocities were estimated to be in the range of 10 to 100 µm/s. The result in Fig. 23 suggests that these small flow velocities are sufficient to change the SDAS compared to an environment, which definitively is convection free. This result points to a possible pitfall of laboratory experiments: there seems to be no sufficient control on the fluid flow within laboratory facilities for directional solidification and thus a comparison of the results with theoretical predictions seems to be difficult and not free enough from fit parameters.

The results of the TEXUS 39 and 41 experiments will be improved with two experiments on MAXUS 7 (spring 2006) and a Polyzon experiment in fall 2006 (FOTON capsule). An experiment series in the MSL of the ISS will be needed to clarify if the observations made on TEXUS 39 are accidental. With the series of experiments we intend to replace the few data points in fig. 23 by a number of points to which a theory can be fitted.

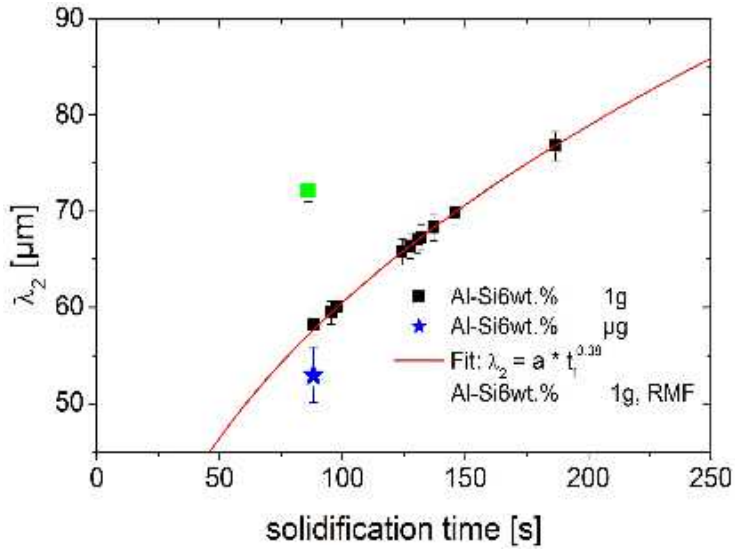

Figure 22 – SDAS in AlSi6 as measured in the laboratory (black squares), in TEXUS 39 (blue star) and in the laboratory using the same solidification conditions with a RMF of 6mT (grey square).

Acknowledgements: The MICAST team gratefully acknowledges financial support by ESA under contract No. 14347/00/NL/SH, DLR (contract Nos. 50WM0042 & 50WM0043), CNES and the Hungarian Space Office within the ESA-MAP project MICAST AO-99-031).

References

[1] C. Beckermann: Int. Mat. Rev. 47 (2002) 243
[2] W.Kurz, D. J. Fisher, *Fundamentals of Solidification*, TransTechPubl, Ackermannsdorf, 1989
[3] M.C. Flemings, G.E.Nereop, Trans. AIME, 239 (1967) 1449.
[4] P.A. Davidson, F. Boysan, Appl. Sci. Res., 44 (1987) p. 241
[5] M. Hainke, J. Friedrich, G. Müller, J. Mat. Sci., 39 (2004). 2011
[6] N. Govindaraju, B.Q. Li, Energy Conv. Management: 43 (2002) 335 –344; B.Q.Li, JOMe 50 (1998): www.tms.org/pubs/journals/9802/Li/Li-9802.html
[7] W.D. Griffiths, D.G. McCartney, Mat.Sci.Eng. A 216 (1996) 47 –60; P.A. Davidson Ann.Review Fluid Mech. 31 (1999) 273 - 300
[8] R. Sampath, N. Zabaras, J. Comp. Phys. 168 (2001) 384 – 411; K. Moeinipour, K.Eigenfeld, Giessereiforschung 50 (2004) 103 - 109
[9] M.E. Glicksman, M.B. Koss, L.T. Bushnell, J.C: LaCombe, E. A. Winsa, in: Materials and Fluids under Low Gravity, Lecture Notes in Physics, Eds. L. Ratke, H. Walter, B. Feuerbacher, Springer Verlag, Heidelberg, 1996, pp.63 - 75
[10] "Thermochemical database for light metal alloys", ed. I. Ansara, European Commission, 1995
[11]] J. Lacaze , R. Valdes, communication at the TOFA meeting, Vienna, 2004
[12]] H. Feufel, T. Gödecke, H.L. Lukas, F. Sommer, J. Alloys and Compounds, 247 (1997) 31-42
[13] J.Alkemper, PhD-thesis, RWTH Aachen 1996
[14] J.Alkemper, S.Sous, C.Stöcker, L.Ratke, *J.Cryst.Growth 191* (1998) 252-260
[15] J. Alkemper, L. Ratke, S. Sous, in Proc. 4th Decennial Conf. 'Solidification Processing Sheffield, Ed. J. Beech, H. Jones, Sheffield University, 1997, pp. 463-467.
[16] S. Sous, PhD-thesis, RWTH Aachen 1999

[17] M. Hainke, *Computation of convection and alloy solidification with the software package CrysVUn*. PhD-Thesis, Tech. Fac. Erlangen-Nuremberg (2004).
[18] P. Lehmann, R. Moreau, D. Camel, R. Bolcato, *Journal of Crystal Growth,* 183 (1998)690-704
[19] J.D. Hunt, S.Z. Lu, Met. Mat. Trans. 27A (1996). 611
[20] J. Friedrich, J. Dagner, M. Hainke, G. Müller, Crys. Res. Technol., 38, no. 7-9, (2003) p. 726
[21] S. Ahrweiler, A. Diefenbach, G. Mathiak, H.D. Masslow, L. Ratke, ESA SP-454, 1st Int. Symp. Micro. Grav. Res. & Appl. Phys. Sci., p. 979 (2000).
[22] M. Hainke, J. Dagner, J. Friedrich, G Müller, Microgravity Sci. & Tech. J., accepted.
[23] J. Dagner, M. Hainke, J. Friedrich, G Müller, in: 4th Int. Conf. On Electromagnetic Processing of Materials, EPM2003, 2003.
[24] X. Wang, A. Ciobanas, Y. Fautrelle, this conference
[25] A. Ciobanas, Y. Fautrelle, this conference
[26] I.Kuti, A. Roosz, Mat. Sci. Forum Vol. 329-330 (2000) 49 - 56
[27] I.Kuti, A. Roosz, Mat. Sci. Forum Vol. 215-216 (1996) 169 - 178
[28] A. Roósz, J. Kovács this confeence
[29] H.-J. Diepers, A. Karma: Globular-Dendritic Transition in Equiaxed Alloy Solidification. Solidification Processes and Microstructures: A Symposium in Honor of Prof. W. Kurz, ed. by M. Rappaz (et al.), Warrendale : TMS, 2004, p. 369-371.
[30] J. C. Ramirez, C. Beckermann, A. Karma, H.-J. Diepers: Physical Review E 69 (2004), 051607.
[31] H.-J. Diepers: Simulation des Primärabstandes gerichtet erstarrter Dendriten mit der Phasenfeldmethode, Aachen : Shaker, 2003 (Gießerei-Institut: Forschung, Entwicklung, Ergebnisse ; Bd. 38, Diss.).
[32] S. Ahrweiler, L. Ratke. H.D. Masslow, in: Proceedings of the 16th Symposium on European Rocket and Balloon Programmes and Related, Research, 2 - 5 June 2003, St. Gallen, Switzerland ESA Publications Division ESTEC, Nordwijk, Netherlands, Editor: Barbara Warmbein, ESA SP-530, pp. 107-112
[33] L.Ratke, W. Thieringer, *Acta metal.,* **1985**, *33*, 1793-1802
[34] C. Diepers, C. Beckermann, I.Steinbach *Acta Mat.* **1999**, *47*, 3663 – 3678

X-ray characterization of Al-Mg-Si alloys

Complément II

II.1 X-ray characterization.

X-ray analysis (XRD) of the four alloys was usually performed with a Seifert 2000 apparatus equipped with a Cu cathode ($\lambda_{K\alpha}$=1.540598 Å) and operated at 40 kV and 30 mA. Samples of 10x18x2 mm^3 were cut out from the as-cast material. Diffractograms were recorded in θ-2θ conditions with 2.θ varying in between 20 and 80° at a scanning rate of 0.04 °.min^{-1}. Additional experiments were however performed on crushed material and with a Co-K_α cathode. Indexing of the different XRD patterns were made with the program CaRine v 3.1 [1] according to the information of Pearson's Handbook [2].

CaRine v 3.1 is a program which can be used to create a phase structure defined from literature data, i.e. space group and lattice parameters. XRD patterns are then calculated and possibly compared to experimental ones. The Figure II-1 shows the structure of the Al_3Mg_2-β phase using phase type and atoms position according to Pearson's handbook [2]. The calculated diffraction diagram with the most intense diffraction peaks indicated is shown in Figure II-2a. It has been checked that the origin and position of the atoms (the cell contains about 1227.84 atoms) agree with international tables [3]. It is interesting to compare the diffraction diagram shown in Figure II-2a to the one published by Donnadieu et al. [4] and presented in figure II-2b. Both patterns correspond with the stable β phase and both can be completely identified referring to Pearson's handbook [2].

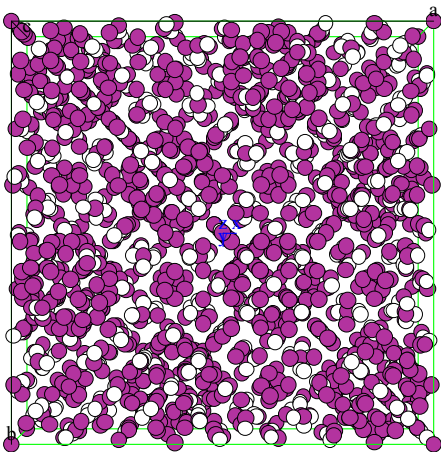

Figure II-1: Cell structure of the Al_3Mg_2-β phase as calculated using Carine. The purple circles correspond to aluminium atoms and the white circles to the magnesium.

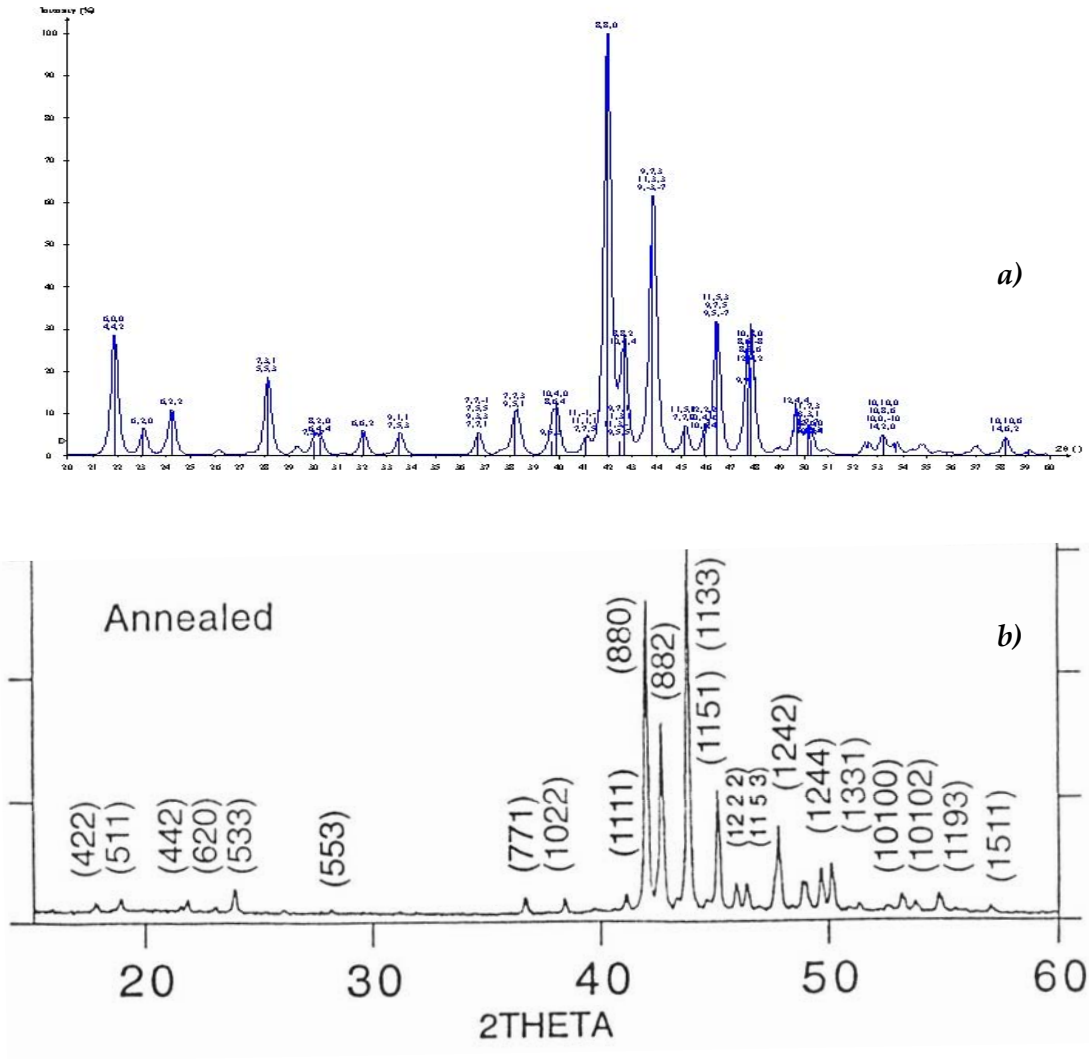

Figure II-2: XRD pattern of a) β phase and b) alloy Mg-61.0 at. % Al annealed at 400°C [4].

The experimental X-ray diffraction diagrams of alloys A30 and D30 in the as-cast state are shown in Figure II-3. The lines may be indexed by accounting for (Al), β and Mg_2Si phases. However, it is seen that the diffraction diagram of the D30 alloy presents much less lines than the other one. As a matter of fact, most of the peaks related to the Mg_2Si phase did not show up in agreement with the fact that the amount of this phase is quite low in this alloy (see the corresponding micrograph in Figure I-3b). In both diagrams, the peaks corresponding to the (Al) phase could be indexed with a = 4.122 Å. This value agrees with data by Schoenitz and Fischer [5] who reported that the peaks of the (Al) phase shift to lower angles with increasing Mg concentration.

By comparison with the X-ray diffraction pattern of the stable β phase [4] and with the one calculated with the software CaRine v 3.1, we can observe in the experimental pattern that the β phase is present in both alloys. However, it is noticed in the experimental pattern of alloy A30 that the peak corresponding to the family of planes (8,8,2), i.e. to an angle $2\Theta = 36.58°$, is lacking. This diffraction pattern should be recorded again.

For A45 alloy, it was necessary to crush the material and to make the experiment with CoKα radiation (λ = 1.7889nm). The experimental diagram is show in the Figure II-4. All lines of the XRD pattern can be indexed according to the γ and Mg_2Si phases. The X-ray diffraction pattern of the γ phase can be compared with the ones shown in Figure II-5 for rapidly solidified Mg-Al alloys with various Al contents [6]. It is seen that most of the peaks are similar, but the one at $2\theta \approx 43.0$ ° which is not observed in Figure II-4 while it is expected from Figure II-5 as the composition of the phase is about 45 at. % Mg (55 at. % Al). This peaks relates to the splitting of the (330) peak as the γ phase becomes commensurate at decreasing Mg content.

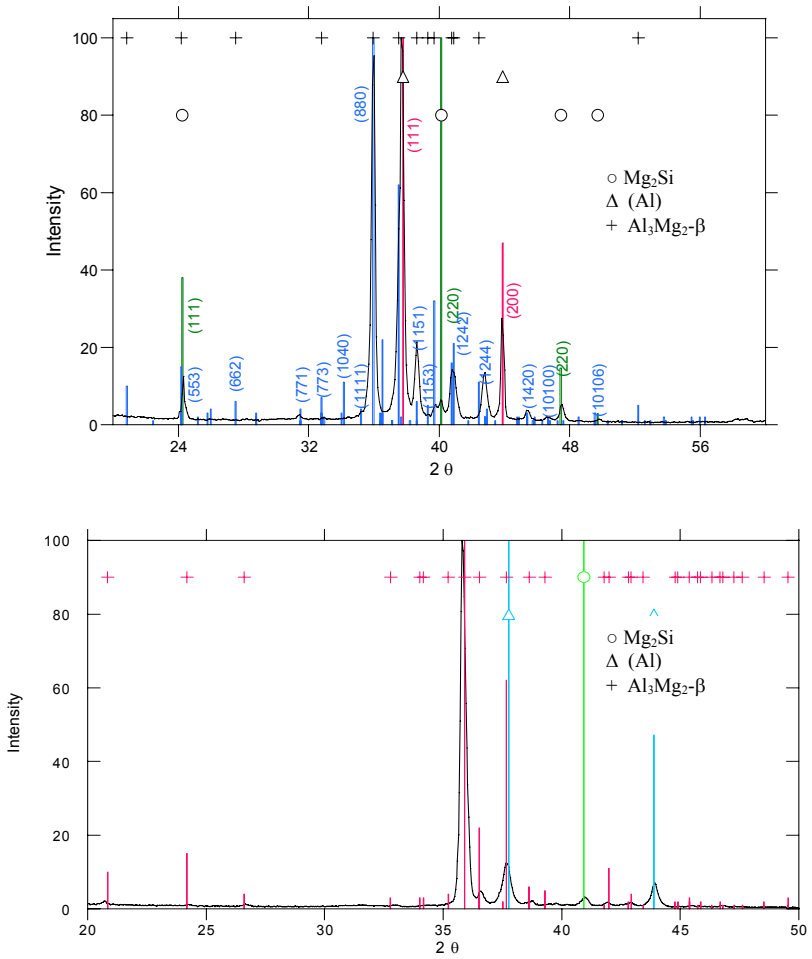

Figure II-3: X-ray diffractogram of the as-cast alloys A30 (above) and D30 (below) with the lines identified superimposed. Cu radiation.

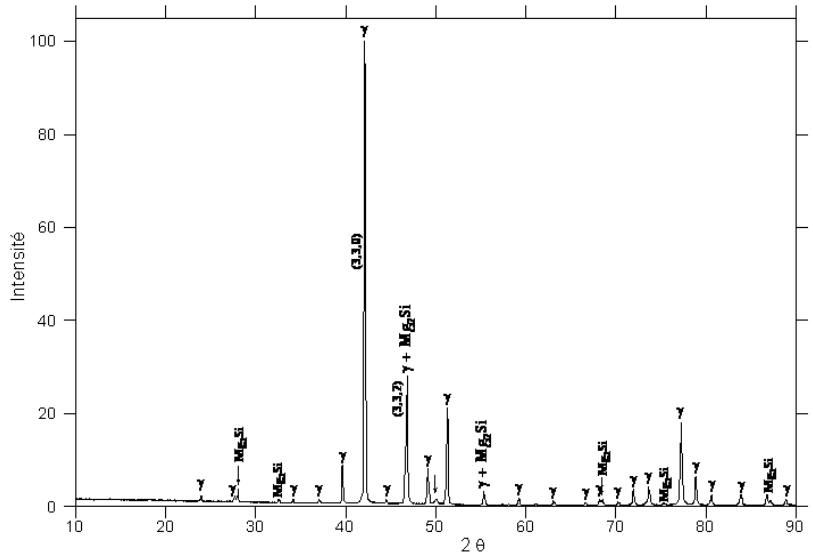

Figure II-4: X-ray diffractogram of alloy A45 with the lines identified superimposed. CoKα radiation

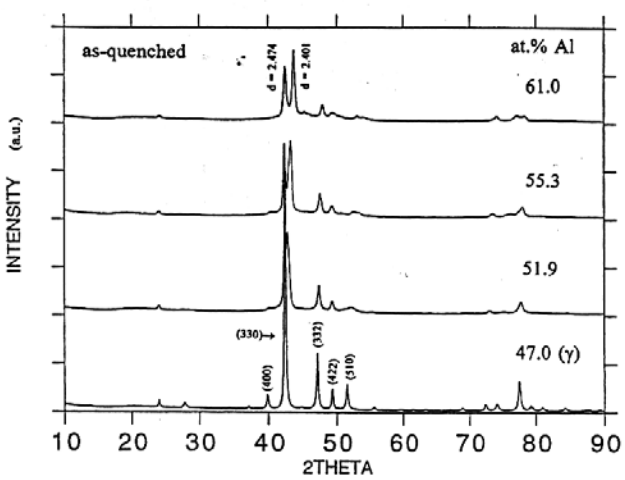

Figure II-5: X-ray diffractogram for rapidly cooled Mg-Al alloys containing 47, 51.9, 51.9, 55.3 and 61 at. % Al [6].

Figure II-6 shows the powder pattern of alloy A70, in which the peaks have been indexed according to Mg_2Si, (Mg) and γ data. The parameters used for (Mg), a=3.17 Å and c=5.2112 Å, were obtained from published experimental information on the effect of Al content on the hexagonal lattice [7]. The peaks corresponding to the γ phase were indexed with a=10.57 Å as before. There is an overall good agreement of these indexations with the experimental record. However, there is one peak which remains not indexed. The position of this peak (2θ=43.094 °) is much alike the one due to the splitting of the (330) peak of the γ phase mentioned above for low Mg content. The possibility that this splitting appears also at high Mg content should be investigated further, e.g. by looking at the effect of cooling rate.

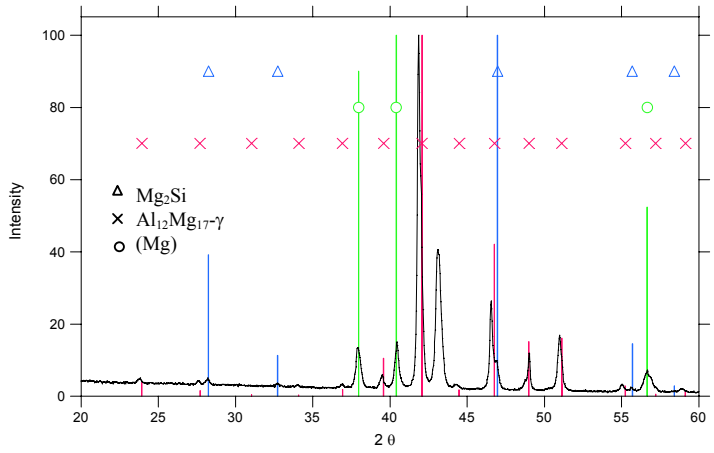

Figure II-6: X-ray diffractogram for as-cast A70 alloy.

[1] http://pro.wanadoo.fr/carine.crystallography/. CaRine v3.1.

[2] Villars P. Pearson's Handbook Desk Edition. ASM International 1997.

[3] "International Tables For X-Ray crystallography", The International Union of Crystallography, 1965

[4] Donnadieu P, Harmelin M., Su H., Seifert H., Effenberg G., Aldinger F. A quasicrystal with Inflation Symmetry and no forbidden symmetry Axes in a rapidly solidified Mg-Al Alloy. Z. Metallkd 1997;88:33.

[5] Schoenitz M., E D. Structure and properties of Al-Mg mechanical alloys. J. Mater Res., 2003;18:1827.

[6] Donnadieu P., Su H., Proult A., Harmelin M., Effenberg G., Aldinger F. From Modulated Phases to a quasiperiodic structure with a cubic point group and inflation symmetry. Journal de Physique I France 1996;6:1153.

[7] Luo H.L., Chao C.C., Duwez P. Metastable Solid Solutions in Aluminum-Magnesium alloys. Transtactions of the metallurgical society or aime 1964;230:1488.

Phase equilibria and solidification of Mg-rich Al-Mg-Si alloys

Valdés R., Freulon A.L., Deschamps J-B., Ma Quian., Lacaze J., Materials Science Forum Vol. 508. (February 2006) pp. 621-628.

Phase equilibria and solidification of Mg-rich Al-Mg-Si alloys

R. Valdes[1], A. Freulon[1], J.-B. Deschamps[1], Ma Qian[2], J. Lacaze[1]
1- CIRIMAT, UMR 5085, ENSIACET, 31077 Toulouse cedex 4, France
2- Brunel Centre for Advanced Solidification Technology, Brunel University, UB8 3PH, UK
Contact: jacques.lacaze@ensiacet.fr

Keywords: Al-Mg-Si alloys; Solidification; Phase equilibria; Differential thermal analysis

Abstract. The solidification and solid-state phase equilibria of four Al-Mg-Si alloys containing 30-70%Mg and 0.5-3.5%Si, selected on the basis of an isothermal section of the Al-Mg-Si system calculated at 300 °C, have been investigated. Solidification paths of Mg-rich Al-Mg-Si alloys finish on ternary eutectics and the temperatures of two of these eutectic reactions, i.e. L↔(Al)+β+ Mg_2Si and L↔(Mg)+γ+ Mg_2Si, have been determined to be at ~ 448 °C and ~ 436 °C respectively by DTA. The characteristic temperatures recorded on the DTA curves are analysed and a linear relationship is found between the peak temperature and the square root of the scanning rate.

Introduction

Aluminium and magnesium alloys containing silicon are well known for their age hardening characteristics. Owing to their good castability, they are of high industrial relevance. Although increasing demand for higher strength and better service properties has led to the development of more complex alloys, the Al-Mg-Si system remains of great importance for understanding the solidification and heat-treatment of many relevant industrial alloys. While there are a few studies available related to the liquidus surface of this system and quite a lot on solid-state equilibria in the Al corner, very scarce information deals with Mg-rich alloys, in particular the solid-state equilibria in the Mg corner. The present study was intended to check available descriptions of the Al-Mg-Si phase diagram against new experimental results on high Mg alloys in the Al-Mg-Si system.

Experimental details and characterisation of the as-cast alloys

Fig. 1 shows an isothermal section of the Al-Mg-Si phase diagram calculated at 300 °C using a new set of optimised parameters presented elsewhere [1] based on the COST 507 [2] data bank. The bold lines are limits between various domains, where the phases present are indicated on the right-hand side of the diagram. (Al) and (Mg) stand for the fcc and hcp solid solutions rich in Al and Mg respectively, while $Al_{30}Mg_{23}$ (ε), Al_3Mg_2 (β) and $Al_{12}Mg_{17}$ (γ) are compounds from the binary Al-Mg system. Three alloy compositions, shown as crosses in Fig. 1, were chosen from three different phase fields along the interrupted line. A fourth alloy, much closer to the Al-Mg side (see square in Fig. 1), was also prepared for this study. Table 1 lists the nominal compositions of these alloys.

Samples taken out from the as-cast ingots were prepared by standard metallographic techniques and first observed by optical microscopy. Figs. 2(a) to 2(d) show typical views of the microstructure of each alloy. The phases observed were ascertained by chemical microanalysis and X-ray diffraction (XRD), as will be detailed later. In each alloy, the primary phase appears as faceted dark crystals of Mg_2Si. This is in agreement with the liquidus surface of the Al-Mg-Si system. Alloy D30, which contains only 0.5 wt.% Si, shows much less primary Mg_2Si crystals. In alloys A30 and D30 which both contain 30 wt.% Mg, (Al) dendrites are seen enveloped within a matrix of β. Alloy D30 shows a finer microstructure because its cooling rate was higher than the cooling rates for the other alloys. Numerous small dark precipitates, which present the same contrast as primary Mg_2Si, were found within the β phase in alloy D30 (Fig. 2(a)). Similar precipitates were also seen in alloy A30 but they were much less in quantity and generally located close to the (Al) phase. It is unclear if these precipitates are associated with the expected ternary eutectic (liquid↔(Al)+β+ Mg_2Si) or if they form during cooling after solidification finishes. This will be addressed subsequently.

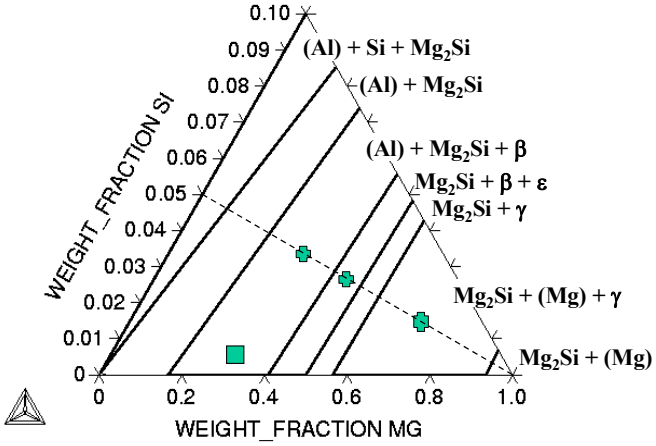

Figure 1 - Isothermal section of the Al-Mg-Si system at 300 °C.

Table 1 - Nominal composition of the alloys studied (wt %).

Alloy table	*Al*	*Mg*	*Si*
A30	66.5	30.0	3.5
A45	52	45	3
A70	28	70	2
D30	69.5	30	0.5

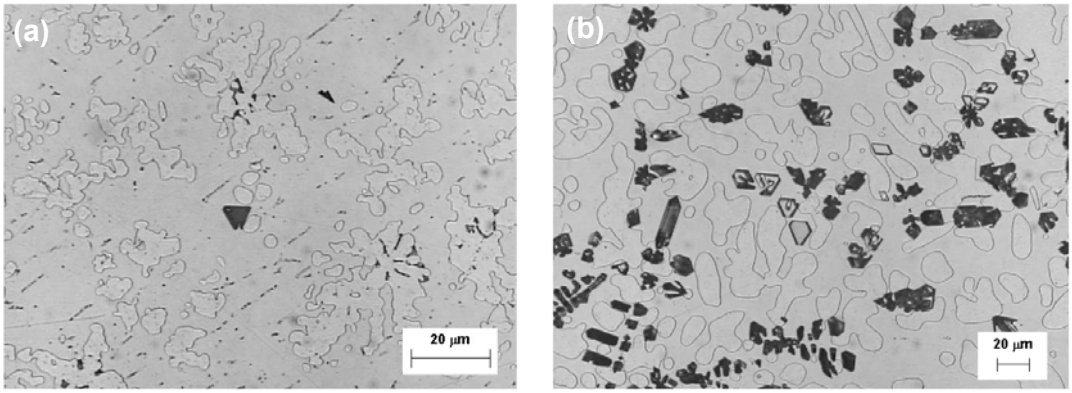

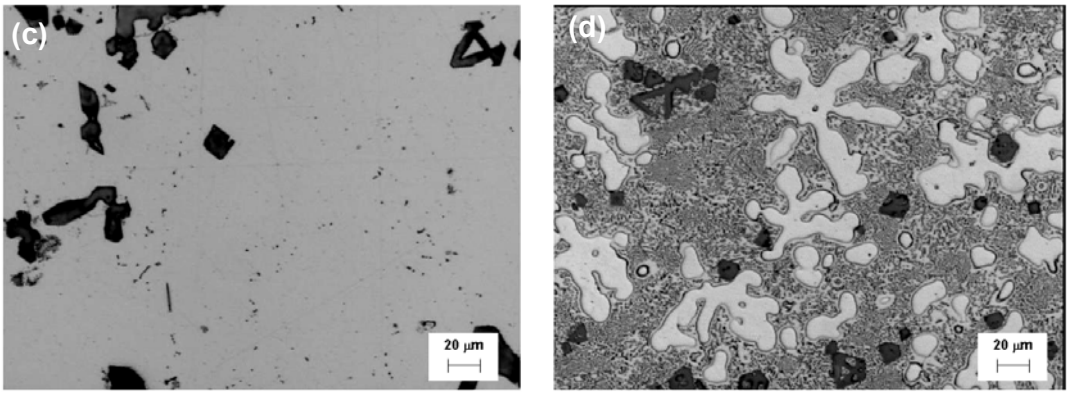

Figure 2 - Optical micrographs of the as-cast microstructures of the four alloys studied: (a) D30; (b) A30; (c) A45; (d) A70. Alloys A30, A45 and D30 were etched with Keller's reagent while alloy A70 with a solution of 0.5 % HNO_3 in etanol.

In addition to primary Mg_2Si crystals, alloy A45 is essentially made of the γ phase. Also observed are some fine precipitates similar to those found in alloys D30 and A30. Apart from blocky precipitates of Mg_2Si, well-developed dendrites of the (Mg) phase are observed in the microstructure of alloy A70. These dendrites are surrounded by a halo of the $Al_{12}Mg_{17}$-γ phase and the remaining volume is occupied by a rod-like eutectic made of γ and (Mg) phases. However, the presence of Mg_2Si was not resolved within this eutectic, which should be the terminal three phase (Mg_2Si+(Mg)+γ) eutectic. An estimate of the eutectic composition was made by EDS analysis on areas of 30µm × 40µm and was found to be ~ 30.1 wt.% Al and ~ 69.9 wt.% Mg.

X-ray diffraction analyses of the four alloys were performed with a Seifert 2000 apparatus equipped with a Cu cathode ($\lambda_{K\alpha}$=1.540598 Å) and operated at 40 kV and 30 mA. Indexing of the different XRD patterns was made with the software Carine v.3.1 [3] according to the information given in Pearson's handbook [4]. It was found that only phases expected from the stable phase diagram were present. Each alloy was subjected to differential thermal analysis (DTA) using a SETSYS apparatus from SETARAM. The DTA signal was recorded on heating and cooling with various scanning rates, 2.5, 5 and 10 $K.min^{-1}$. The scanning rates used for heating and cooling were the same and a new sample was used in each run. The DTA samples thus obtained were then prepared for metallographic observations. Scanning electron microscopy (SEM) was performed by means of an LEO scanning electron beam microscope operated under 15 kV. Microanalysis was achieved with an energy dispersive spectrometer IMIX from PGT, using pure elements as standards. For microanalysis, the probe current was maintained at 1.5 nA and the spectra were cumulated during 200 seconds.

A diffusion couple with an Al-5wt%Si alloy (cast at DLR Germany) on one side and alloy A70 on the other side was prepared and introduced in an ampoule sealed under low argon pressure. It was then maintained at 300 °C for 7 months to allow equilibrium at the junction.

Diffusion couple

Fig. 3 presents an SEM micrograph across the junction of the diffusion couple, demonstrating the microstructural changes that have taken place after 7 months at 300°C. The phases identified according to EDS analyses are indicated on the micrograph. The initial location of the junction contains many large pores. On the outmost part of the Al-Si side, silicon lamellae appear white in the (Al) matrix. Close to the junction, these lamellae are replaced by Mg_2Si precipitates with grey contrast. On the other side of the couple, the three Al-Mg compounds, β, ε and γ, appear in a sequence with an increase in the Mg content. The microstructure in the zone at the outmost right-hand side of the micrograph is composed of dark dendrites of the (Mg) phase in a matrix of γ and some large faceted crystals of Mg_2Si, where these Mg_2Si crystals are invisible due to the poor contrast with the γ phase in backscattered imaging mode. Similar Mg_2Si precipitates were present together with β and γ but not in the zone with ε. The dark spots in the γ+Mg_2Si zone are pores.

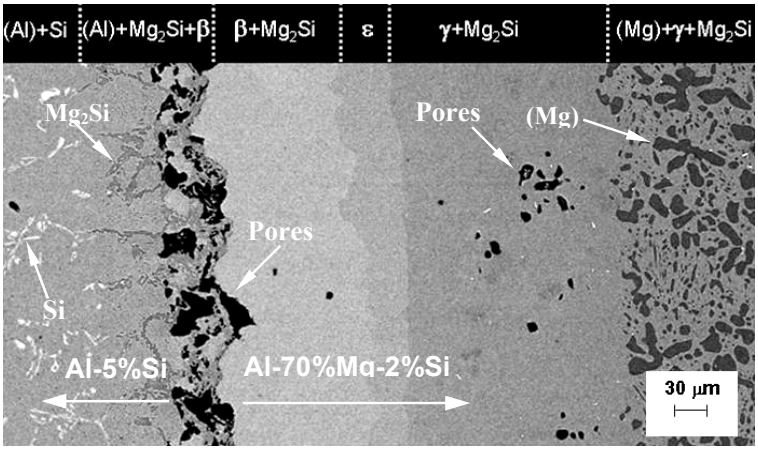

Figure 3 – SEM micrograph showing the junction of the diffusion couple after 7 months at 300 °C (backscattered electron imaging).

The composition across the inter-diffusion zone was estimated by means of line profiles with spot measurements made at every 3 μm in spacing. Mg_2Si was found to have the same composition in whatever equilibrium it is involved. Also, the amount of silicon was found to be less than 0.1wt% in any of the three Al-Mg compounds (ε, β and γ) and in each of the (Al) and (Mg) phases as well. The very low silicon content in the ε phase was also confirmed with WDS in an electron probe microanalyser. Based on these quantitative analyses, the compositions of the various phases at the boundary of each microstructural zone were carefully evaluated, giving estimates of the tie-lines in three phase equilibria (two phases from the Al-Mg system plus Mg_2Si). These compositions are reported in Table 2 with the silicon content being set at zero. Since the amount of silicon that may enter the Al-Mg compounds (ε, β and γ) is very low, it is expected that the composition of any of these phases in equilibria in the ternary system is very close to its composition in the binary system. The set of data in Table 2 was thus plotted into the calculated phase diagram shown in Fig. 4, together with data collected from literature [5-9].

Table 2 – Magnesium content (wt %) of the phases at the limits of the microstructural domains in Fig. 3.

(Al)	*β*		*ε*		*γ*		*(Mg)*
5.8	36.0	36.4	40.6	41.5	50.5	58.0	94.1

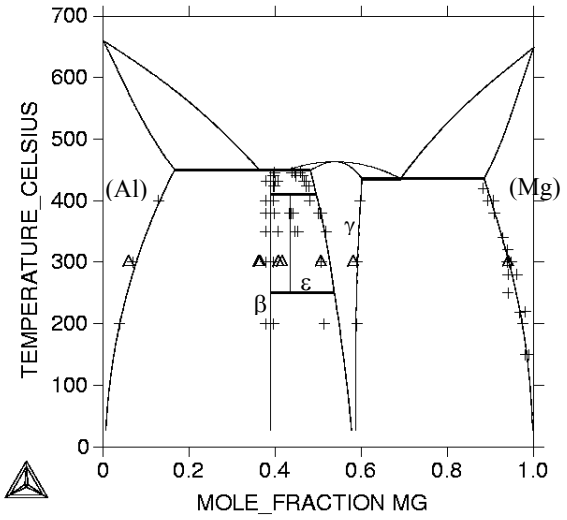

Figure 4 – Al-Mg phase diagram with experimental phase compositions from literature (crosses) and from Table 2 (triangles).

DTA results

Fig. 5 presents the DTA records obtained on cooling alloys A30, A45 and A70 at a scanning rate of 2.5 $K.min^{-1}$. There is a first thermal arrest which appears at about 700 °C for all three alloys. An intermediate arrest shows up for alloys A30 and A70 but not for alloy A45. The final arrest is marked in any case, with even some recalescence for alloy A30. The records obtained from other scanning rates were similar for each alloy. Moreover, examination of the microstructure of each of the DTA samples confirmed similar microstructural features to the as-cast samples, although large primary Mg_2Si crystals were found in the upper part of some samples. It is thus clear that the high temperature arrest is associated with the formation of Mg_2Si and the intermediate arrest with the growth of (Al) for alloy A30 and the growth of (Mg) for alloy A70. The final arrest corresponds to the formation of β for alloy A30 and the formation of γ for both of alloys A45 and A70.

Based on the DTA records, an attempt was made to characterise the temperature of the final invariant reaction undergone by each alloy. Fig. 6 compares the DTA records obtained at various scanning rates in a temperature range across all possible solidification events for alloy A30. Upon heating, the very start of melting should correspond to the temperature at which the signal deviates from the nearly horizontal basal line. This temperature appears not to be sensitive to the heating rate and was found equal to 448±1°C for alloy A30, 458±1°C for alloy A45 and 436±1°C for alloy A70. The peak temperature is another characteristic temperature and was found to shift to a higher value as the heating rate was increased. Upon cooling, the temperature corresponding to the start of the final reaction recorded by the DTA is influenced by the undercooling experienced by the material. So, the peak temperature, which in this case was found to

shift to a lower value as the scanning rate was increased, is more useful as a characteristic temperature. A particular feature is observed in the case of alloy A30 where the peak is seen to split into two parts, a main peak and a marginal one. This feature will be further discussed below.

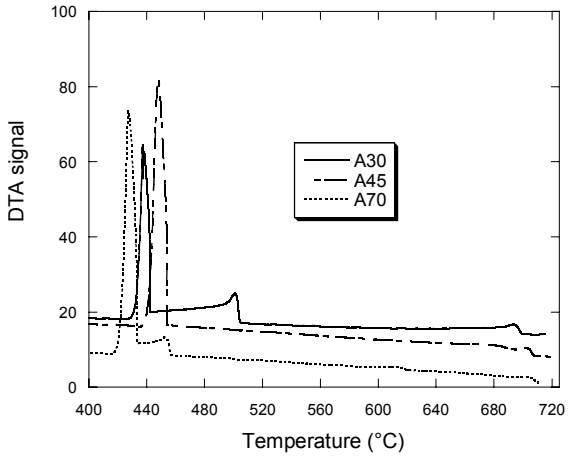

Figure 5 - DTA records obtained on cooling alloys A30, A45 and A70 at 2.5 K.min^{-1}.

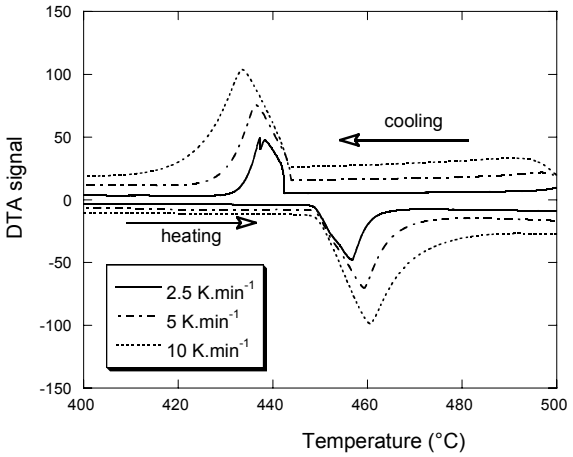

Figure 6 - DTA records for alloy A30 at various scanning rates in the temperature range of the final invariant reaction.

The characteristic temperatures, thus evaluated, are plotted in Fig. 7. Two series of DTA were made for alloy A30 and these are represented with empty triangles either upwards or downwards. The temperature of the second peak on cooling, when present, has been added with solid triangles. It was found that a linear relationship could be drawn through the peak temperature data against the square root of the scanning rate for each series. Furthermore, the resultant linear relationships extrapolate well to the experimental temperatures for the very start of melting of each alloy studied which have been plotted on Fig. 7 at a zero scanning rate. It is satisfying to notice that the absolute values of the slope of these lines are all very similar, indicating that the experiments are reproducible although a new sample was used in each run.

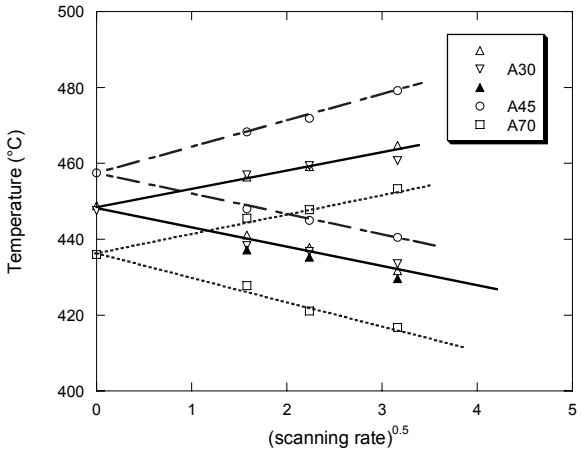

Figure 7 - Effect of scanning rates on the characteristic temperatures of the peak related to the final invariant reaction.

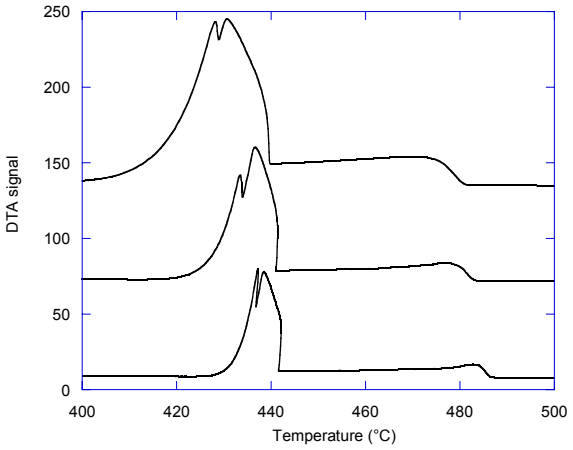

Figure 8 - DTA records for alloy D30 at cooling rates of 2.5, 5 and 10 K.min^{-1}.

At first glance, it was thought that the marginal peak recorded on the DTA curve of alloy A30 could be an artefact due to inhomogeneous temperature in the sample. This assumption was ruled out as it was never observed with alloys A45 and A70. The transformation is supposed to be the three phase invariant reaction, where some undercooling is required for the nucleation of new Mg_2Si crystals as the primary crystals of Mg_2Si have all become enveloped within (Al) or β. Accordingly, as can be inferred from Fig. 7, the potential linear relationship between the marginal peak temperature and scanning rate, represented by solid triangles in Fig. 7, would extrapolate to a lower temperature than the estimated incipient melting temperature. These hypotheses are supported by the fact that the marginal peak is well observed for alloy D30 for all three cooling rates, as illustrated in Fig. 8. The DTA samples of alloy D30 showed much more small precipitates than did the as-cast samples. As can be seen from Fig. 9(a), they are present in some regular patterns. Apparently, they were formed during the eutectic reaction. However, solid-state diffusion may have affected the solidification structure as very few (Al) phases have been found in the eutectic areas. As shown in Fig. 9(b), clear signs of growth of β at the expenses of the (Al) phase are observed in samples after a DTA run.

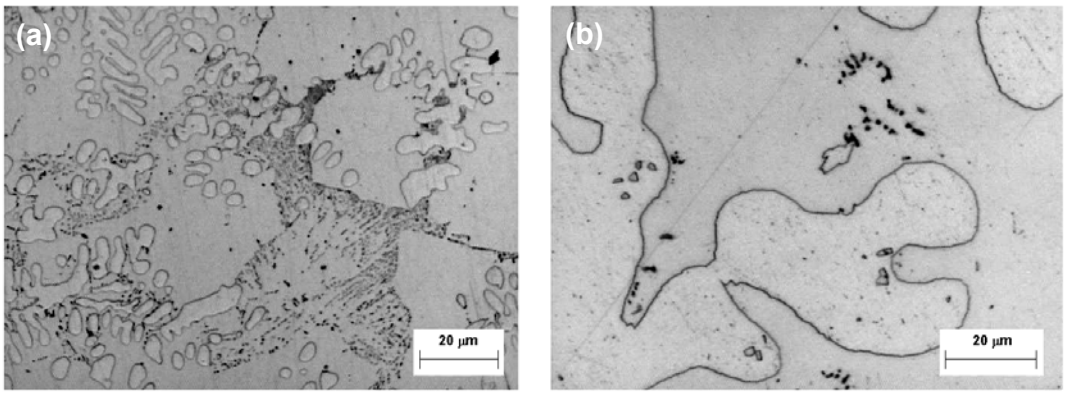

Figure 9 – Optical micrographs showing the microstructure of alloy D30 after a DTA run.

Summary

Solidification paths of Mg-rich Al-Mg-Si alloys finish on ternary eutectics located very close to the Al-Mg side of the composition triangle. These eutectics involve Mg_2Si and two phases of the Al-Mg system. The silicon content in any of these Mg-Al phases in the ternary eutectics has been found lower than 0.1 wt%. The temperatures of two of these ternary eutectic reactions, i.e. liquid ↔(Al)+β+ Mg_2Si and liquid↔(Mg)+γ+ Mg_2Si, have been determined to be at about 448 °C and 436 °C respectively by DTA.

Acknowledgements

Part of this study is supported by ESA through the MICAST programme under contract 14347/00/NL/SH. Thanks are due to M. Palm (MPI-E Düsseldorf) for WDS measurements and to L. Ratke and S. Steinbach (Institute for Space Simulation, DLR, Germany) for providing alloys.

References

[1] Lacaze J. and Valdes R., communication at the TOFA meeting, Vienna, 2004
[2] "Thermochemical database for light metal alloys", ed. I. Ansara, European Commission, 1995
[3] http://pro.wanadoo.fr/carine.crystallography/
[4] Villars P., "Pearson's Handbook Desk Edition", ASM international, 1997
[5] E. Schurmann,Giesserei-Forschung, 32, 163-174, 1980
[6] P. Liang et al., Z. Metallkd, 89, 536-540, 1998
[7] M.I. Zacharowa, W.K. Tschikin, Zeitschrift fur Physik, 95, 769-777, 1935
[8] E.Schimd, G. Siebel, Zeitschrift fur Physik, 85, 36-55, 1933
[9] P. Saldau, M. Zamotorin, Journal of the Institute of Metals, 48, 221-226, 1933

Diffusion couples Al-Si /Al-Mg-Si, preparation and exploitation

Complément IV

IV.1 Diffusion couples Al-Si/Al-Mg-Si, preparation and exploitation.

To study the phase relations in multicomponent systems we used one of the most usual procedures; namely the diffusion couple technique where two alloys are clamped together and annealed at one temperature. The analysis of these experiments is well established when the diffusion zone consists of several single-phase layer while it is complicated by the presence of layers with more than one phase. The resulting microstructure of the reaction zone can be visualized with the aid of the diffusion path. This is a line on the ternary isotherm representing the locus of the average composition in planes parallel to the original interface across the diffusion zone. The information on phase diagram of the Al-Si, Al-Mg and Mg-Si binary systems was presented in the introduction, while limited experimental information on the ternary Al-Si-Mg system has been reported for the Mg corner. The only work found is due to Rokhlin and Pepelyan [1] who reported isothermal sections at 300, 400 and 430 °C. The present study focused on the investigation of the Al-Mg-Si phase diagram at 300 °C.

Diffusion couples with an Al-5 wt % Si alloy on one side, one of the three other alloys of the AlSiMg series on the other side, were prepared. Blocks of 5x5x5 mm^3 were cut out from the casts and one face was carefully polished. The diffusion couples were then prepared by clamping together the blocks two by two, in contact with their polished flat surface. The clamps were made of stainless steel plates maintained under a slight pressure. The diffusion couples were then introduced in a quartz ampoule sealed under low argon pressure and held 7 months at 300 °C. At the end of this treatment, the ampoule was cooled to room temperature and broken. The diffusion couples were sectioned perpendicular to the bond interface with a low speed diamond saw. These samples were mounted in bakelite and the cross-sections were prepared by standard metallographic

techniques to a surface finish of ¼ μm. At the very end of metallographic preparation, the samples were electropolished to remove any surface contamination.

The composition of the intermetallic compounds formed in the interdiffusion layer was determined with EDS by spot analysis. Composition profiles were obtained by means of various methods: spot counting along lines and different types of area mappings. These latter could be recorded either on large areas (and then divided in successive rectangles) or on contiguous rectangles of limited width but parallel to the contact zone. The conditions used will be detailed in each case.

Figure IV-1a, b and c present SEM micrographs across the interdiffusion zone of the three diffusion couples between the Al-Si alloy and the pairs of alloys. The very left side corresponds in each diffusion couple to the Al-Si alloy where the silicon lamellae appear whiter than the (Al) matrix. The right part of these micrographs corresponds to areas with the same phases than the bulk of the respective Al-Mg-Si alloy. In the three diffusion couples, on the left side of the junction, close to the bounding interface, the silicon lamellae have been replaced with Mg_2Si which appears with a darker contrast. In the same area, Mg_2Si has also precipitated within the aluminium matrix and appears as dusky little crystals.

Figures IV-1 d to f present enlarged views of the microstructures as observed far from the bounding zone. A comparison of the as cast and heat treated microstructures will be presented for each diffusion couple. As will be seen later with the composition profiles, the three diffusion couples may be classified as semi-infinite, which means that the couple ends inherited their original compositions after diffusion annealing.

The phases present in each of the fields that can be observed were identified by EDS analysis and are indicated in the upper part of the micrographs (in some cases, only detailed examination of the sample allowed observation of some phases, as is the case of Mg_2Si when mixed with β or ε compounds). It is seen that the microstructures in the reaction zone, are essentially composed by two-phase domains, though one single phase domain made of the compound ε is seen in Figure IV-1c. In the ternary systems there is an

additional degree of freedom allowing concentration gradients, and therefore diffusion to occur in two-phase regions as well as in one phase region.

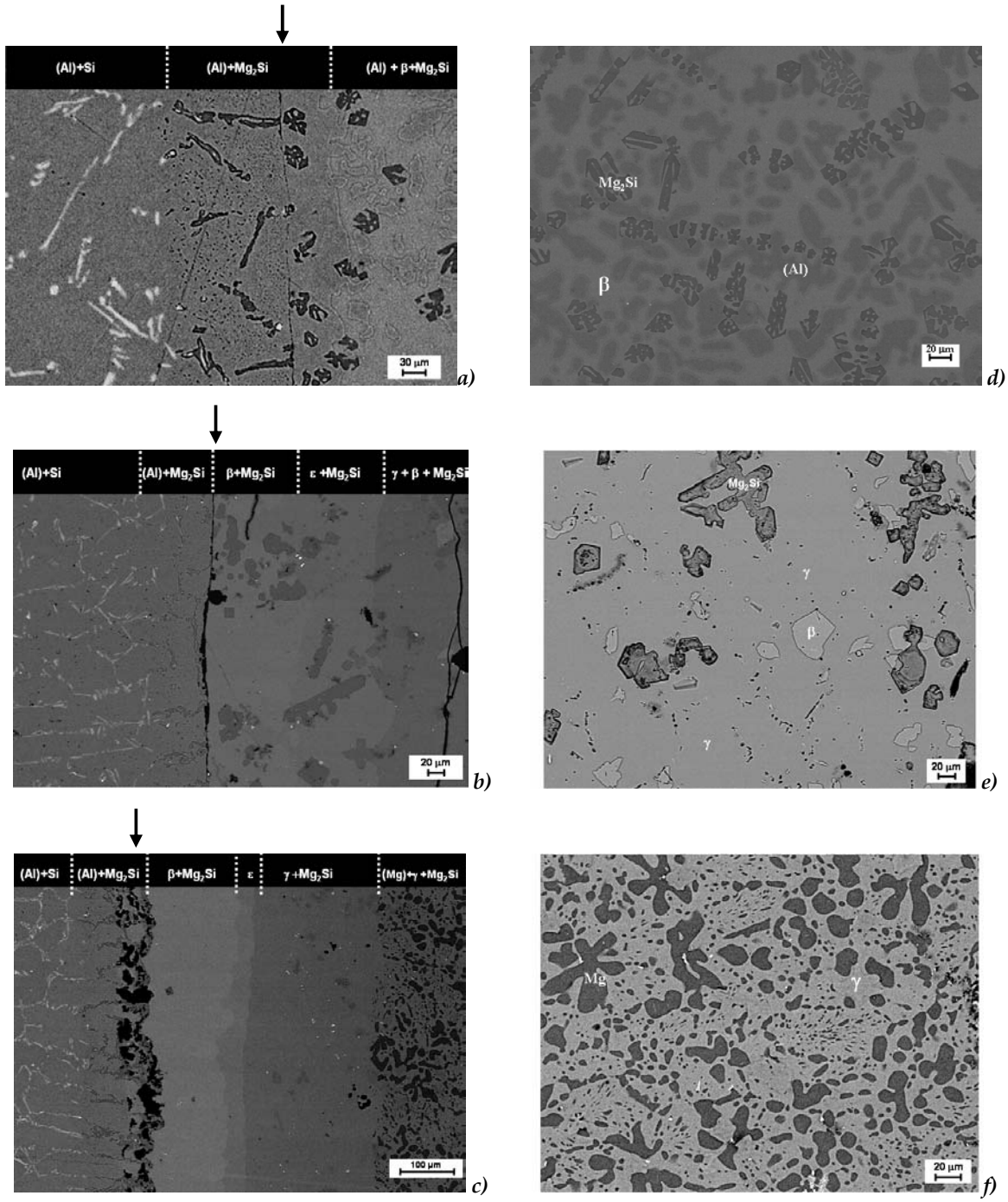

Figure IV-1: SEM micrographs showing the junction part of the three diffusion couples: AlSi/A30 a); AlSi/A45 b); AlSi/A70 c). Figures d, e and f show the microstructure of the respective bulk Al-Mg-Si alloy far from the reaction zone of each diffusion couple. Arrows indicate the original couple interface.

IV.1.1 Al-5Si/A30

For the first diffusion couple AlSi/A30, the bounding joint is continuous and free from any porosity. As indicated before, in the left side of the interface, the Si lamellae were replaced by Mg_2Si precipitates. On the right side of the interface, the same two-phase (Al)+Mg_2Si layer is observed but the Mg_2Si precipitates come from the as cast microstructure. The development of this layer is due to magnesium diffusion from right to left, leading to the disappearance of the Al_3Mg_2-β phase. The Mg_2Si precipitates in both sides of these layers have the same composition whatever its morphology. This later layer is followed by a three-phase zone that corresponds to the initial microstructure of alloy A30. Coarsening of the aluminium dendrites occurred.

Average composition profile. The composition profiles were obtained from two different kinds of mappings:

a) An area mapping was carried out on the reaction area (254 x 204 pixels image) shown in Figure IV-1a. The mapping was recorded during 5 hours, leading to a total counting time of 0.35 seconds for each pixel. In this X-cartography one pixel is equal to 1 micron. From this mapping, the average concentration profile was estimated by averaging data in each column (1 x 204 pixels) or for successive sets of 10 x 204 pixels. Both profiles are shown in Figure IV-2 for all three elements, where the continuous line represents the average profiles estimated from one pixel in width whereas the interrupted lines with solid symbols are the average profiles for contiguous rectangles of 10 pixels in width. As already mentioned in the introduction, the accuracy of measurements was not always sufficiently high because the acquisition time by pixel was not long enough. From the profile we can see the variation of the composition for the three elements in each phase. The composition of silicon was constant in the reaction zone.

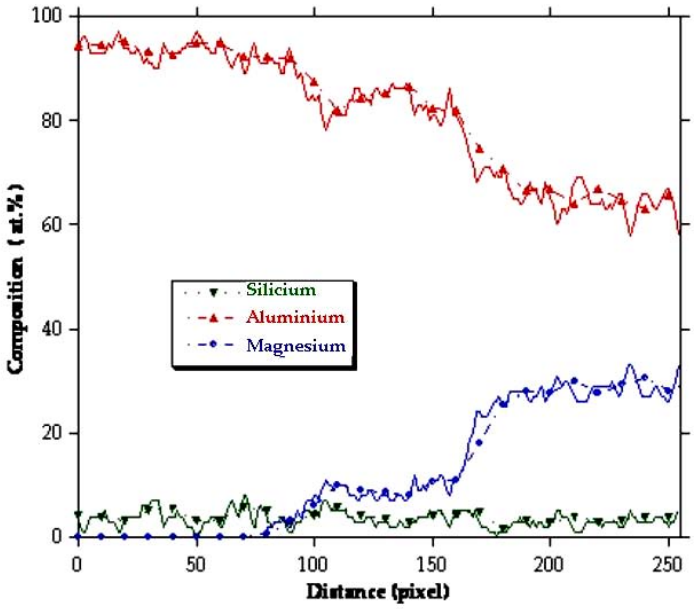

Figure IV-2: Average concentration profiles from the Figure IV-1a. (1 pixel = 1µm)

IV.1.2 Al-5Si/A45

Figure IV-1b shows the second couple diffusion (Al-5Si/AlSiMg45). The initial bounding interface presents porosity. In the right side of the diffusion zone appeared two successive two-phase layers of different thicknesses: β + Mg_2Si for the first and ε + Mg_2Si for the second layer. This succession agrees with the phase diagram presented in the introduction according to which the ε phase should be present at the experimental temperature used.

The microstructure of AlSiMg45 far from the interface has evolved with respect to the as cast microstructure. Figure IV-3 compares the microstructure after 7 months at 300 °C to the as cast one. In the microstructure after heat treatment, γ and β phases are observed together with Mg_2Si precipitates, while the β phase was not initially present. Differential thermal analysis was carried out on the A45 part of the diffusion couple but no solid state transformation could be detected. After this analysis we can conclude that

this transformation is probably too sluggish to be observed in DTA and proceds very slowly during long term heat treatment occur very slowly.

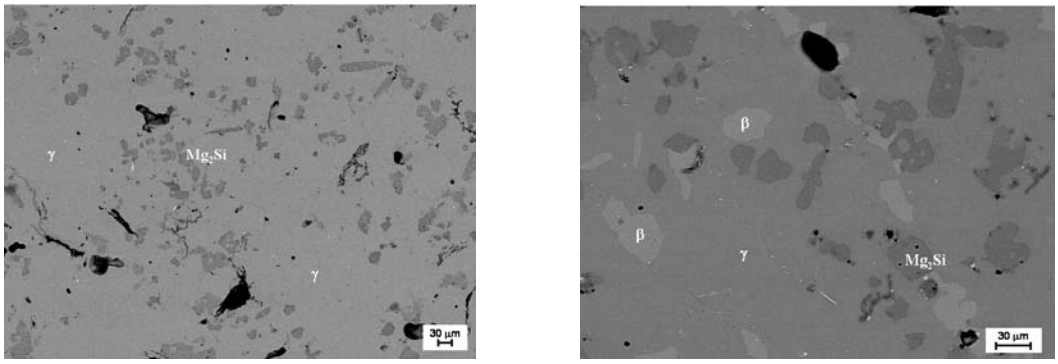

a) *b)*

Figure IV-3: SEM micrographs showing the as cast A45 microstructure a), and the A45 microstructure after heat treatment b).

Average composition profile. The compositions profiles were obtained from two different kinds of mappings:

a) Composition average profiles were acquired from successive X-ray mappings on elongated adjacent boxes (35 x 300 μm) on the area shown in Figure IV-1b. The acquisition time for each box was 100 seconds. In Figure IV- 4 are shown with solid lines the corresponding average concentration profiles for all the elements. The presence of Mg_2Si precipitates in the layers leads to large compositions changes in the profiles.

b) From the same SEM micrograph in Figure IV-1b EDS spot analyses were carried out every 20 μm during 100 seconds, leading to the profiles shown with interrupted lines in Figure IV- 4. In this profile a zone is distinguished in which the atomic percentages of the three elements are fairly constant. After this zone the aluminum concentration diminishes to form the ε phase in equilibrium with Mg_2Si precipitates. This profile will be plotted in the ternary system.

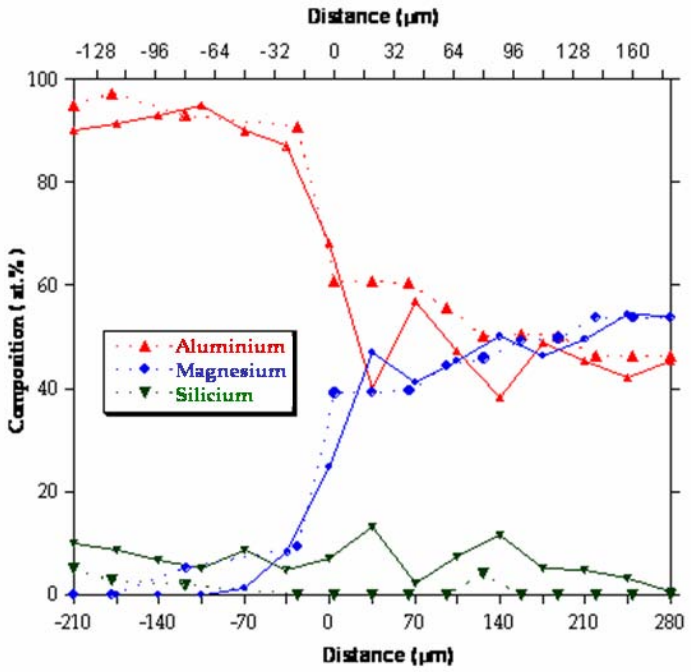

Figure IV- 4 : Composition profiles from the Al-5Si/A45 diffusion couple.

IV.1.3 Al-5Si/A70

The last diffusion couple shown in Figure IV-1c presents at the bounding junction large porosities which appear dark. The micrograph shows the formation of three layers in the diffusion zone. On the right side of the couple, the three Al-Mg compounds, β, ε and γ, appear at correspondingly increasing Mg content. Mg_2Si precipitates were also present together with β and γ but not in the zone where the ε phase appears. The β and ε layers form with a nearly constant composition. Figure IV-5 compares the microstructure of the alloy after heat treatment far from the junction to the as cast one. It is seen that the eutectic γ + (Mg) has coalesced during the heat treatment. Figure IV-6 shows an enlarged view of this diffusion couple where the dark areas in the γ+Mg_2Si zone are porosities. These porosities approximately are of the same shape than (Mg) dendrites, so that it can be assumed that they appeared because of diffusion of magnesium to form the ε and β phases.

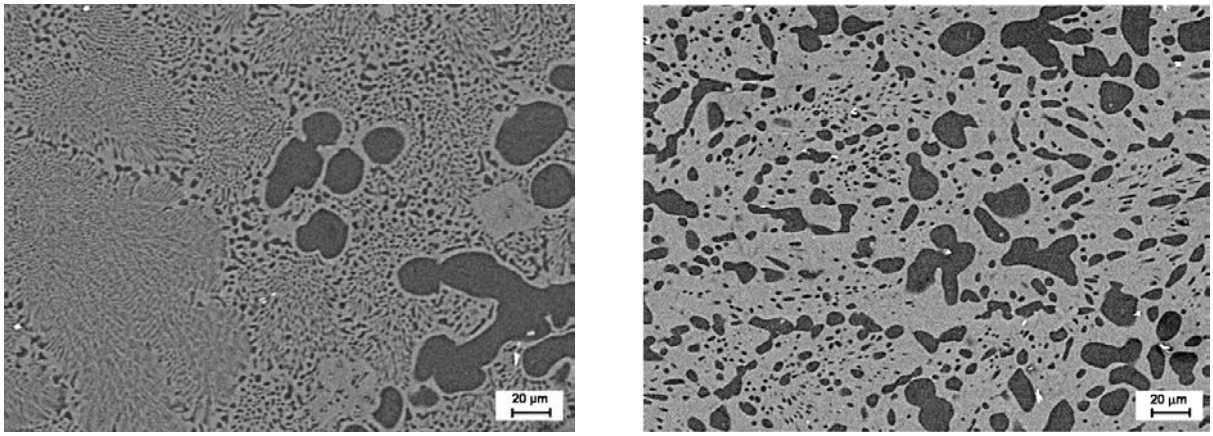

a) ***b)***

Figure IV-5: SEM micrographs of the A70 as cast a) and A70 microstructure after heat treatment b).

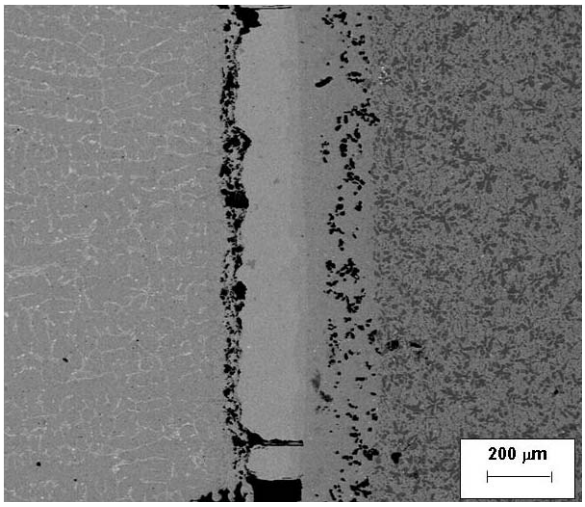

Figure IV-6: SEM micrograph of all the A70 diffusion couple.

Average composition profile. The concentration profiles across the inter-diffusion zone were acquired from X-ray mapping of the area shown in Figure IV-1c that lasted for 5 hours (254 x 204 pixel image). The acquisition time for each pixel was thus 0.35 seconds. Figure IV-7 shows the corresponding average profiles for all the elements with solid symbols and solid lines. The average profile on the layers confirms the presence of three compounds of the Al-Mg phase diagram. The composition ranges indicated by EDS closely match those of the Al_3Mg_2-β, $Al_{30}Mg_{23}$-ε and $Al_{12}Mg_{17}$-γ at 300°C.

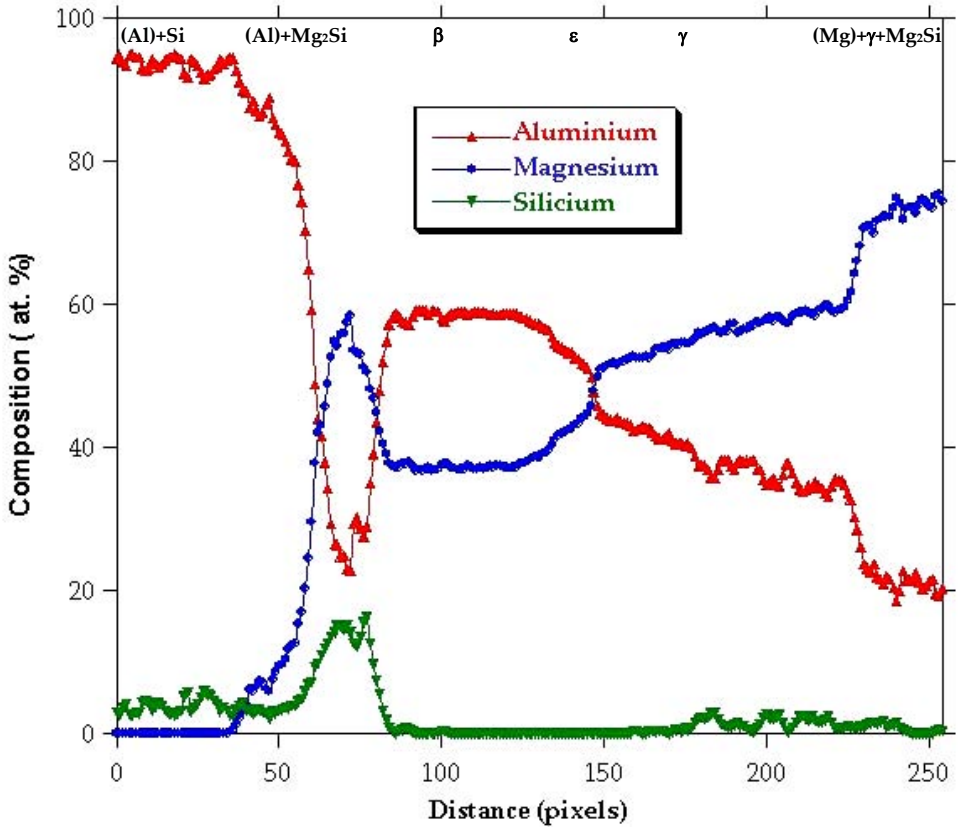

Figure IV-7: Concentration profile across the diffusion zone of the diffusion couple shown in Figure IV-1c.

A further analysis was devoted to the investigation of the ε layer. In the central part of the SEM micrograph shown in Figure IV-8, a composition profile was recorded by EDS spot analysis, with counting performed every 3 μm during 100 seconds. The compositional changes that characterize a boundary crossing can be easily observed. The phase boundaries from left to right are shown in the Figure IV-8. The values of the concentrations at each of these interfaces can be evaluated from the concentration profile and will be used in the ternary phase diagram.

In the $Al_{30}Mg_{23}$-ε layer the content of the elements do not vary, in opposition with the profile observed in the Figure IV-7. Nevertheless, for both profiles, the measured silicon content was always zero; confirming that the solubility of silicon in the ε phase is limited.

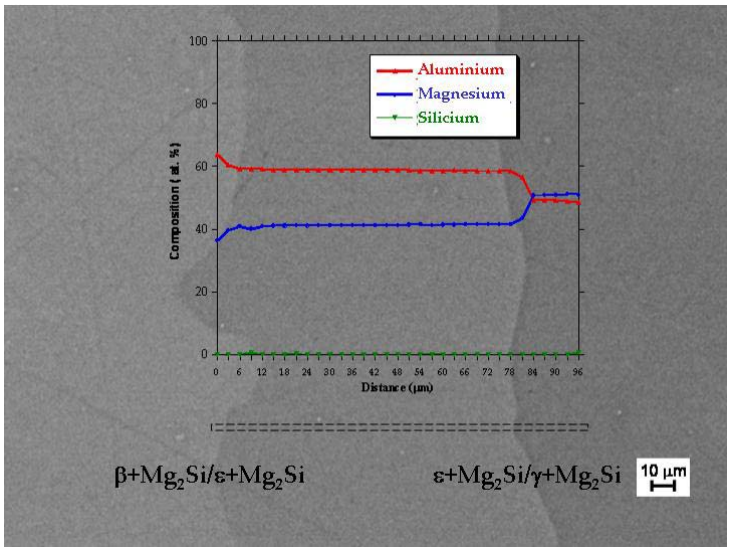

Figure IV-8: Localisation of the profile done in the layer $Al_{30}Mg_{23}$-ε.

IV.2 Phase compositions

Al least three precise measurements were obtained by counting during 100 seconds on each phase in various locations along each of the diffusion couples. The estimated average compositions of each phase for the three diffusion couples are presented in Table IV-1, where the bold line represents the bonding interface. In all the diffusion couples, the Mg_2Si precipitates were found to have the same composition in whatever equilibrium it is involved. The phase composition of the beta phase was checked with WDS in an electro probe microanalyser (at MPI-E Düsseldorf) and the results are shown in Table IV-2. The amount of silicon in β phase was found to be less than 0.1 at. %.

	Al-5Si			***A30***			
	Far away					***Far away***	
	(Al)	(Al) + Si	(Al)+ Mg_2Si	(Al)	β	(Al)	β
Al	97.7	98.8	94.8	92.9	62.3	95.3	62.3
Mg	0	0	4.3	7.1	37.7	4.8	37.7
Si	2.3	1.2	0.9	0	0	0	0
	Al-5Si			***A45***			
	Far away					***Far away***	
	(Al)	(Al) + Si	(Al)+ Mg_2Si	β	ε	β	γ
Al	94.9	96.0	92.8	60.4	55.6	60.2	46.3
Mg	0.0	0.05	5.2	39.6	44.4	39.8	53.7
Si	5.0	3.8	2.0	0.0	0.0	0.0	0.0
	Al-5Si			***A70***				
	Far away						***Far away***	
	(Al)	(Al) + Si	(Al)+ Mg_2Si	β	ε	γ	γ	(Mg)
Al	98.9	95.9	94.6	60.7	55.7	44	37.7	5.8
Mg	0	0	5.07	39.3	44.3	56	61.4	94.1
Si	1.12	4.08	0.29	0	0	0	0	0

Table IV-1: Phase composition in the three diffusion couples (at. %) across the reaction layer. EDS spot analyses.

	Al_3Mg_2–β			
Al	62.5	62.6	62.8	62.6
Mg	37.4	37.3	37.1	37.3
Si	0.15	0.13	0.12	0.13

Table IV-2: β-phase compositions in the A30 diffusion couple (at. %) determined by WDS.

From the concentration profile of the A70 diffusion couple shown in Figure IV-7, the average compositions of the phases as measured at the interfaces by EDS spot analysis were carefully evaluated (two phases from the Al-Mg system plus Mg_2Si). These compositions are reported in Table IV-3 with the silicon content set at zero.

At 300 °C there is one intermetallic phase ε between the γ and β phases. As a matter of fact, the central part of the Al-Mg system has been controversial as for phase equilibria, phase compositions and temperature range of stability. There is no doubt about the existence of two intermediate phases: Al_3Mg_2-β and $Al_{12}Mg_{17}$-γ [2-4]. An assessment of the

Al-Mg system presented by Murray [2] indicates the existence of another phase, noted R, that was confirmed as ε by Su et al. [4]. The chemical composition of this phase was suggested to be 42 at. % [2] or 43.5-45 at. % Mg [4]. On the contrary the phase designated by Zuo [3] as ζ and by Su et al. [4] as λ phase was not confirmed by other investigations. Besides the β, γ and ε phases, the existence of another phase has been dismissed by Donnadieu et al. [3-6] who state that ζ (or λ) constitutes a commensurate modulation of the γ phase.

In this work, the homogeneity range of ε extends from 40.6 to 41.5 at. % Mg. The data in Table IV-3 was thus plotted on the calculated binary Al-Mg phase diagram shown in Figure IV-9, together with data from H.L. Su et al. [4] who investigated the Mg-Al phase diagram by XRD, SEM, TEM and DSC. The results are well reproduced by Thermocalc and the solubility ranges observed for the intermetallic phases are in agreement with the literature [2-4, 7].

(Al)	**β**		**ε**		**γ**		**(Mg)**
5.8	36.0	36.4	40.6	41.5	50.6	58.1	94.1

Table IV-3: Magnesium composition (at. %) of the phases at the limit of the microstructure domains.

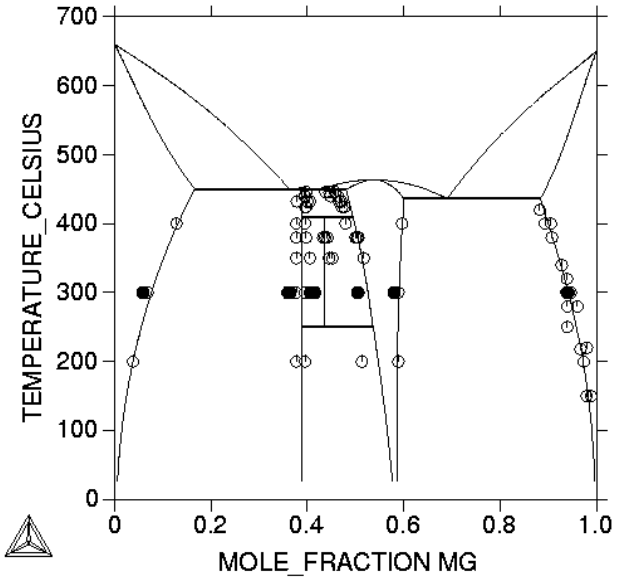

Figure IV-9: Al-Mg diagram with experimental phase compositions from literature (empty symbols) and from Table IV-3 (solid symbols).

The boundary concentrations of the diffusion profiles of the three diffusion couples after annealing at 300 °C for 7 months are plotted on the isothermal section of the Al-Mg-Si phase diagram showed in Figure IV-10. The tie lines are limits between various domains, with the phases present indicated within or on the right side of the diagram. (Al) and (Mg) stand for the fcc and hcp solid solutions respectively rich in Al and Mg, ε, β and γ designate compounds from the binary Al-Mg system. The solid circles correspond to the initial composition in both sides of the diffusion couples. The others symbols represent the compositions on either side of the boundary at each interface along the diffusion path of each diffusion couple. The measured average composition of the initial alloys is given in Table IV-4. The diffusion paths for the three couples have a discontinuous or zigzag shape. This deviation is due to the presence of the Mg_2Si precipitates. In spite of these precipitates, the diffusion path moves during the interdifffusion process in the binary Al-Mg system.

The results of the determination of phase boundaries on the Al-Mg-Si phase diagram at 300°C by the diffusion couple technique are in a satisfactory agreement with the isothermal cross-section established.

The diffusion couple technique is an easy and quick approach to determine and study the phase relations in multicomponent systems.

Alloy label	*Al*	*Mg*	*Si*
Al-5Si	97.1	0	2.9
A30	66	29	5
A45	45.5	52	2.5
A70	29	69	2

Table IV-4: Average composition of alloys (at. %)

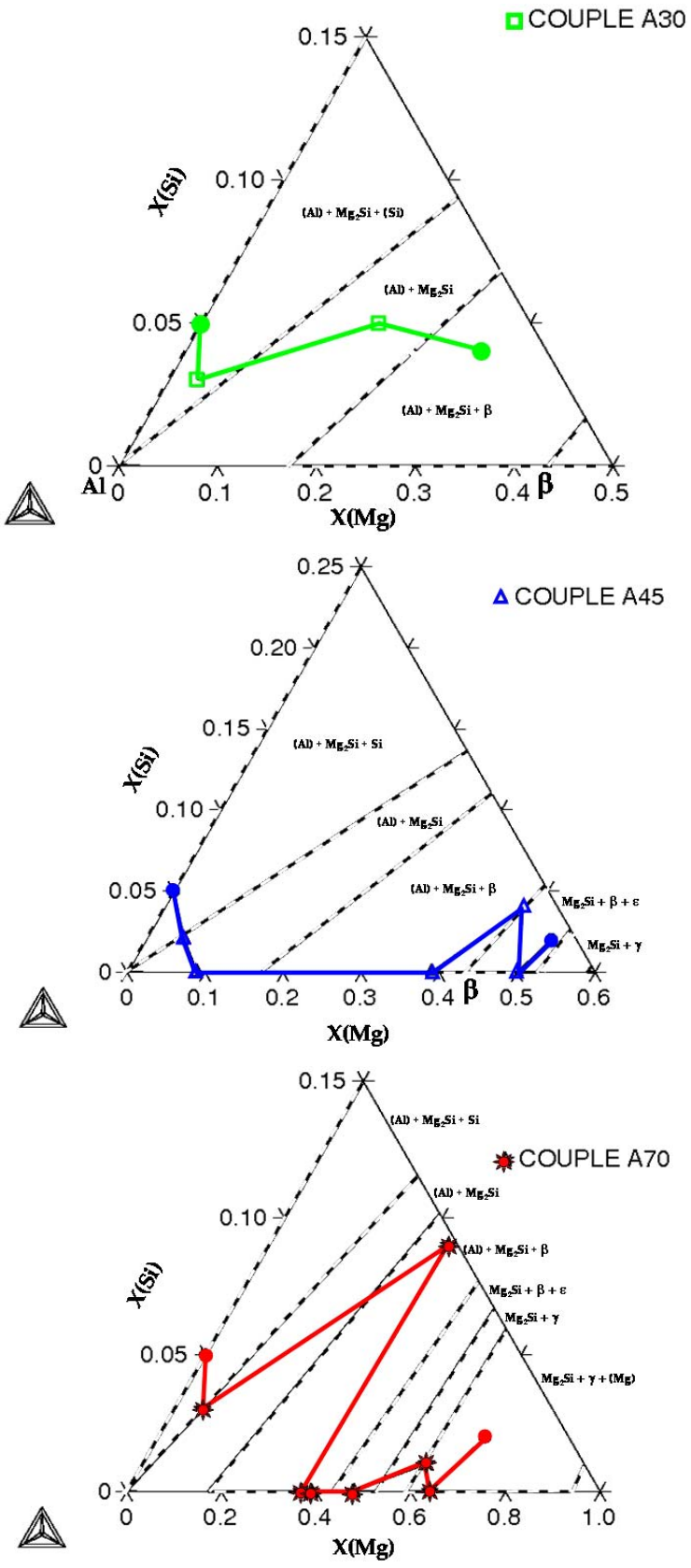

Figure IV-10: Enlargement of the isothermal section at 300°C of Al-Mg-Si with the diffusion paths.

[1] Rokhlin L. L., Pepelyan A.G. Phase equilibria in the Mg-rich region of the Mg-Al-Si system. Metally 1988;6:172.
[2] Murray J.L. The Al-Mg System. Bulletin of Alloy Phase Diagrams 1982; 3:60.
[3] Zuo Y. CYA. Thermodynamic calculation of the Al-Mg Phase diagram. CALPHAD. Vol.17, No.2. pp 161-174. 1993.
[4] Su H.L., Harmelin M., Donnadieu P., Beatzner C., Seifert H., Lukas H.L., Effenberg G., F. A. Experimental investigation of the Mg-Al phase diagram from 47 to 63 at.% Al. Journal of alloys and compounds 1997;247:57.
[5] Donnadieu P, Harmelin M., Su H., Seifert H., Effenberg G., Aldinger F. A quasicrystal with Inflation Symmetry and no forbidden symmetry Axes in a rapidly solidified Mg-Al Alloy. Z. Metallkd 1997;88:33.
[6] Donnadieu P, Harmelin M., Seifert H., Aldinger F. Commensurately modulated stable states related to the gama phase in the Mg-Al Alloys. Philosophical Magazine A 1998;78:893.
[7] N.Saunders. A Review and thermodynamic assessment of the Al-Mg and Mg-Li systems. CALPHAD. Vol.14, No.1. pp 61-70. 1990.

CALPHAD-type assessment of the Al-Mg-Si System

Jacques Lacaze, Rocio Valdés., Monatschefte für Chemie, Chemical monthly, 136, 2005, 1899-1907.

CALPHAD-type assessment of the Al-Mg-Si system

Jacques LACAZE, Rocio VALDES

CIRIMAT, UMR CNRS 5085, ENSIACET, 31077 Toulouse cedex 4, France
Contact person : jacques.lacaze@ensiacet.fr

Keywords
Phase diagrams, analytical description, CALPHAD, aluminium, magnesium, silicon

Abstract
The parameters describing ternary interactions in the liquid phase of the Al-Mg-Si system have been improved slightly with respect to the COST 507 data base by accounting for a larger set of liquidus data than previously considered. As no other parameter was modified, the description thus obtained presents the same high efficiency for solid-solid equilibria as previously achieved, in particular, for the solubility limits in the Al-rich solid solution.

Introduction

Precise knowledge of the Al-Mg-Si system is of interest for applications of both aluminium and magnesium alloys. Accordingly, it has been the subject of many investigations and assessments since long [1], although most of them focused on the aluminium-rich corner. A few CALPHAD-type assessments using the lattice stabilities compiled by Dinsdale [2] are available [3-6] but the system may be reconsidered because it appears that none of these assessments discussed all the information available. Recently, reviews of the available information have been made by Chakraborti and Lukas [7] and Kumar et al. [8]. After a section devoted to the limiting binary systems, a more detailed presentation of the available information on the ternary system is given. Then, a new assessment of the ternary interaction parameters for the liquid phase is presented and predictions made with this new data are compared with available experimental information.

Binary systems

Table 1 lists the binary solid phases, which are the only solid phases under consideration as there is no ternary stable solid phase appearing in the Al-Mg-Si system. The Al-Si system is quite well known and various assessments following the CALPHAD method are available, in particular as part of higher order system descriptions [6, 9-12]. As all of these assessments lead to very close results, the one selected for the COST 507 data bank [13], which is now public, was chosen for this work. The Mg-Si system has also been assessed several times in relation with the study of ternary systems, in particular Al-Mg-Si [3-6]. While the Mg-Si phase diagram appears to be well established, the authors of these assessments emphasized the very large discrepancies in the thermodynamic data reported for this system. As pointed out by Feufel et al. [4], this is unfortunate as the solubility limits of Mg and Si in the aluminium-rich phase are given by the boundary between the phase fields of this phase and of Mg_2Si, and thus by the Gibbs energy and enthalpy of

formation of the compound. Although the description by Yan [6, 14] of the Mg-Si system may appear to be more effective than the others, it fails to reproduce this boundary. Moreover, this author did not represent the Gibbs energy function of the Mg_2Si phase in a way appropriate for extrapolation to higher order systems. Kevorkov [5, 15] carried out a new optimization in order to avoid a liquid miscibility gap appearing far above 2000 °C as in the previous assessments. Because the assessment by Kevorkov [5, 15] was based on the previous work by Xinyan Yan [14], and will therefore suffer from the same drawbacks as detailed above, the description of the Mg-Si system given in the COST 507 data base was preferred considering that the miscibility gap in the liquid phase appears at temperatures much above any domain of interest.

Following a detailed experimental investigation, Su et al. [16] modified the central part of the Al-Mg phase diagram with respect to the version in the COST 507 data base. The resulting phase diagram is illustrated in Figure 1. As a matter of fact, it is in agreement with the older assessment made by Murray [17] and accepted by Chartrand and Pelton [18]. In this diagram, the ζ phase reported by Schürmann and Voss [19] does not appear, while the ε phase is stable only up to about 410 °C to decompose giving β and a commensurate variation of the γ phase. Metastable phases are readily formed on rapid cooling of alloys with compositions in the middle of the Al-Mg system, and this may account for the difficulty in establishing the phase diagram. Liang et al. [20] provided a CALPHAD-type assessment of the Al-Mg system which takes into account the work of Su et al. [16]. This description has been included in the COST 507 data base [13]. It will be used in the present study.

Ternary Al-Mg-Si system

There have been three experimental studies of the ternary liquidus [4, 21-22]. Losana [21] studied by thermal analysis the solidification and solid state transformations of 150 alloys with aluminium contents varying from 99 to 0.4 wt. %. The alloys were prepared from aluminium, magnesium and silicon of respectively 99.8, 99.7 and 99.4 wt % purity. The cooling rate varied between 100 and 400 °C/hour (1.67 and 6.67 °C/min). The results of Losana have not been considered in the earlier CALPHAD-type assessments because of apparent discrepancies with other data, in particular for Mg-rich alloys [6]. Although the table provided by Losana undoubtedly contains typing errors that can be only partially corrected, it seemed of value to use this information for comparison purposes in the present work. Similarly, Schürmann and Fisher [22] studied the whole liquidus surface by thermal analysis (cooling rate not given), selecting alloys along 15 lines in the whole composition triangle. These authors used 99.0 % purity silicon and observed, in some cases, the presence of intermetallic phases other than those expected. Feufel et al. [4] used high purity materials to prepare alloys with either 80, 85, 90 or 95 wt. % Al. These alloys were homogenized and then submitted to differential thermal analysis (scanning rate in the range 2 to 5 °C/min) on heating and cooling. As it will be seen later, these three sets of data are in overall agreement. A few thermodynamic data are also available which are however limited to dilute Al-rich alloys. Table 2 lists the binary and ternary invariant equilibria involving the liquid phase with labels given by Chakraborti and Lukas [7].

In the course of the optimization of the Al-Mg-Si system, Chakraborti and Lukas [3] first reassessed the Al-Si and Mg-Si systems using experimental information on both phase equilibria and thermodynamics. To describe the ternary system, these authors added ternary interaction parameters only for the liquid phase, arguing that the solubility of the third element is low for any of the solid phases in the system. They seem to have used data for solid-state equilibria corresponding only to the Al-rich corner. For equilibria involving the liquid phase, they mainly considered the work by Schürmann and Fischer [22]. In a later study, Feufel et al. [4] improved the available thermodynamic data, measuring the specific heat and formation enthalpy of Mg_2Si, and provided new vertical sections of the Al-Mg-Si system in the Al-rich part, as mentioned above. These authors performed a new CALPHAD-type assessment of the system using both their new experimental information and the same data considered previously Chakraborti and Lukas [3].

Owing to the large discrepancies in the thermodynamic data for the Mg-Si system and to the fact that ternary interactions in the Al-rich fcc phase are too small to be considered, Feufel et al. [4] emphasized that the properties of the Mg-Si system could be optimized by also considering the solubility limits of Si and Mg in the aluminum rich phase. Both Chakraborti and Lukas [3] and Feufel et al. [4] considered that there was not enough information available to determine the temperature dependence of the coefficients describing the ternary interactions in the liquid phase and adopted a linear relationship between the constant and temperature dependant coefficients. This appears quite in contrast with the fact that the description of the interactions in the liquid phase of the Mg-Si system involves 5 temperature dependent parameters in both of these studies, corresponding to 8 independent coefficients. Finally, it is worth noting that Xinyan Yan [6] showed that the assessment of Feufel et al. [4] did not reproduce satisfactorily one of the sections determined by Schürmann and Fischer [22], numbered 15 in the original paper, and representing the isopleth at 2 wt. % Si.

Reassessment of the ternary Al-Mg-Si system

This reassessment was achieved using Thermocalc® with the same assumptions used previously, i.e. that ternary interaction parameters are significant only for the liquid phase. By considering the largest possible set of experimental data for the liquidus temperatures, based on the works by Schürmann and Fischer [22] and Feufel et al. [4], the optimization procedure was repeated assuming 6 independent coefficients. It was found that the coefficients for the temperature dependent terms were not significant, so that only three constant coefficients were needed to describe the ternary interactions in the liquid. The values of these parameters are :

L_{Al}=+11882, L_{Mg}=-24207 and L_{Si}=-38223.

A very good agreement was obtained with all the experimental information shown as isoplethal sections in the earlier works [4, 22]. Figure 2 shows the section numbered 15 by Schürmann and Fischer [22] which was not well described by the previous assessment by Feufel et al. [4], as pointed out by Xinyan Yan [6]. In this figure, experimental points from

Schürmann and Fischer [22] as well as from Losana [21] are shown. As a matter of fact, these latter results show a degree of scatter for the liquidus temperatures while they show very good consistency with other data for the terminal (eutectic) reactions. Similarly, Figure 3 compares the predicted isoplethal section for 5 wt % Al with data from Losana [21] and a few results taken from Schürmann and Fischer [22]. The agreement appears again quite satisfactory for the liquidus but this figure shows that detailed examination of the effect of microsegregation on the solidification path during thermal analysis could be of interest. Figure 4 presents the isoplethal section at 85 at. % Al with experimental data from Feufel et al. [4] and Losana [21]. The overall agreement obtained appears to be much better than the one shown by Kevorkov [5]. For any other section, the agreement obtained was as good as the ones shown by Xinyan Yan [6] or Kevorkov [5].

In a parallel investigation [23], solidification and solid-state equilibria of Mg rich alloys were studied. Using as-cast and heat treated alloys with 30, 45 and 70 wt. % Mg, respectively 3.5, 3 and 2 wt. % Si, it was verified that the Al-Mg compounds do not contain any significant amount of Si, in practical terms less than the resolution of EDS i.e. about 0.1 wt. %. DTA analysis gives 448 °C and 436 °C as the temperatures for points E2 and E4 respectively. These temperatures compare well with those reported in table 2. Using a sample of alloy of composition Al-70Mg-2Si heat treated at 300 °C for seven months in a quartz ampoule filled with argon, it was possible to characterize the equilibrium between (Mg), Mg_2Si and γ. The composition of the (Mg) phase is reported on the calculated isothermal section in figure 5. As expected, the Al content in (Mg) in equilibrium with γ and Mg_2Si does not differ significantly from its value in the binary system. This result is however very different from the only other reported data, from Rokhlin and Peplyan [24] who studied the phase boundaries between the two phase domain (Mg)+Mg_2Si and the three phase domain (Mg)+Mg_2Si+γ at 300, 400 and 430 °C. In figure 5, it is seen that there is a huge discrepancy between the limit proposed by these authors at 300 °C and the present experimental and calculated limits. A similar difference appears between the calculated limit and the data from Rokhlin and Peplyan [24] for the other temperatures. It seems reasonable to disregard their results.

Finally, figure 6 shows the liquidus projection along the monovariant lines close to the Al-Mg side of the ternary system. There are three invariant eutectic points appearing with two saddle points in between. The calculated temperatures for points E2 (450 °C) and E4 (436 °C) are in good agreement with experimental data (table 2). The temperature of point E3 could not be determined experimentally and is calculated at 449 °C. Unfortunately, no experimental information is available to check the compositions of these points are correct.

Conclusion

The description of the interaction parameters in the liquid phase of the Al-Mg-Si system as given in the COST 507 data base has been improved slightly by accounting for a larger set of liquidus data than considered previously. The best description was obtained by assuming temperature independent parameters. As no other parameter was modified, the data set thus obtained maintains its highly efficient description of the solid-solid equilibria

which was due in particular to an appropriate description of the properties of the Mg_2Si phase [4]. This capability appears as an essential feature when comparing the present results to those recently proposed in similar CALPHAD-type assessments of the Al-Mg-Si system [5-6].

Acknowledgments
Partial support from ESA through the MICAST project under contract number 14347/00/NL/SH is greatly appreciated.

References

[1] Phillips H.W.L., The Institute of Metals, report n° 25, 1959
[2] Dinsdale A.T., NPL report DMA 195, 1989
[3] Chakraborti N., Lukas H.L., CALPHAD 16, 1992, 79-86
[4] Feufel H., Gödecke T., Lukas H.L., Sommer F., J. Alloys Compounds, 247, 1997, 31-42
[5] Kevorkov D., PhD thesis, Technical University of Clausthal, 2001
[6] Xinyan Yan, PhD thesis, University of Wisconsin-Madison, 2001.
[7] Chakraborti N., Lukas H.L., in Ternary alloys comprehensive compendium on constitutional data and phase diagrams, 16, 1999, 382-398
[8] Kumar K.C.H., Chakraborti N., Lukas H.L., Bodak O., Rokhlin L., in Ternary phase diagrams, ed. by Landolt and Boerstein
[9] Gröbner J., Lukas H.L., Aldinger F., CALPHAD 20, 1996, 247-254
[10] Jacobs M.H.G., Spencer P.J., CALPHAD 20, 1996, 307-320
[11] Liu Z.K. and Chang Y.A., Metall. Mater. Trans. A, 30A, 1999, 1081-1095
[12] Hansen S.C., Loper C.R., CALPHAD 24, 2000, 339-352
[13] "Thermochemical database for light metal alloys", edited by I. Ansara, European Commission, 1995; and COST 507, European Commission, EUR 18171, 18499 and 18475, 1998
[14] Xinyan Yan, Zhang F., Chang Y.A., J. Phase Equilibria, 21, 2000, 379-384
[15] Kevorkov D., Schmid-Fetzer R., Zhang F., J. Phase Equilibria Diffusion, 25, 2004, 1-12
[16] Su et al., J. alloys and Compounds 247, 1997, 57-65
[17] Murray J.L., Bull. Alloy Phase Diagrams, 3, 1982, 60-74
[18] Chartrand P., Pelton A.D., J. Phase Equilibria, 15, 1994, 591-605
[19] Schürmann E., Voss H.J., Giessereiforschung 33, 1981, 43-46
[20] Liang P. et al., Z. Metallkd. 89, 1998, 536-540
[21] Losana L., La Metallurgia Italiana, 23, 1931, 367-382
[22] Schürmann E., Fischer A., Giessereiforschung 29, 1977, 161-165
[23] Valdes R., Freulon A., Deschamps J.-B., Ma Qian, J. Lacaze, proceedings of the Fourth Conference on Solidification and Gravity, 2004, in press
[24] Rokhlin L.L., Pepelyan A.G., Russian Metallurgy, 6, 1988, 176-179
[25] Birchenall C.E., Riechman A.F., Metall. Trans 11A, 1980, 1415-1420

Table 1- Characteristics of the stable solid phases of the Al-Mg-Si system [7].

Phase	*Prototype*	*Pearson symbol*	*Space group*	*Lattice parameters (Å)*	*Formula (COST 507)*
(Al)	Cu	c*F*4	$Fm\bar{3}m$	a=4.0494	solid solution
(Mg)	Mg	h*P*2	*P*63/mmc	a=3.2094 c=5.2107	solid solution
Si	C (diamond)	c*F*8	*F*d3m	a=5.4306	solid solution
Mg_2Si	CaF_2	c*F*12	*F*m3m	a=6.338	Mg_2Si
β	Al_3Mg_2	c*F*1832	$Fd\bar{3}$	a=28.239	$Al_{140}Mg_{89}$
ε	$Co_5Cr_2Mo_3$	h*R*53	$R\bar{3}$	a=12.8254 c=21.7478	$Al_{30}Mg_{23}$
γ	αMn	c*I*58	$I\bar{4}3m$	a=10.4811 to 10.5791	$Mg_5(Mg,Al)_{12}(Al,Mg)_{12}$

Table 2 - Equilibria involving the liquid phase : experimental and calculated (this work) invariant reactions in the ternary Al-Mg-Si system (reactions are labelled according to Kumar et al. [8]).

Reaction	*temperature (°C)*	*Mg (at. or wt. %)*	*Si (at. or wt. %)*	*reference*
Liquid=(Al)+Si+Mg_2Si	558	4.97	14.6	*
point E1	550	4.8	14.1	22
	560	5.1	12.6	25
	558			4
	557	5.5	13.6	this work
Liquid=Mg_2Si+(Al)	595	8.3	4.6	*
point e3	593			22
	595			4
	596	10.1	4.0	this work
Liquid=Mg_2Si+(Al)+β	448	33.9	0.07	*
point E2	444	34.5	<0.2	22
	448			23
	450	36.6	0.06	this work
Liquid=Mg_2Si+β				
point e6	451	39.0	0.06	this work
Liquid=Mg_2Si+β+γ				
point E3	449	42.5	0.05	this work
Liquid=Mg_2Si+β+γ				
point e5	463	53.8	0.08	this work
Liquid=Mg_2Si+γ+(Mg)	434	67.5	<0.2	22
point E4	436	69.9	<0.1	23
	436	69.0	0.06	this work

* Hanemann E. and Schrader A. ("Ternäre Legierungen des Aluminiums", Düsseldorf, 1952), cited by Schürmann and Fischer [22]

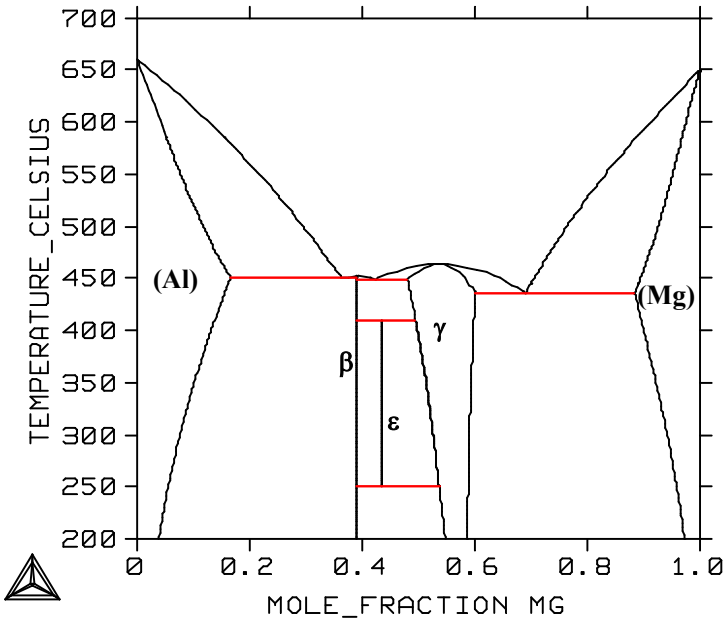

Figure 1 - Al-Mg phase diagram calculated with the COST 507 data base.

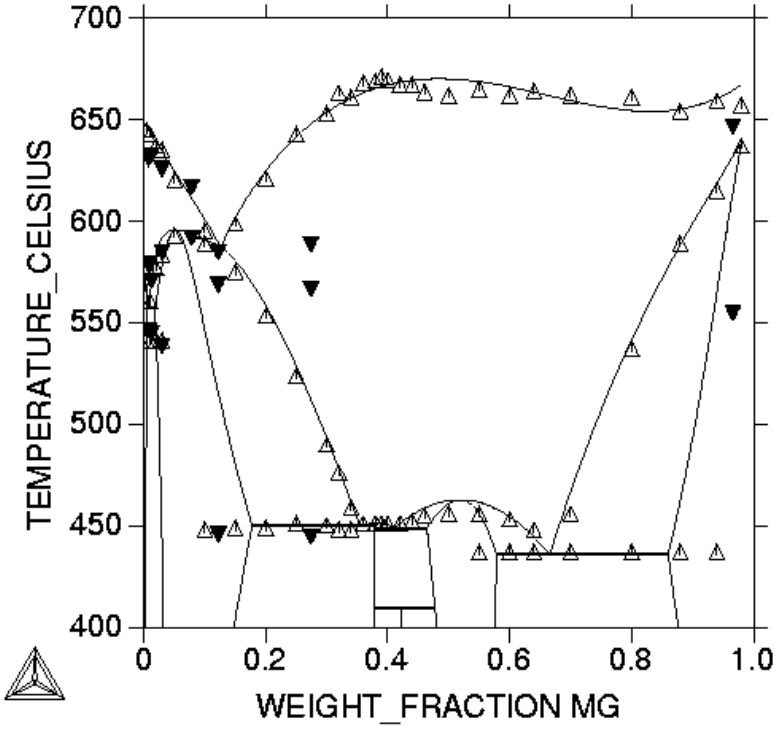

Figure 2 - Isoplethal section at 2 wt % Si of the Al-Mg-Si system. Open and solid triangles show experimental points from Schürmann and Fischer [22] and Losana [21] respectively.

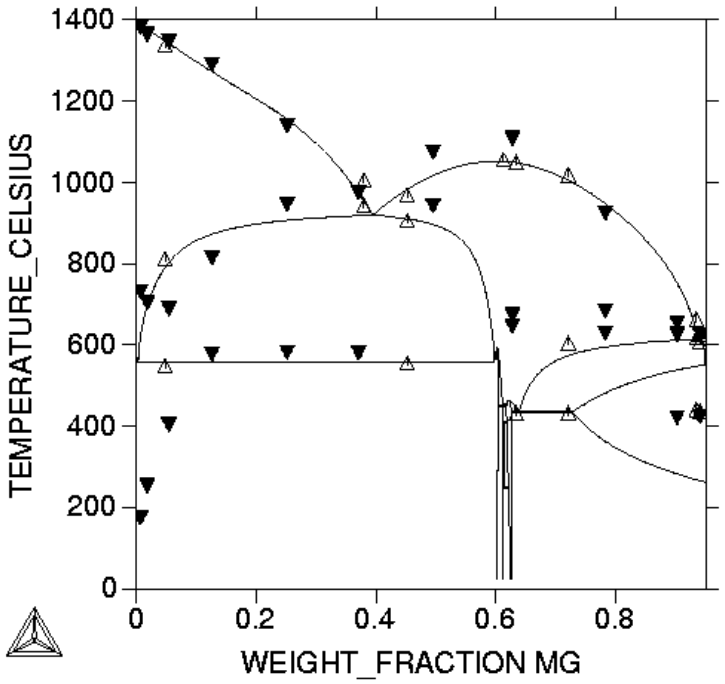

Figure 3 - Isoplethal section at 5 wt % Al of the Al-Mg-Si system. Open and solid triangles show experimental points from Schürmann and Fischer [22] and Losana [21] respectively.

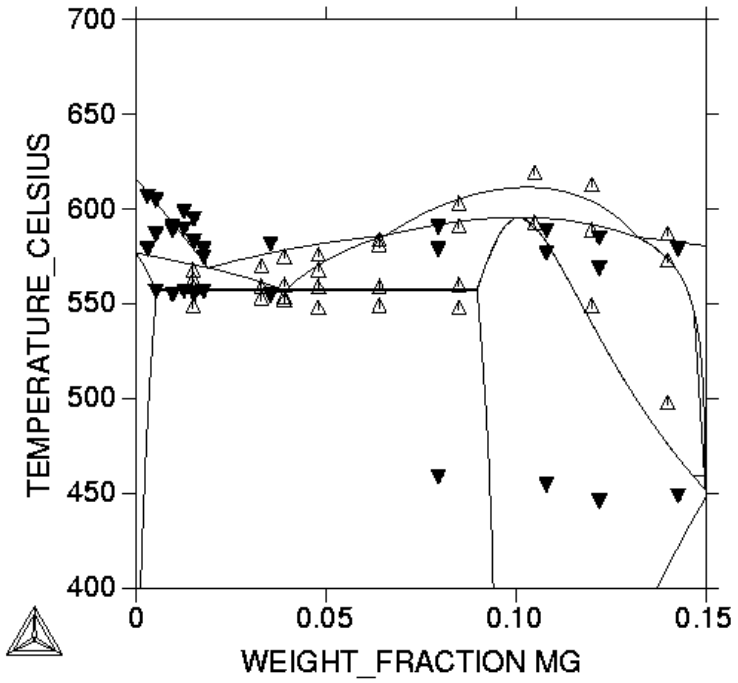

Figure 4 - Isoplethal section at 85 wt % Al of the Al-Mg-Si system. Open and solid triangles show experimental points from Feufel et al. [4] and Losana [21] respectively.

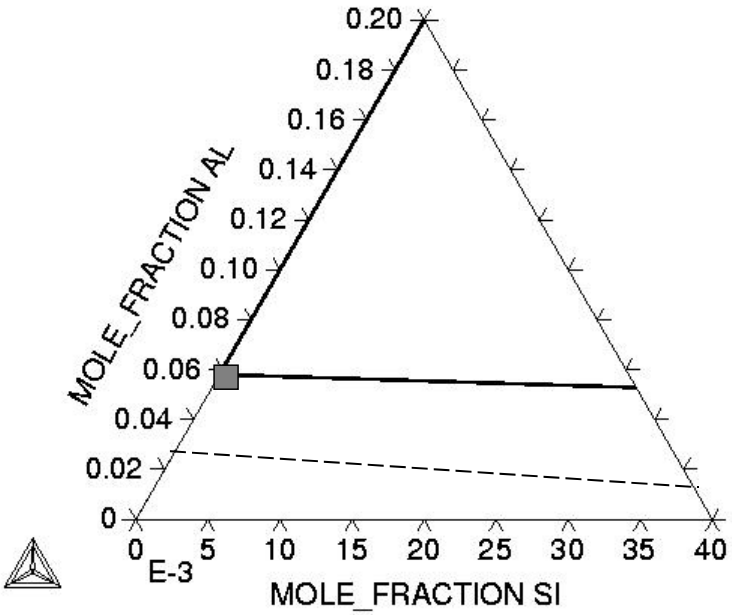

Figure 5 - Isothermal section at 300 °C comparing the calculated (solid line) and experimental (dashed line) [24] limit between the (Mg)+Mg_2Si and (Mg)+Mg_2Si+γ phase fields. The grey square represents experimental data according to Valdes et al. [23].

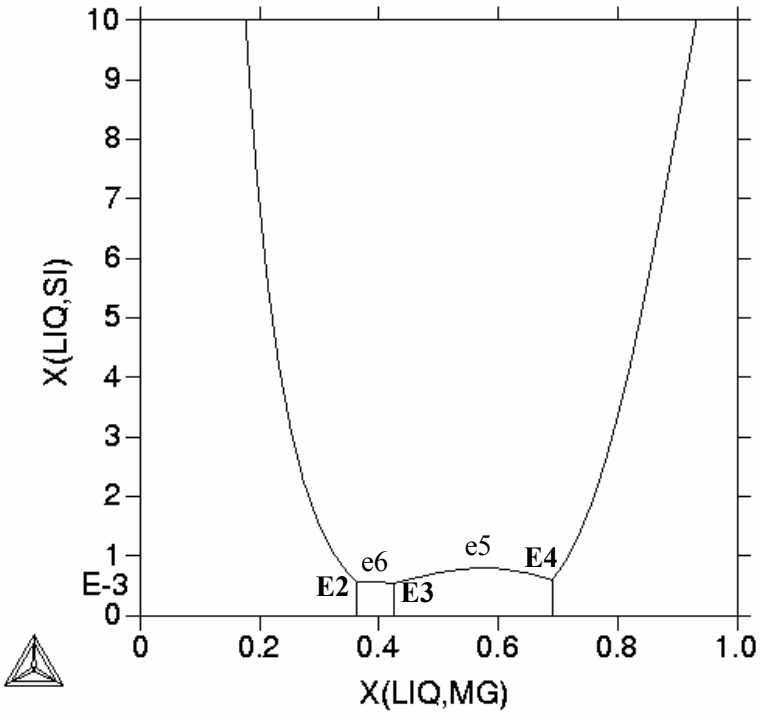

Figure 6 - Enlargement of the liquidus projection close to the Al-Mg binary edge.

Phase equilibria in Al-Mg-Si-Mn system

Complément VI

VI.1 Phase equilibria and solidification in Al-Mg-Si-Mn system.

Manganese plays a critical role as iron remover in aluminium and magnesium alloys [1], it may be used as grain refiner for nucleating primary magnesium grains [2], and its most important effect is on the corrosion resistance of aluminium alloys [1-3]. For a better understanding of solidification and phase transformations in aluminium and magnesium alloys, a CALPHAD-type description of the Al-Fe-Mn-Si system would be useful. In this line, attempts to get new experimental information through solid/solid and solid/liquid diffusion couples were carried out.

A review of the Al-Mn-Si ternary system has been reported recently by N. Krendelsberger et al. [4] who identified and characterized ten ternary stable phases τ_1, τ_2 … τ_{10}. The main characteristics of these phases are summarized in Table VI-1. Young Du et al. [5] published a CALPHAD-type thermodynamic assessment of the Al-Mn-Si system which agrees satisfactorily with the experimental data showed in [4]. The 550 °C isothermal section of the phase diagram is shown in the Figure VI-1. Nine ternary phases and several extended ternary solid solution of binary phases occur. A thermodynamic description of the ternary Al-Mg-Mn is included in the COST 507 base that is only valid for the Al rich part [6]. M. Ohno and R. Schmidt-Fetzer [7] presented recently a thermodynamic description of the whole Mg-Al-Mn system which agrees with previous experimental information. The set of parameters assessed of the Al-Mn system presented in the introduction of this manuscript have been introduced in the COST 507 database to calculate the Al-Mn-Si ternary system. It was found not possible to obtain the isothermal section shown in Figure VI-1, in particular because the domain of the τ_8 phase was not described satisfactorily.

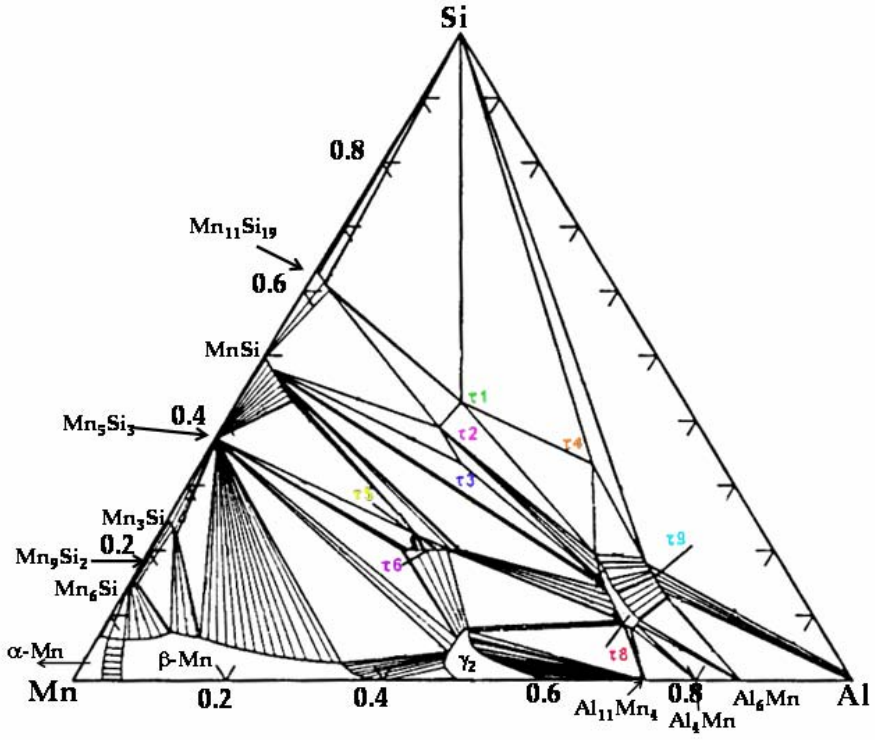

Figure VI-1: Isothermal section at 550 °C calculated by Young Du et al. [4].

Phase denomination	*Formulae*	*Space group / Pearson symbol/ Type*	*Compositions observed (at.%)*	T_f *(°C)*
τ_1	$Al_2Mn_2Si_3$	$P\bar{6}$ / *h*P21	28 Mn, 28.5 Al, 43.5 Si	830
τ_2	$Mn(Al_{1-x}Si_{1+x})$ x = 0.12	$P6_222$ / *h*P9 / $CrSi_2$	34 Mn, 29 Al, 37 Si	949
τ_3	AlMnSi	F*ddd* / *o*F24 / $TiSi_2$	34 Mn, 34 Al, 32 Si	893
τ_4	Al_3MnSi_2	P4/n / *t*P48	15.5 Mn, 52 Al, 32.5 Si (If Fe replaces Mn, it seem to be the δ-phase)	773
τ_5	$Al_3Mn_4Si_2$	Unknown but not FeSi-type as proposed by Gasik	45 Mn, 33 Al, 22 Si	1023
τ_6	$Al_{2-x}Mn_{2+x}Si$ $0 < x < 0.5$	Unknown but not FeSi-type as proposed by Gasik	45 Mn, 40 Al, 15 Si	1035
τ_7	$Al_{\sim 5}Mn_{\sim 4}Si_{\sim 1}$	Unknown	39 Mn, 50 Al, 11 Si 37 Mn, 52 Al, 11 Si	Not determined
τ_8	β-AlMnSi $(Al,Si)_{10}Mn_3$	$P6_3/mmc$ / *h*P26 / $Al_{10}Mn_3$	26Mn, 61 Al, 13 Si 25 Mn, 70 Al, 5 Si	1058
τ_9	α-AlMnSi Al_9Mn_2Si	$Pm\bar{3}$ / *c*P138 / Al_9Mn_2Si	17.1 Mn, 71 Al, 11.9 Si	576
τ_{10}	Al_2MnSi_3	I4/mcm / *t*I24 / Ga_5Pd as Panday[8]	17 Mn, 35 Al, 48 Si	844

Table VI-1: Description of the ternary solid phases of the system Al-Mn-Si [4]. T_f is the decomposition temperature.

To prepare solid-solid diffusion couples, we tried to fabricate sintered compacts from powders. A mix of manganese, magnesium and silicon powders, all of purity 99.99%, was prepared and compacted by Spark Plasma Sintering (SPS) with a die 8 mm in inner diameter. During SPS processing, a uniaxial pressure of 50 MPa was applied upon the sample through the graphite punches and maintained during heating up to 400 °C and during a 5 min hold at that temperature. The compact was then polished to remove the surface carbon contamination and its microstructure was observed using scanning electron microscopy (SEM) as illustrated in Figure VI-2. It was noted a very loose contact between the different powder grains, mainly because of the presence of oxides everywhere.

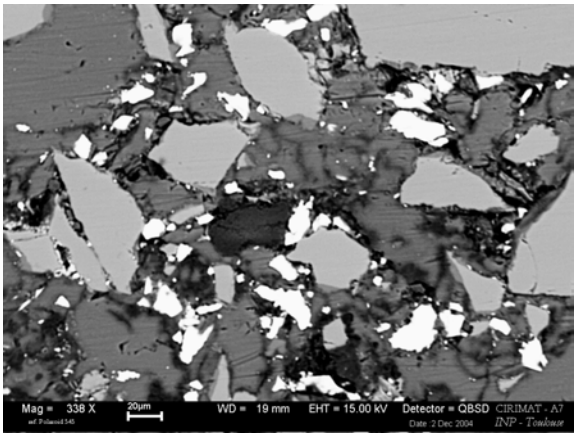

Figure VI-2: SEM micrograph of sample sintered at 400 °C.

As we did not succeed to fabricate Al-Mn-Si alloys, pieces remaining from previous studies were kindly provided by N. Krendelsberger and J.C. Schuster (University of Vienna). Solid-solid diffusion couples were thus prepared by assembling a small piece of one of these alloys with a piece of A70 alloy. The diffusion couples thus prepared were heat-treated in vacuum furnace at 400 °C during 15 days. After optical and SEM observation, no reaction zone could be identified.

These attempts to achieve solid-state diffusion couples having failed, we found it possible to prepare diffusion couples with a liquid phase provided by the ternary A70 alloy in which the eutectic made of $Al_{12}Mg_{17}$ and (Mg) phases melts at 436 °C. Solid/liquid diffusion couples were prepared with the experimental set-up shown in Figure VI-3. The

chemical composition of the Al-Mn-Si alloys used in this work and the annealing conditions are listed in Table VI-2.

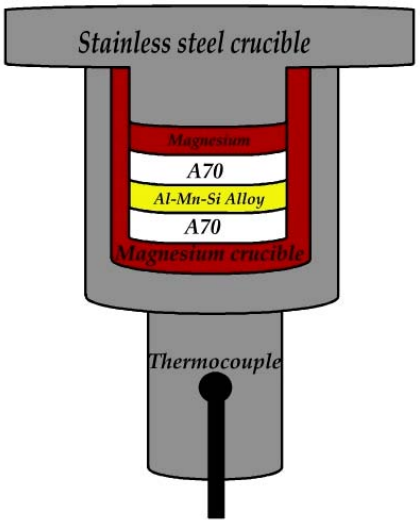

Figure VI-3: A cross-section of the experimental set-up. The stainless steel cylinder is placed onto the thermocouple.

Reference	*Al*	*Mn*	*Si*	*T_1 (°C)*	*t_1 (min)*	*T_2 (°C)*	*t_2 (hr)*	*Phases formed*
N59	45	45	10	600	180			Dissolution
				550	240			$Al_{11}Mn_4$-($Al_{72}Mn_{25}Mg_3Si_1$)
N55	36	45	19	600	120			Dissolution
				550	180			$Al_{11}Mn_4$ – ($Al_{75}Mn_{24}Si_1$)
E	20	45	35	600	120			Dissolution
N72	30	40	30	600	15	550	3	$Al_{11}Mn_4$-($Al_{72}Mn_{26}Si_2$)
F	10	40	50	600	5	550	4	Dissolution
A	5	75	20	550	15	450	8	$Al_{67}Mn_{32}Si_1$ Mn_3Si-($Mn_{74}Si_{22}Al_4$)
B	20	70	10	550	15	450	8	$Al_{66}Mn_{27}Si_1$
C	65	20	15	600	15	450	8	Dissolution

Table VI-2 : Al-Mn-Si composition (at. %), annealing conditions and the phases formed at the interface.

For the first five preliminary experiments, a pre-treatment of the A70 tablets was first performed at 550 °C. Each tablet was introduced in an Mg crucible and hold at temperature during 30 minutes under argon. This led to partial melting of the material and settling of undissolved Mg_2Si crystals in the lower part of the sample, so that they would not perturb the contact between the melt and the surface of the Al-Mn-Si pellet during diffusion coupling with the solid Al-Mn-Si alloy. For the final assemblage of the diffusion couple, a number of steps were achieved:

- The A70 tablet was removed from the Mg crucible and its upper surface was polished and cleaned ultrasonically, and finally replaced at the bottom of the crucible;
- The Al-Mn-Si tablets, which were conserved under vacuum as long as possible to avoid oxidation, were finally rinsed in dilute nitric acid before being placed above the A70 tablet;
- Finally a second tablet of A70 was placed on top.

It was expected that this assemblage would guarantee that the Al-Mn-Si alloy should be wet by the liquid. The Mg crucible was closed with a piece of pure Mg and then fitted in a stainless steel crucible on the top of which a cover was simply put as shown in Figure VI-3. This assemblage was then placed onto a thermocouple maintained with an alumina rod and introduced inside a lamp furnace that was then evacuated and later filled with argon. During the experiments, a low argon flux was maintained. After annealing for a time t_1 at temperature T_1 (both given in Table VI-2), the samples were cooled by switching off the power and increasing the argon flux. The rate of cooling was of the order 2 °C per minute.

For the N72, F, A, B and C solid/liquid diffusion couples, the pre-treatment of the A70 alloy was not made. Instead, the diffusion couple was first heated for a time t_1 at a temperature T_1 higher than the one planned for equilibration (time t_2, temperature T_2). This first stage ensured that a large quantity of melt formed and wetted the solid Al-Mn-Si pellet. The experiments performed are listed in Table VI-2.

After cooling, the solid/liquid diffusion couples were mounted and polished down to the middle of the sample. SEM observation and EDS analysis of the cross sections was carried out to obtain the composition of the phases, and in some cases concentration profiles across the diffusion zone were acquired. All the figures presented below are SEM micrographs across the lower junction of the "sandwich" diffusion couples with the Al-Mn-Si alloy on the right side and the A70 alloy on the left side. Figure VI-4 shows the interface of the first three diffusion couples in Table VI-2, which were equilibrated at 600°C. The surfaces of the Al-Mn-Si alloys became irregular and recessed compared to their initial position showing intense dissolution. As observed in Figure VI-4, the details of the dissolution process differ from one Al-Mn-Si alloy to another. Also, we can note in Figure VI-4b the presence of small Mn-rich precipitates (which appear with bright contrast) within the re-solidified A70 alloy but far away of the interface.

For the solid/liquid diffusion couple N59 a EDX profile composition was taken every 2 μm along the line line 1-2 as seen in Figure VI-5a. The analyses were carried out using an acceleration of 15 keV and 1.5 nA current and processed for ZAF correction. The concentration profiles across the diffusion zone are shown in Figure VI-5b. Unless expected, there is no Mg having entered the phases in alloy N59, and no measurable Mn was found in A70 alloy apart for the small Mn-rich precipitates. The identification and characterization of the Al-Mn-Si phases was done by comparison to the compositions reported by Krendelsberger et al. [4].

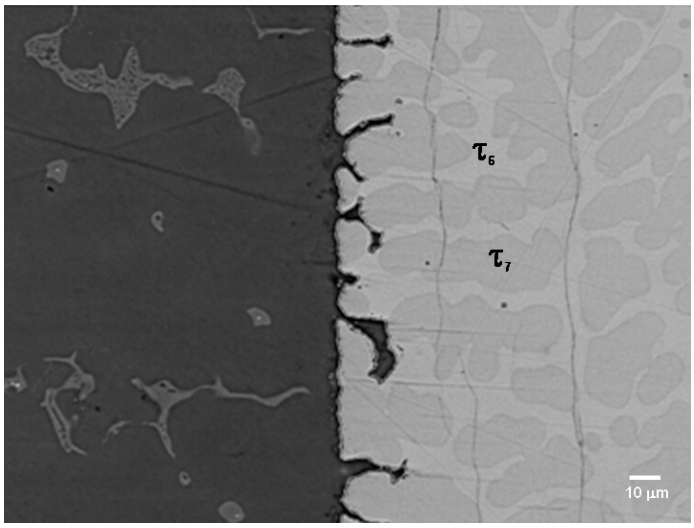

a) N59

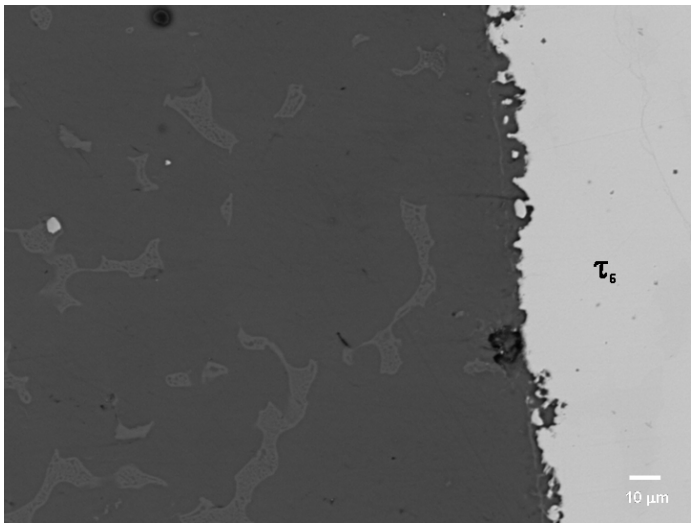

b) N55

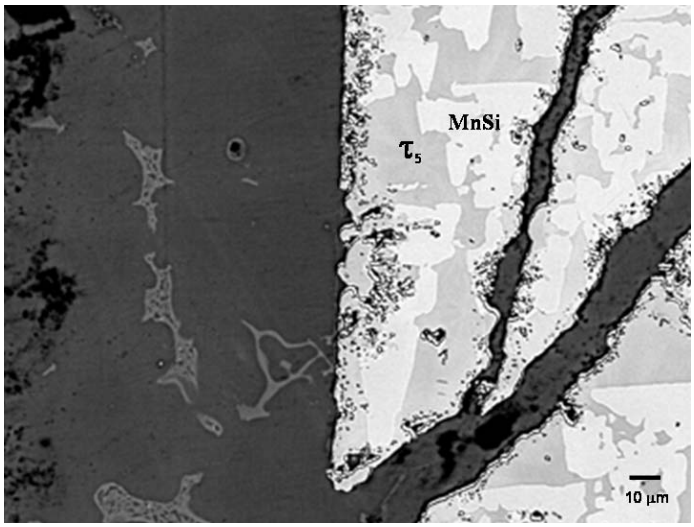

c) E

Figure VI-4: Solid/liquid diffusion couples equilibrated at 600 °C.

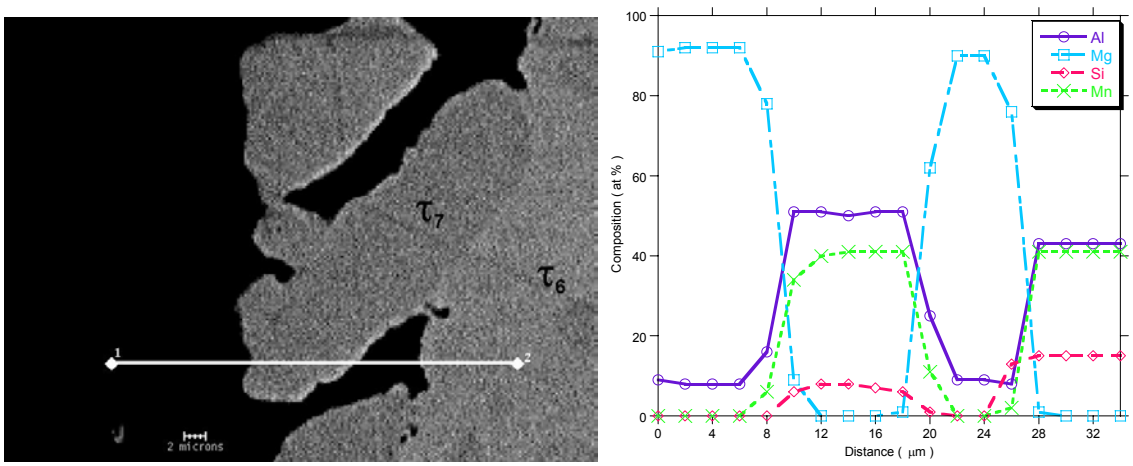

a) *b)*

Figure VI-5: Enlargement of the N59 boundary diffusion couple (a) and profile quantitative (b).

Figure VI-6a shows an enlarged view of the interface of the A70/E diffusion couple. The dark spots and areas on the right side of the interface are due to A70 liquid alloy having penetrated the E alloy. Figure VI-6b shows the concentration profiles along the line indicated in Figure VI-6a. Spot countings were made every 4 µm. It is seen again that no measurable Mn was found in A70 alloy and that no Mg entered in τ_5 phase. Additional spot measurements showed that the other phase in this alloy is MnSi. There is a significant dissolution of the Al-Mn-Si alloy within the liquid phase.

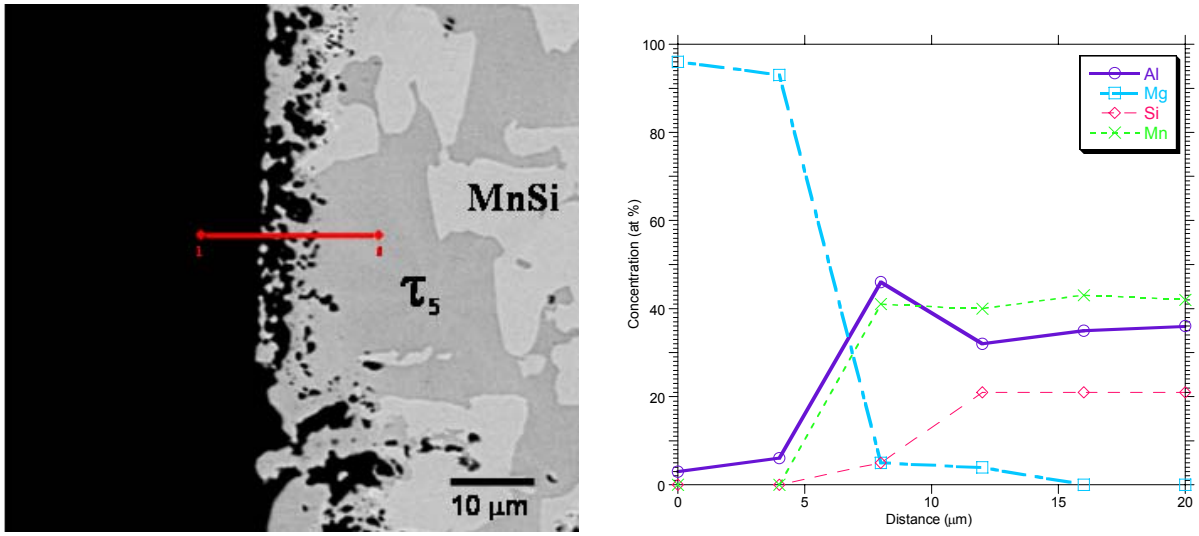

a) *b)*

Figure VI-6: Backscattered-electron micrograph of the A70/E couple annealed at 600 °C for 2 hours (a). Concentration profiles through the interface (b).

Figure VI-7a and b show the two diffusion couples of the first series equilibrated at 550 °C where it is seen that a continuous but irregular layer was developed at the interface. Some cracks throughout the N55 alloy are observed. EDX analysis of the cross section of the N55 couple was carried out using a stabilised electron beam of 15 keV energy and 1.5 nA current for 100 seconds to obtain the concentration profiles across the diffusion zone, that were determined by spot counting every 1 μm along the two lines showed in Figure VI-7b and are plotted in Figure VI-7 c and d, respectively. For both diffusion couples, the intermetallic $Al_{11}Mn_4$ (75 at.% Al, 24 at. % Mn, 1 at. % Si) formed at the interface between the Al-Mg-Si liquid and the Al-Mn-Si alloy.

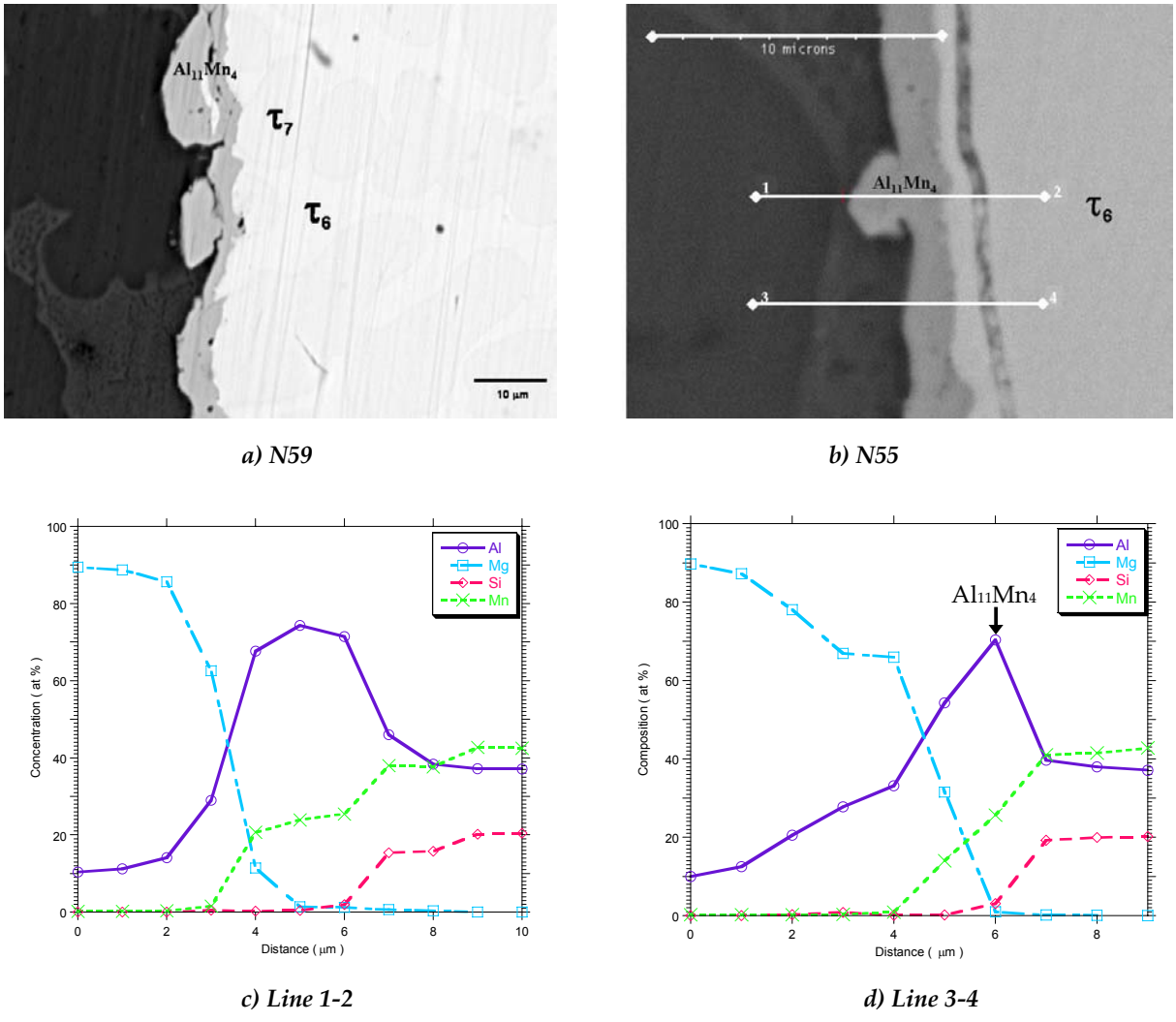

a) N59

b) N55

c) Line 1-2

d) Line 3-4

Figure VI-7: N59 (a) and N55 (b) diffusion couples equilibrated at 550 °C, and concentration profiles along lines 1-2 (c) and 3-4 (d) for the couple A70/N55.

The change between the first and second series of experiments was decided at the end of this first series in order to shorten the trials. The initial idea was that melting of the eutectic $Al_{12}Mg_{17}$ + (Mg) would lead to a better homogenisation of the liquid, with possibly partial dissolution of the Al-Mn-Si alloy and later precipitation of quaternary compounds upon cooling after the equilibration treatment. After the two-step annealing, the diffusion couples were polished and observed in SEM as before. EDX measurements were performed on every sample on all the phases observed. However, some problems arose when attempting to analyse a thin layer (<1 μm) in which case the EDX signal from the layer was convoluted with the one from the substrate. In those cases, the analyses were done again with an acceleration of 8 keV and the counting time was increased to 200 seconds to improve the analysis accuracy as was described in the introduction.

Figure VI-8a shows a cross section SEM micrograph of the A70/N72 diffusion couple at the issue of the two treatments. The contact between the upper A70 alloy and the Al-Mn-Si alloy was not achieved. The A70 microstructure is mainly composed of (Mg) dendrites, i.e. most of Al and Si solutes that are part to the eutectic (Mg + $Al_{12}Mg_{17}$) diffused to the Mg crucible. Figure VI-8b shows the microstructure at the lower interface between these two alloys. A continuous Mg_2Si layer separates the (Mg) dendrites from the Al-Mn-Si alloy. In the centre of the Al-Mn-Si sample, the microstructure is composed of the MnSi and τ_3 intermetallics originally detected in the as-cast microstructure. Some small $Al_{11}Mn_4$ precipitates and a two-phase network composed of $Al_{11}Mn_4$ and a second phase having the same colour than (Mg) dendrites formed between the Mg_2Si layer and the intermetallics. From these microstructures, we can assume that during the first treatment (600 °C) the dissolution process of the MnSi and τ_3 phases started at the solid/liquid interface. In the second step of the treatment at 550 °C, the Mg_2Si layer developed and subsequently or together started the growth of the $Al_{11}Mn_4$ network. It is possible that during the cooling the Mg_2Si layer increased in thickness while the network of $Al_{11}Mn_4$ and the dark phase formed. EDX measurements were made in the different phases of the diffusion couple, including several locations of the layer, and the results are shown in Table VI-3.

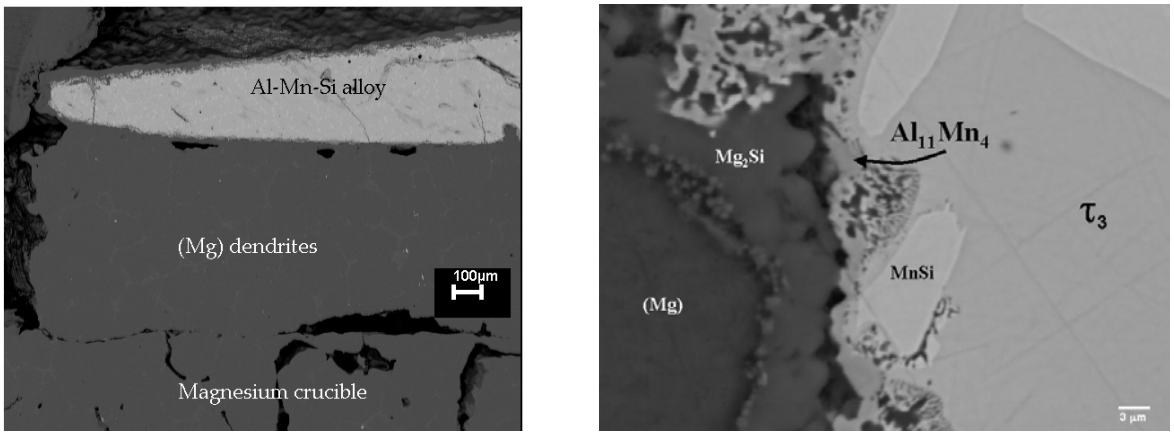

a) *b)*

Figure VI-8: A cross section from A70/N72 (T_1= 600 °C, 15 min; T_2=550 °C, 3 h) diffusion couple a). A solid/liquid interface b).

N72	*Al*	*Mg*	*Mn*	*Si*
Mg_2Si	0	62.86	0	37.15
(Mg)	7.31	92.64	0	0.05
$Al_{11}Mn_4$	71.77	0.20	25.57	2.47
MnSi	7.39	0.00	43.47	49.14
τ_5	37.52	0.00	29.84	32.64

Table VI-3: Phase compositions in the A70/N72 couple.

A low magnification SEM micrograph of the A70/F couple annealed at 600 °C for 5 min and at 550 °C for 4 hours is presented in Figure VI-9a that shows the entire diffusion couple with the Al-Mn-Si alloy dissolving between the two A70 pallets. Some white fine Mn rich particles were observed in the upper A70 alloy and in the Mg tablet. The microstructure in the centre of the Al-Mn-Si was composed of three phases that were identified as MnSi, τ_2 and $Mn_{11}Si_{26}$. Between these phases and the (Mg) dendrites, at the interface, numerous white intermetallics were present as is indicated in Figure VI-9b. Their compositions were measured by EDX and are given in Table VI-4. The white small Mn-rich precipitates seen in Figure VI-9a correspond to $Al_{11}Mn_4$ compound, and could possibly form during cooling of the sample to room temperature. Near to the Al-Mn-Si alloy and to the magnesium dendrites, $Al_{11}Mn_4$ precipitates were possibly formed by the dissolution of the τ_2 phase. Around of the MnSi precipitates, as shown in Figure VI-9c, these precipitates are surrounded by a network that shows the probable formation of an eutectic structure with the (Mg) dendrites.

	Al	***Mn***	***Mg***	***Si***
$Al_{11}Mn_4$	73.1	25.7	0.2	0.3
τ_2	27.63	34	0	38.33
$Mn_{15}Si_{26}$	3.2	36.9	0	59.9
MnSi	1.2	50	0	48.8
(Mg)	4.0	0.0	96.0	0.0
Mg_2Si	0.0	0.0	67.0	33.0

Table VI-4: composition (in at. %) of the phases in the A70/F couple.

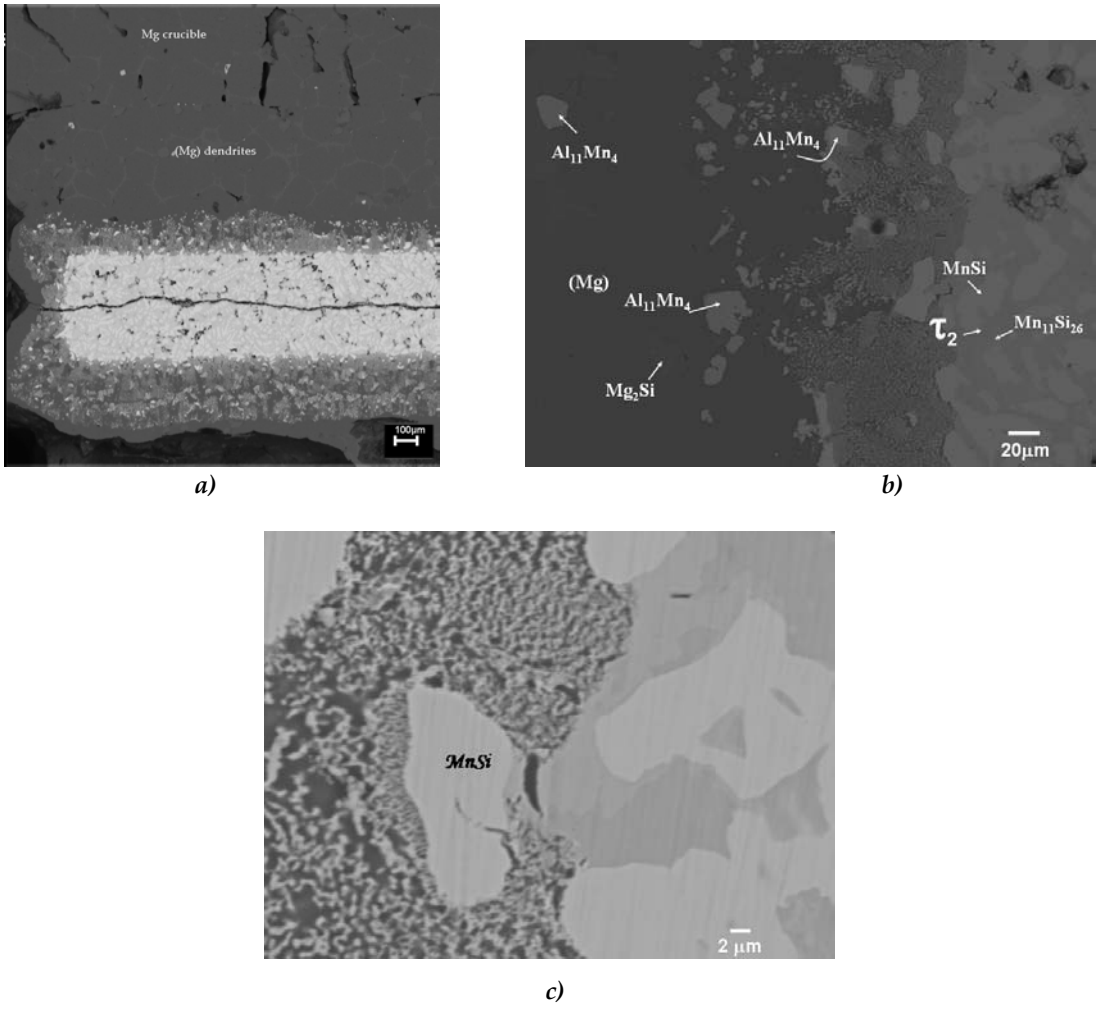

Figure VI-9: SEM images of A70/F (5Al-75Mn-20Si) annealed at 550 °C for 4 hours. Cross section (a). The microstructure of the $Al_{11}Mn_4$ phase in the Mg liquid and the Al-Mn-Si microstructure of the three-phase fields MnSi +τ_2 + $Mn_{11}Si_{26}$. (b). An MnSi precipitate that shows a eutectic-like structure of the MnSi and magnesium.

The initial state of the C alloy was characterized by N. Krendelsberger who found the τ_8 and τ_9 phases by X-ray and EDX technique. A section of the A70/C diffusion couple annealed at 450 °C is shown in Figure VI-10a and an enlargement in Figure VI-10b. The phase characterisation was done from the EDX measurements as indicated in Figure VI-

10b. According to the reaction scheme for the entire Al-Mn-Si system calculated by N. Krendelsberger the temperature established for the ternary eutectic L = τ_9 + (Si) + (Al) is 576 °C. During the first stage of heating at 600 °C, the temperature is high enough to starts melting of both eutectics [L = (Mg) + $Al_{12}Mg_{17}$ and L = τ_9 + (Si) + (Al)] whilst the τ_8 phase remains solid. Therefore the liquid will be enriched in these elements (Al, Mn, Si). During the cooling from 600 to 450 °C polygonal grey crystals of Mg_2Si solidified at about 510°C, (see the Figure IV-10b). The partial solidification continues with precipitation of (Mg) and transformation of the $Al_{11}Mn_4$ phase and ends with the eutectic L = (Mg)+ $Al_{12}Mg_{17}$. All these phases are indicated in the Figure VI-10b. The intermetallic τ_8 (62 at. % Al, 23.6 at. % Mn, 14.0 at. %Si) is surrounded by the $Al_{11}Mn_4$ (72.5 at. %Al, 26.9 at. % Mn, 0.3 at. % Si, 0.34 at. % Mg). This microstructure (L = (Mg) + $Al_{12}Mg_{17}$ + $Al_{11}Mn_4$) is quite consistent with the isotherm at 430 °C calculated by M. Ohno [7]. M. Ohno and R. Schmid-Fretzer [7] assessed the Mg-Al-Mn system with experimental data based on the solubility of manganese in Mg-rich alloys and showed some calculated isothermal section in the Mg-rich corner which they compared with experimental data. The more important information on the types of precipitating phases was carefully determined by [9] and is quite consistent with the results calculated by M. Ohno.

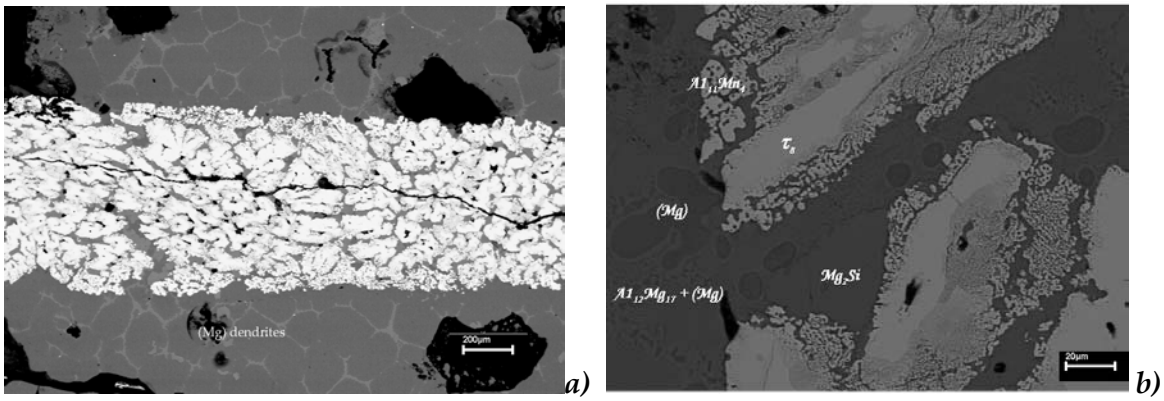

a) *b)*

Figure VI-10: Backscattered-electron micrographs of the A70/C couple annealed at 450 °C for 8 hours a) and enlarged microstructure at the centre of the couple. The $Al_{11}Mn_4$ precipitates have a globular morphology in the $Al_{12}Mg_{17}$ + (Mg) region, leaving the possibility of an eutectic transformation b).

Alloy A was characterized by N. Krendelsberger who found β_{Mn} and Mn_3Si phases by X-ray and EDX. The cross section of the annealed couple is shown in Figure VI-11 a and b.

The contact between the two alloys was not well established in some places whereas in other areas it was possible to observe the formation of two layers of approximately 4 μm in width each as seen in Figure VI-11b. The first of these layers is single phase whereas the second contains two phases. The concentration profile recorded across the diffusion zone, along the line marked with crosses, is shown superimposed upon the micrograph in Figure VI-11b. This profile shows that the first layer has a composition close to the one of Al_8Mn_5. In the second layer, the phase β_{Mn} was observed as little precipitates appearing in white contrast within in a gray like matrix of Mn_3Si. The layers have been formed with a constant concentration.

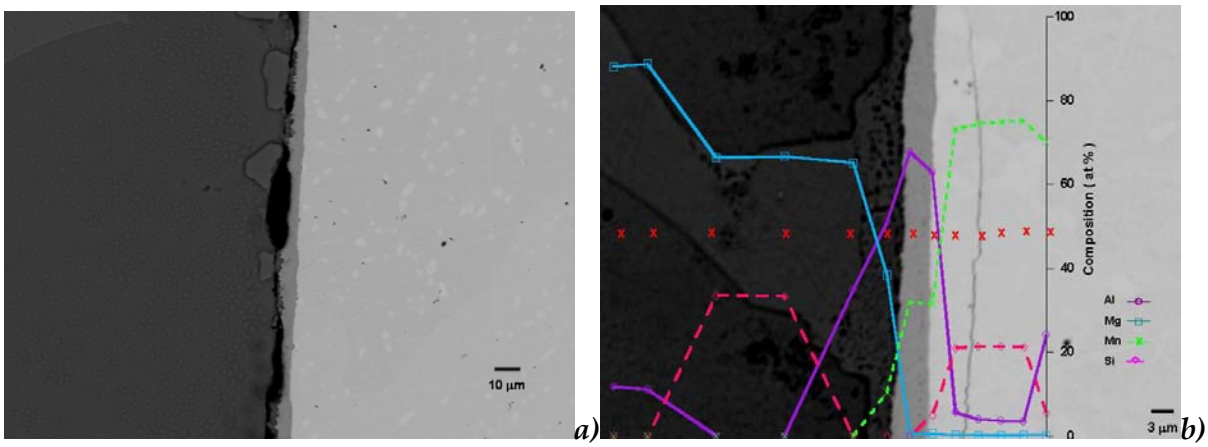

a) ***b)***

Figure VI-11: SEM images of A70/A diffusion couple annealed at 450 °C for 8 hours and composition profile across the interface.

Figure VI- 12 presents the observations made on the diffusion couple A70/B annealed at 450 °C during 8 hours. The microstructure close to the solid/liquid interface shows dark spots that contain oxygen as shown in Figure VI-12a. The microstructure consists of a one-phase layer of a phase with a composition near to the one of Al_8Mn_5. A close inspection of the Al_8Mn_5 layer reveals isolated τ_6 precipitate of 1 μm with an average composition of 36.1 at. % Al, 42.3 at. % Mn and 21.5 at. % Si dispersed along the Al_8Mn_5/Mn_5Si_3 interface. This indicates the existence of the three-phase equilibrium $Al_8Mn_5+\tau_6+Mn_5Si_3$ in the Al-Mg-Mn-Si system at this temperature. The Figure VI-12b shown the concentration profiles recorded across the diffusion zone, along the indicated lines. The solid and dashed lines relate respectively to the profiles recorded along lines 1-2 and 3-4. In the area with lighter

contrast at the right, the aluminium, manganese and silicon contents were constant. Due to the poor contrast, Figure VI-12a and b do not show that the layer with light contrast is in fact composed of three phases, β_{Mn}, Mn_5Si_3 and Al_8Mn_5. This is demonstrated with the average composition profiles recorded by means of rectangles (20x110µm) which are shown in Figure VI-12c. In the light grey layer, a composition gradient in aluminum was observed which is related to the presence of the three phases mentioned above. Away from this layer, the profile shows a constant composition until the end of the sample.

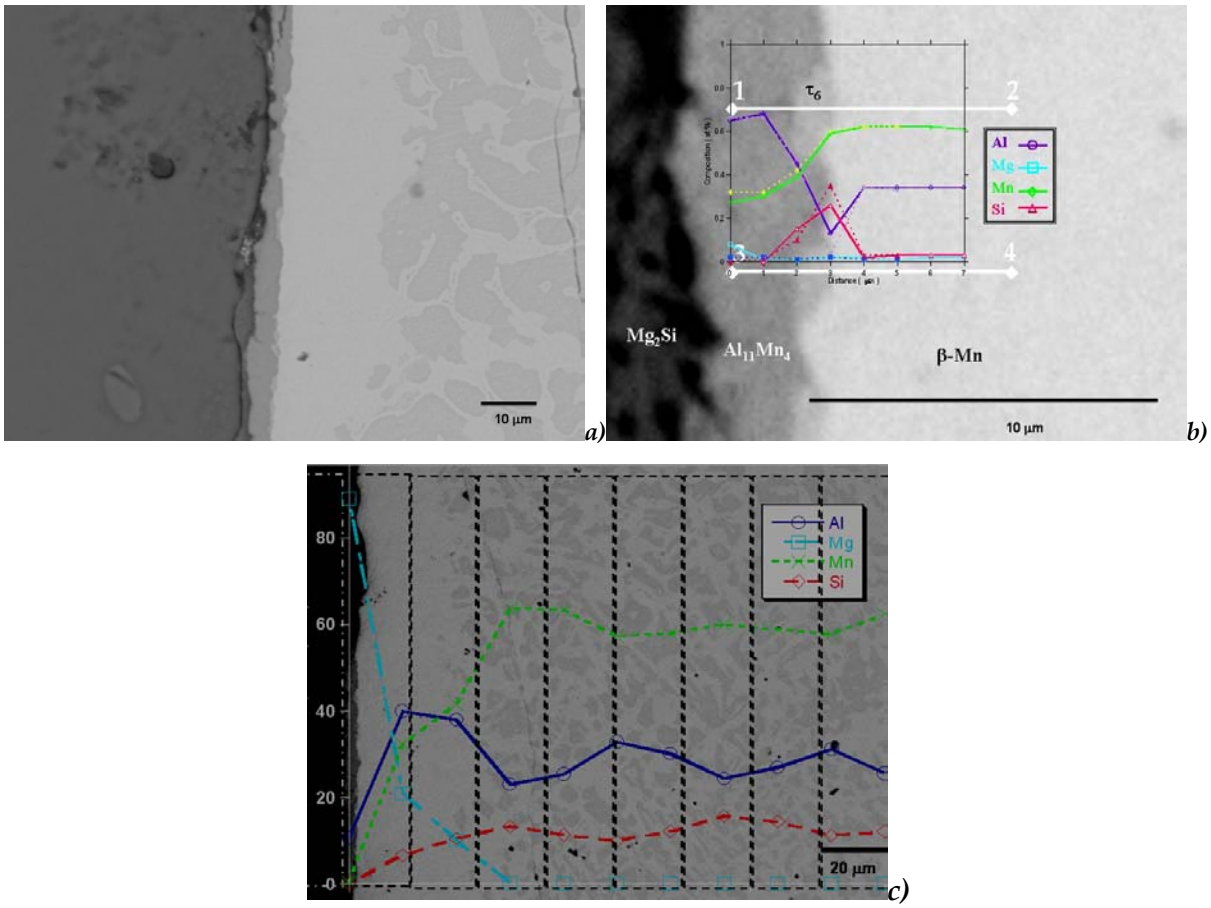

Figure VI- 12 : SEM micrographs of A70/B diffusion couple annealed at 450 °C for 8 hours a). Localisation and composition in the interdiffusion zone d). A70/B diffusion couple on the right side of the interface and where the profiles have been traced c).

The microstructure and composition of the intermetallics in the Al-Mn-Si-Mg system has been studied by diffusion couple experiments. The $Al_{11}Mn_4$ compound was observed as a layer at the liquid/solid interface of the diffusion couples. The solubility of Si in this phase is limited, at most 0.01 at. %. From these results we can conclude that the annealing

temperature between 550°C and 600°C of the diffusion couples has been too high to form new ternary intermetallics. None of the binary or ternary phase of the Al-Mn-Si system were found to contain Mg.

[1] Mondolfo L. The effect of manganese on the properties of aluminum. Light Metals Age 1979;February:20.
[2] Peng Cao, Ma Quian, David H. StJohn. Effect of manganese on grain refinement of Mg-Al based alloys. Scripta Materialia 2006;54:1853.
[3] M. Zamin. The role of Mn in the corrosion behavior of Al-Mn alloys. National association of corrosion engineers; Corrosion -Nace 1981;37:627.
[4] Krendelsberger N., Weitzer F., Schuster J.C. On the constitution of the systme Al-Mn-Si. Metallurgical and Materials Transaction A 2002;33A:3311.
[5] Du Y., Schuster J.C., Weitzer F., Krendelsberger N., Huang B., Jin Zhanpeng., Gong Weiping., Yuan Zhaohui., Xu Honghui. A thermodynamic description of the Al-Mn-Si system over the entire composition and temperature ranges. Metallurgical and Materials Transaction A 2004;35A:1613.
[6] I. Ansara, A.T. Dinsdale, Rand MH. Thermochemical database for light metal alloys. 1998 July,;European Commission and COST 507.
[7] Munekazu Ohno, Rainer Schmid-Fetzer. Thermodynamic assessment of Mg-Al-Mn phase equilibria, focusing on Mg-rich alloys. Z. Metallkd. 2005;96:857.
[8] Panday P.K., Schubert K. Journal of the Less-common metals 1969;18:175.
[9] Simensen C.J., Oberlander B.C., Svalestuen J., Thorvaldsen A. Determination of the equilibrium phases molten Mg-4wt% Al-Mn alloys. Z. Metallkd 1988;79:537.

Identification of intermetallic precipitates formed during re-solidification of brazed aluminium alloys

M. Dehmas, R. Valdés, M.-C. Lafont, J. Lacaze, B. Viguier.
Scripta mater., 55, 2006, 191-194

Identification of intermetallic precipitates formed during re-solidification of brazed aluminium alloys

Moukrane Dehmas, Rocio Valdés, M-C Lafont, Jacques Lacaze, Bernard Viguier
CIRIMAT, ENSIACET-INP, UMR CNRS 5085, 31077 Toulouse cedex 4, France

Keywords
Aluminium alloys, solidification, intermetallic compounds, electron diffraction

Abstract
Following recent investigations, the present study shows that Fe and Mn bearing phases in Al-Si alloys containing low level of Fe and Mn are essentially cubic α-Al(Fe,Mn)Si with Im3 space group and δ-AlFeSi which is observed with both tetragonal and orthorhombic structures. As this latter phase is not expected to form according to the ternary Al-Fe-Si phase diagram, the present results suggest that it is stabilized in the quaternary Al-Fe-Mn-Si system with respect to other phases such as β-Al_4FeSi.

Introduction
An analysis of the solidification sequence of some brazed aluminium clad alloys was presented previously [1, 2]. The material consisted of a core made of AA3003 (essentially an Al-Mn alloy) clad on its two faces with AA4343. This latter alloy is an Al-Si alloy with some low level iron. During brazing, the assemblage is heated for a few minutes at a temperature where the overlay melts whilst the core material remains solid. Most of the liquid fills the joints between the various parts in contact but some remains on the flat surfaces. After brazing, both the joint and the re-solidified overlay were slightly enriched in Mn due to partial dissolution of the core material during the process. This enrichment leads to the formation of precipitates containing Al, Si, Mn and Fe in addition to the (Al) matrix and the silicon lamellae. In the joint, these precipitates were either blocky in a three-phase eutectic with (Al) and silicon lamellae or Chinese-script in two-phase deposits with (Al) [1, 2]. In the re-solidified overlay, the precipitates were again blocky in the three phase eutectics in the valleys between the (Al) grains, or plate-like, when isolated inside or at the surface of the (Al) grains, as illustrated in figure 1.

EDX analyses performed in a SEM showed that both types of precipitates have similar silicon content, 10 to 12 at. %, with Mn and Fe apparently substituting each other with a sum of their contents at 15 to 16 at. % [1, 2]. By comparison to literature data, these results suggested that these precipitates correspond to the cubic α-Al(Mn,Fe)Si phase most often designated as $Al_{15}(Fe,Mn)_3Si_2$ [3]. However, there is so much controversy in the literature concerning the structure and composition of the compounds appearing upon solidification of aluminium alloys containing Si, Mn and Fe [4, 5], that it was decided to resort to TEM examination coupled with EDX analysis to ascertain the previous conclusion.

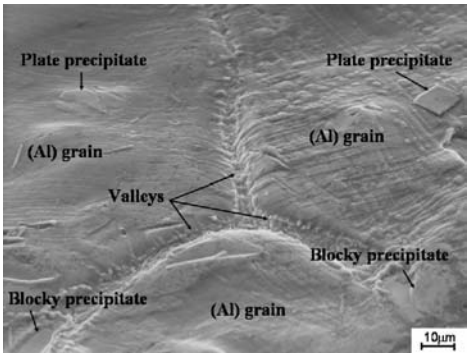

Figure 1 – SEM micrograph of the surface of the re-solidified cladding (*SEI* detector, 15 kV, 32 mm, tilt 54°).

Experimental procedures

To prepare TEM samples, sheets of the flat surfaces of the brazed assemblages were polished down to a thickness of 150 µm while preserving intact one of the re-solidified surfaces. Disks with a diameter of 3 mm were then cut by mechanical punch and the side opposite to the initial surface was gently dimpled before ion milling to transparency with a precision ion bean polishing (Gatan *PIPS™)*. Ion polishing was done during a few hours till a hole has formed. During this step, the disk was observed from times to times with an optical microscope to ensure that the hole was seemly located. Figure 2 presents an optical micrograph of two of the thin foils thus prepared, where precipitates located nearby the hole have been indicated with arrows. All the observations reported below were made on these two samples which will be referred as samples 1 and 2. On the micrographs in figure 2, the valleys are easily recognized in darker contrast. It is seen that the lower precipitate in sample 1 is located within a (Al) grain while the other precipitate as well as the one in sample 2 are within a valley.

TEM investigations were carried out on a JEOL JEM-2010 operating at 200 kV and fitted with a double tilt specimen holder allowing tilts of ± 30 ° around two orthogonal axes. Chemical analyses were achieved by energy dispersive X-ray (EDX) coupled with the TEM, with a spot size of about 40 nm. The EDX spectra were recorded with an acquisition time of 60 seconds, and treated semi-quantitatively using k-factor and including all usual correction (absorption and fluorescence).

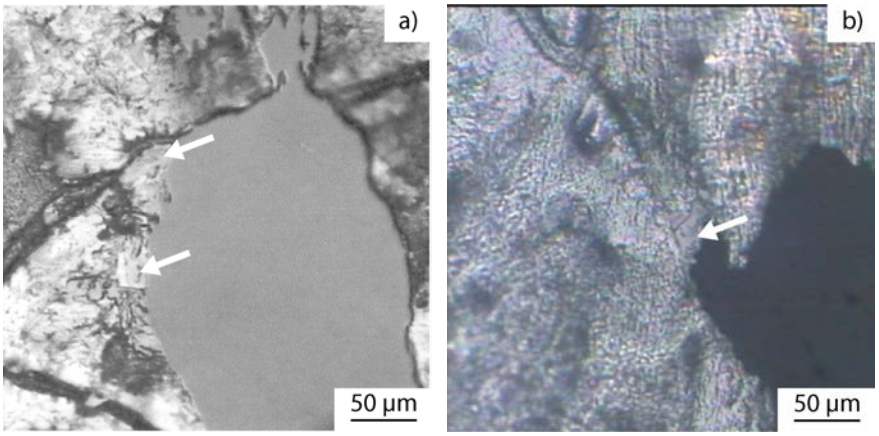

Figure 2 – Optical micrographs of two TEM foils (a: sample 1; b: sample 2) prepared by ion milling showing the hole and precipitates located either in a valley between (Al) grains or within a (Al) grain.

Experimental results

Figure 3 shows a TEM micrograph of each of the two precipitates of sample 1 identified in figure 2. Figures 3-a and 3-b relate respectively to the precipitate in the (Al) grain and to the one in the valley. The numbers on the micrographs refer to locations where EDX measurements were performed. The whole set of measured compositions is listed in Table 1.

The compositions measured on the precipitate in the (Al) grain are very similar to the values previously obtained by SEM-EDX [1, 2]. They are in agreement with the composition of the α-Al(Fe,Mn)Si phase measured on as-cast alloys by various authors as reviewed previously [2], but also with measurements on heat-treated alloys [6-9]. Munson [10] showed that there is a family of quaternary α-AlFeMSi phases (with M being either V, Cr, Mo, W, Cu and Mn) having bcc unit cells very similar to that of the simple cubic ternary α-AlMnSi phase. With increasing the Mn:Fe ratio, the bcc α-Al(Mn,Fe)Si phase would thus transform to the cubic α-AlMnSi phase. Cooper [11] investigated precipitates of this phase with a ratio Fe:Mn=4:1 (corresponding to the formula $Al_{19}Fe_4MnSi_2$) and performed a refinement of its structure starting with the model of the α-AlMnSi phase which has a Pm3 space group [12].

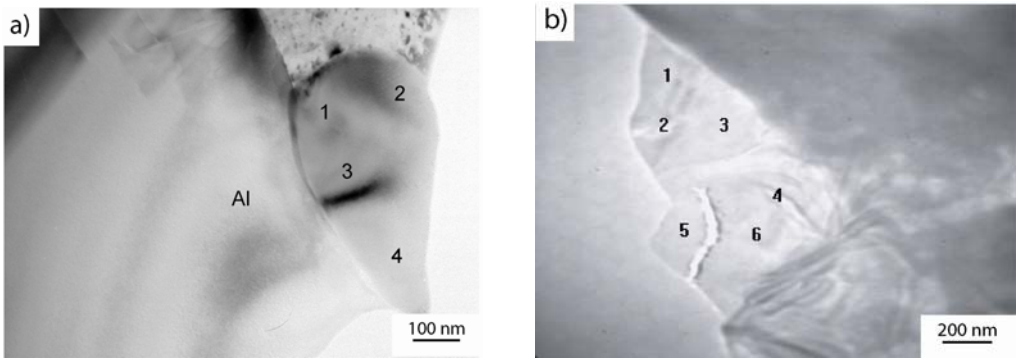

Figure 3 – Bright field images showing the two kinds of precipitates in sample 1: a) precipitate in aluminum grain; b) precipitate in the valley.

Through this refinement, Cooper showed that the α-Al(Fe,Mn)Si has a Im3 space group [11], and this has been found by other authors since then [13]. Donnadieu et al. [14] investigated further the Im3 and Pm3 structures through TEM analysis of precipitates in 6xxx aluminium alloys, and showed that there is a transition between the two structures which depends on the Mn:Fe ratio in the intermetallic phase. However, to the best of knowledge of the authors, no information is available on the type of transition involved.

Electron diffraction patterns along [111] and [230] zone axes recorded on the precipitate shown in figure 3-a are reproduced in figure 4-a and 4-b respectively. Also, diffraction patterns for the Im3 and Pm3 structures were simulated using the EMS software [15] and are shown also in figure 4. The calculations were performed with the description of the phases given by Cooper [11]. It is seen that along the [111] zone axis, the extinctions are similar for both space groups while along the [230] zone axis the reflections for which h+k+l is odd appear for the Pm3 group and not for the Im3 one. From this, it is concluded that the α-Al(Fe,Mn)Si phase observed in this study is cubic with Im3 space group with a

unit cell parameter close to 12.5 Å. This result agrees with the previous study by Donnadieu et al. [14] as the Mn:Fe ratio of the observed precipitate is quite low at 0.4 (table 1).

	Precipitate in the (Al) grain				*Precipitate in the valley*					
	1	2	3	4	1	2	3	4	5	6
Al	75	71	77.8	73.5	54	58.6	49	88	100	87
Si	10.5	10	10.2	9.7	35	29.8	42.5	8	-	8.2
Fe	10	14	8	12.3	8.5	9	6.5	3.5	-	3.7
Mn	4.6	4.2	4	4.5	2.3	2.6	2	0.7	-	0.8

Table 1 – Compositions (at. %) measured by EDX in the TEM on the two precipitates in sample 1.

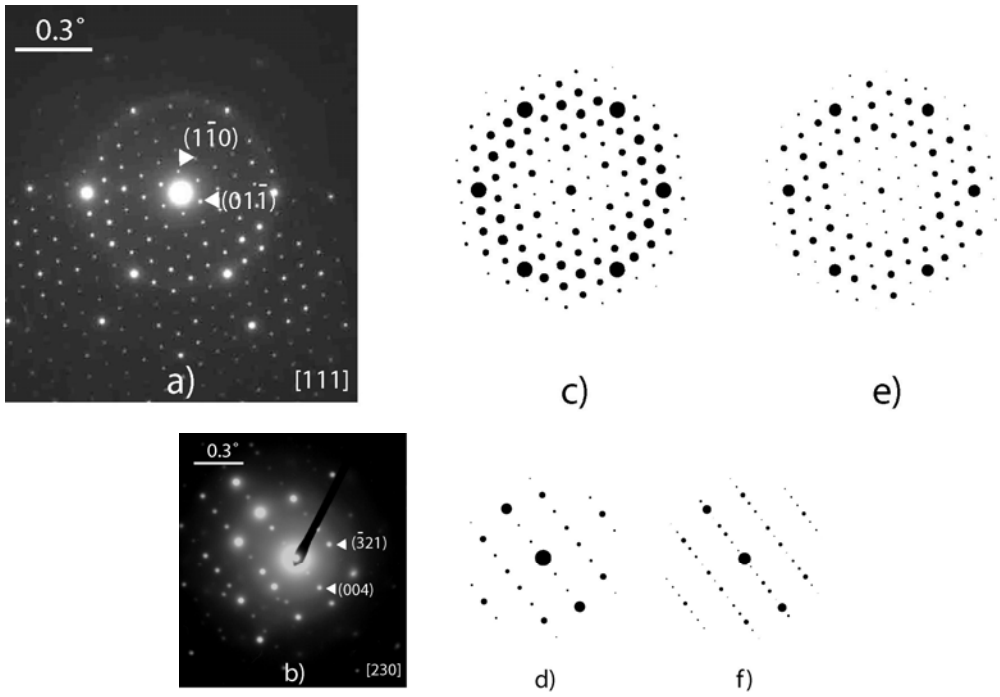

Figure 4 - Experimental selected area diffraction patterns (SAD) of the precipitate located in the (Al) grain (figures 2-a and 3-a) for the [111] (a) and [230] (b) zone axes, and simulation of the pattern expected at these orientations for Im3 (c, d) and Pm3 (e, f) space groups.

Concerning the precipitate in the valley, it is seen in Table 1 that the measurements may be sorted in two classes, compositions showing either high silicon content (30 to 42.5 at. %) or high aluminum content (more than 87 at. %). These latter values are most likely due to a contribution of the aluminum matrix and will not be considered further. Looking at the various compounds appearing in the Al-Fe-Si system, it was found that this high silicon content may fit with the composition of the Al_3FeSi_2 phase (Fe 15-17 at. %, Si 27-43 at. %, Al 40-58 at. %) as reviewed by Gueneau et al. [16]. This phase is most often called δ-AlFeSi.

The structure of the phase Al_3FeSi_2 has been reported as either orthorhombic [16] or tetragonal [13, 17, 18] with the same unit cell parameters. The orthorhombic structure may be distinguished from the tetragonal one by the presence of superstructure reflections, though there are only few zone axes allowing effectively such a distinction to be made, e.g. the [210] zone axis. Another methodology that was used in the present work to remove the uncertainty is based on the analysis of features of the reflection nets in the diffraction patterns including zero-order Laue zone (ZOLZ), first-order Laue zone (FOLZ) and second-order Laue zone (SOLZ). Simulation of diffraction patterns including High-order Laue zones (*HOLZ)* was performed by using EMS program and the structural data obtained by Panday et al. [17] for the tetragonal structure and by Gueneau et al. [16] for the orthorhombic one. The relative intensity of spots from HOLZ has been arbitrary increased in order to enhance the visual representation of the simulated patterns and the maximum deviation parameter from Bragg position (s_g^{max}) has been fitted to get the right number of spots in the ZOLZ. The identification of the structure was performed on a series of conventional selected area electron diffraction patterns (SAD) of different orientations with large angular separations recorded from the same area of the particle. Figure 5 presents the experimental diffraction pattern along [135] zone axis (a) and the corresponding calculated patterns according to the tetragonal (b) and orthorhombic (c) unit cells. The comparison between the two simulated patterns reveals the absence of reflections in the FOLZ for the tetragonal structure in contrast to the orthorhombic structure. Comparison to the experimental SAD pattern shows that the structure is tetragonal with the I4/mcm space group (a = 6.1 Å; c = 9.5 Å), and the other electron diffraction patterns recorded on this precipitate were easily indexed considering a tetragonal unit cell.

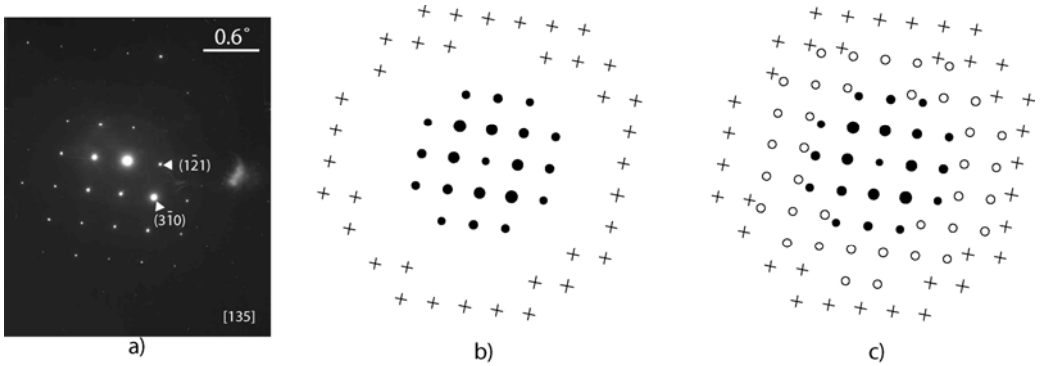

Figure 5 – Experimental electron diffraction patterns for the precipitate in the valley of sample 1 along the [135] zone axis (a) and corresponding calculated patterns according to a tetragonal (b) and orthorhombic unit cell (c) for $s_g^{max} = 0.1\ nm^{-1}$ (solid disks: ZOLZ; empty circles: FOLZ; crosses: SOLZ).

Figure 6 shows a bright field image of the precipitate in sample 2 (figure 2-b) that is also located in a valley. EDX measurements were performed in various locations indicated with numbers on the figure and are reported in Table 2. The compositions obtained could

be sorted in two groups, one rich in silicon (23 to 37 at. % Si) expected to correspond to the Al_3FeSi_2 phase as above and the other lower in silicon (7.1 to 17 at. % Si) that could correspond to the Al_4FeSi phase [18]. Attention was focused only in the present work on the areas with high silicon content. Figure 7 shows the experimental pattern along the $[3\bar{1}5]$ zone axis (a) and the simulated patterns corresponding to the tetragonal (b) and orthorhombic (c) structures. It is seen that additional reflections in the first-order Laue zone are consistent with an orthorhombic structure (Pbcn space group), while the unit cell parameters are the same as those considered for the tetragonal structure.

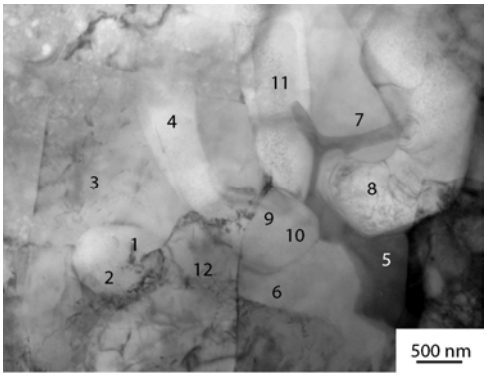

Figure 6 – Bright field image of the precipitate in the valley of sample 2. The numbers refer to locations of EDX measurements.

	1	*2*	*3*	*4*	*5*	*6*	*7*	*8*	*9*	*10*	*11*	*12*
Al	76.5	58.9	79.8	76.8	71.0	66.0	70.9	57.4	83.2	58.9	78.8	88.0
Si	17.0	35.1	12.8	15.9	24.0	28.0	23.1	37.1	10.3	35.1	13.8	7.1
Fe	4.6	4.21	5.1	5.0	4.0	4.6	4.2	3.9	4.5	4.2	5.1	3.5
Mn	1.9	1.71	2.2	2.1	1.5	1.9	1.7	1.5	1.8	1.7	2.1	1.4

Table 2 – Compositions (at. %) measured by EDX in the TEM on the precipitate in sample 2.

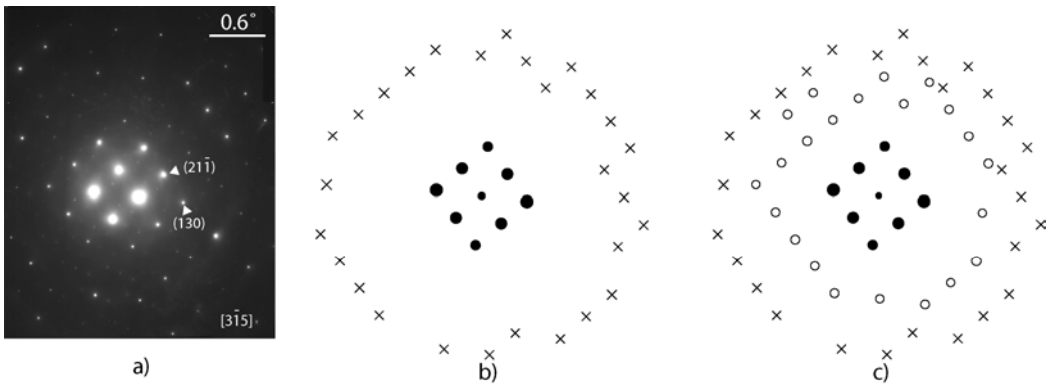

Figure 7 – Experimental electron diffraction patterns for the precipitate in the valley of sample 2 along the $[3\bar{1}5]$ zone axis (a) and corresponding calculated pattern indexed according to the tetragonal (b) and orthorhombic (c) unit cells for $s_g^{max} = 0.07\ nm^{-1}$ (solid disks: ZOLZ; empty circles: FOLZ; crosses: SOLZ).

Conclusion

The present study showed, in agreement with recent work [4], that the Fe and Mn bearing phases in Al-Si alloys containing low level of Fe and Mn are essentially cubic α-Al(Fe,Mn)Si with Im3 space group and δ-AlFeSi. This latter phase was found with both tetragonal and orthorhombic structures in the same sample. This phase appears in the ternary Al-Fe-Si diagram and has a composition most often referred to as Al_3FeSi_2, but should better be written $Al_3(Fe,Mn)Si_2$ when dealing with alloys containing both Fe and Mn. As there is no equilibrium between the (Al) and δ-AlFeSi phases in the ternary Al-Fe-Si phase diagram, the formation of this latter phase rather than the Al_5FeSi phase upon solidification of Al-Si alloys should be investigated further. The present study suggests this to be due to a stabilization of the $Al_3(Fe,Mn)Si_2$ phase with respect to the β-Al_4FeSi phase in the quaternary Al-Fe-Mn-Si system.

References

[1] Tierce S, Pébère N, Blanc C, Mankowski G, Robidou H, Vaumousse D, Lacaze J. International Cast Metals Research Journal 2005;18:370.
[2] Lacaze J, Tierce S, Lafont M-C, Thebault Y, Pébère N, Mankowski G, Blanc C, Robidou H, Vaumousse D, Daloz D. Mater. Sci. Eng. A 2005;413-414:317.
[3] Mondolfo LF. Aluminium alloys: structure and properties. London: Butterworths and co.; 1976
[4] Kral MV. Materials letters 2005;59:2271.
[5] Zakharov AM, Guldin IT, Arnold AA, Matsenko YA. Russian Metallurgy 1989;4:209.
[6] Dehmas M, Archambault P, Serriere M, Gautier E, Gandin C-A. Aluminium 2004;80:619.
[7] Li Y, Arnberg L. Acta Materialia 2003;51:3415.
[8] Tromborg E, Dons AL, Arnberg L. Aluminium alloys, proceedings of ICAA3, Materials Science Forum 1992. 285.
[9] Furrer P, Hausch G. Metal Science 1979;13:155.
[10] Munson D. J. Inst. Met. 1967;95:384.
[11] Cooper M. Acta Cryst. 1967;23:1106.
[12] Cooper M, Robinson K. Acta Cryst. 1966;20:614.
[13] Kral MV, McIntyre HR, Smillie MJ. Scripta Materialia. 2004;51:215.
[14] Donnadieu P, Lapasset G, Sanders TH. Philos. Mag. Lett. 1994;70:319.
[15] Stadelmann P. Ultramicroscopy 1987;21:131.
[16] Gueneau C, Servant C, d'Yvoire F, Rodier N. Acta Cryst. 1995;C51:177.
[17] Panday PK, Schubert K. J. Less-Common Met. 1969;18:175.
[18] Rivlin VG, Raynor GV. International Metals Reviews 1981;3:133.